
UNIVERSITY OF BIRMINGHAM

# A Molecular Dynamics Investigation of The Conformation and Hydration of Polymer Brushes

**by**

**Helen Elizabeth Abbott**

A thesis submitted to the University of Birmingham for the degree of

DOCTOR OF PHILOSOPHY

School of Chemistry

College of Engineering and Physical Sciences

University of Birmingham

October 2022

# ABSTRACT

The unique architecture of polymer brushes (PBs), combined with their ability to respond to external stimuli, have led to numerous applications, for example in biomechanical devices. A thorough understanding of their responsiveness to external stimuli is required to optimise PBs for use in these practical applications. It is well-known that the hydration levels and structural properties of PBs can be modulated by the addition of different types of electrolyte solutions, depending on the categorisation of electrolyte ions within the Hofmeister series.

Atomistic molecular dynamics (MD) simulations have been used to characterise the levels of hydration and conformational behaviour of two different types of PB: (i) strong polyelectrolyte brushes consisting of poly (2-(methacryloyloxy) ethyl trimethylammonium chloride) (PMETAC) and (ii) polyzwitterionic brushes consisting of poly (sulfobetaine methacrylate) (PSBMA) in a range of electrolyte solutions. The chosen atomic parameters successfully reproduced subtle differences in the conformational responses of both types of studied PBs in the presence of highly concentrated chaotropic anions, $ClO_4^-$ and $SCN^-$. The responsiveness of the studied PBs has been linked to the formation of ion pairs. The frequency and size of ion pairing and clustering species have been proposed to influence the hydration and structure of PMETAC and PSBMA brushes.

The presence of strongly kosmotropic anions, $SO_4^{2-}$ anions, caused no discernible change in the properties of the simulated PMETAC and PSBMA brushes. The chosen atomistic parameters, while accurate for the studied PBs with the chaotropic anions, do not seem to appropriately describe specific-ion interactions involving $SO_4^{2-}$ anions.

Chapter 7 is a stand-alone study using basin-hopping global optimisation techniques. Alkyl-dicarboxylate di-anions and alkyl-diammonium di-cations, in which the two distinct charge centres are separated by a flexible alkyl $(CH_2)_m$ chain were investigated in differently solvated conditions. For each di-ion investigated, a conformational transition from linear to folded is observed at a critical hydration number.

# ACKNOWLEDGEMENTS

I wish to thank my supervisors, Melanie Britton and Alessio Alexiadis, for their continued support and encouragement throughout my PhD. I would like to thank you both for always pushing me to be a better scientist and for teaching me so much.

All the members of the Britton group, the Johnston group and the Chakrabati group (particularly Jay and Wes) over the past five years also deserve my gratitude. Thank you for your support and for making me always feel part of the groups (even when I wasn't).

**Dizzy Dozzers:** Thank you for all the weird and wonderful things you've done since we've known each other: you are endlessly entertaining. Thank you for listening to my moaning and for telling me to get on with it – needed and appreciated.

**Big Andy and Dr Christophe:** Thank you to both of you for your surprising amounts of patience, guidance, support, and most importantly, for the constant supply of food and excellent coffee.

**Jacquie and Beth:** Thank you for your consistent support, thank you for coming in every day and going above and beyond your actual jobs. I truly appreciate all the chats we've had, all the strops you've listened to, the endless faith you've showed in me and your top tier pep talks. Also thank you for ignoring my daily requests asking you to do the PhD for me, I think this would be a very different thesis had you agreed! Lots of love from the finally (almost), real Dr Habbott/Dr Helebot.

**My non-science besties:** Thank you all for being so patient and understanding while I became progressively less fun throughout this PhD. Let's all hope it's a reversible reaction.

**Tommy:** thank.

**The Parents:** Thank you for being the best! xxx

And finally, to Professor Roy Johnston. Thank you for giving me the opportunity to work with you and start this journey. I only wish you were here to see the end of it as well. Royz Boyz 4evs!

# CONTENTS

# LIST OF ABBREVIATIONS

| Abbreviation | Definition |
|---|---|
| **PB** | Polymer Brushes |
| **PE** | Polyelectrolyte |
| **PZ** | Polyzwitterion/Polyzwitterionic |
| **LMWA** | Law Of Matching Water Affinities |
| **CIP** | Contact Ion Pair |
| **SIP** | Solvent-Shared Ion Pair |
| **2SIP** | (Double) Solvent-Separated Ion Pair |
| **PMETAC** | poly(2-methacryloyloxy)-ethyl-trimethylammonium chloride |
| **QA** | Quaternary Ammonium |
| **MD** | Molecular Dynamics |
| **RDF** | Radial Distribution Functions |
| **PSBMA** | Poly (sulfobetaine methacrylate ammonium) |
| **QCM-D** | Quartz Crystal Microbalance with Dissipation |
| **NMR** | Nuclear Magnetic Resonance |
| **LAMMPS** | Large-Scale Atomic/Molecular Massively Parallel Simulator |
| **AMBER** | Assisted Model Building with Energy Refinement |
| **CPU** | Central Processing Unit |
| **GPU** | Graphical Processing Unit |
| **pppm** | Particle-Particle Particle Mesh |
| **2D** | Two Dimensional |
| **GAFF** | General Amber Force Field |
| **SPC** | Simple Point Charge Water Model |
| **SPC/E** | Extended Simple Point Charge Water Model |
| **TIP4P** | Transferrable Intermolecular Potential Four Point |
| **DP** | Degree Of Polymerisation |
| **ATRP** | Atom Transfer Radical Polymerization |
| **RESP** | Restrained Electrostatic Potential |
| **PBCs** | Periodic Boundary Conditions |
| **VMD** | Visual Molecular Dynamics Programme |
| **$N_{QA}$** | Nitrogen Atom of Quaternary Ammonium Group |
| **$CA_{anion}$** | The Central Atom of Anion of Interest |
| **$O_W$** | Oxygen Of Water Molecules |
| **$S_{sulfonate}$** | Sulfur of Sulfonate Groups in PSBMA Chains |
| **AFM** | Atomic Force Microscopy |
| **NVT** | Canonical Ensemble |
| **$DC_m$** | Alkyl-dicarboxylate di-anions, $[^{-}O_2C(CH_2)_mCO_2^{-}]$ |
| **$DA_m$** | Alkyl-diammonium di-cations $[^{+}H_3N(CH_2)_mNH_3^{+}]$ |
| ***n**** | Critical Hydration Number |
| **GM** | Global Minimum |
| **DFT** | Density Functional Theory |
| **BH** | Basin-Hopping |
| **PES** | Potential Energy Surface |

# CHAPTER 1: INTRODUCTION

Polymer chains can be chemically grafted to an interface or surface. When tethered with an appropriately high grafting density, polymer brushes (PBs) are formed.[1,2] The characteristics and behaviour of PBs depend on numerous factors, including the type of polymer within the PB,[3,4] the surrounding solvent,[4,5] and the presence of ions.[3,6,7]

The properties of PBs can, therefore, be altered by adding an electrolyte solution to the PB.[3,6–10] It is well-known that the hydration and structural behaviour of PBs is affected by different types of electrolyte ions, regarding their categorisation within the Hofmeister series.[11] This is an example of the Hofmeister effect, otherwise known as the specific-ion effect. Consequently, macroscopic properties of PBs can be controlled by specific-ion effects, thus impacting many valuable applications such as colloidal stabilisation,[12,13] ice nucleation,[14] bio-lubricants on artificial joints,[15] wettability,[11] and lubrication.[16–18] An understanding of specific-ion interactions with PBs, and how to control them, can be achieved by clarifying how ions interact with PBs and their influence on the behaviour of PBs.[19] The aim of this research is to explore specific-ion interactions within PBs using atomistic molecular dynamics (MD) simulations.

## 1.1 Polymer Brushes

PBs contain groups of polymer chains that have been tethered to a surface.[1,2,20] The preferred method of synthesis is the “grafting-from” technique, wherein the PB surface contains an initiator from which direct polymerisation occurs.[2,21–23] The grafting density of the PB, namely the density of polymer chains per surface area, can be controlled during the synthesis step. This

is an important property to regulate, as a brush configuration can only be achieved if the grafting density of the chains is above a critical value.[3]

In solution, a free polymer chain will adopt a coiled arrangement (Figure 1.1a).[3] The effect of tethering polymer chains so closely within a brush, however, prevents this configuration. Instead, chains stretch orthogonally away from the surface to prevent overlapping with one another (Figure 1.1b).[3] The length of a polymer chain within a PB is, therefore, much greater than that of an untethered chain, due to the high grafting density which induces the unique conformation observed for PBs. This results in the ability for PBs to react to external stimuli by altering their conformations.[24,25] Stimuli within the surroundings of a PB such as, the type of solvent,[4,5] pH[26] and the temperature,[3] can alter interactions between PBs and their environment. PBs have been shown to respond in either an attractive or repulsive way, inducing a swollen (Figure 1.1c) or collapsed (Figure 1.1d) conformation.[3,4,24,25] The responsiveness of PB systems can be exploited by industries responsible for creating devices which require switching materials properties upon external signals.[3,15,27]

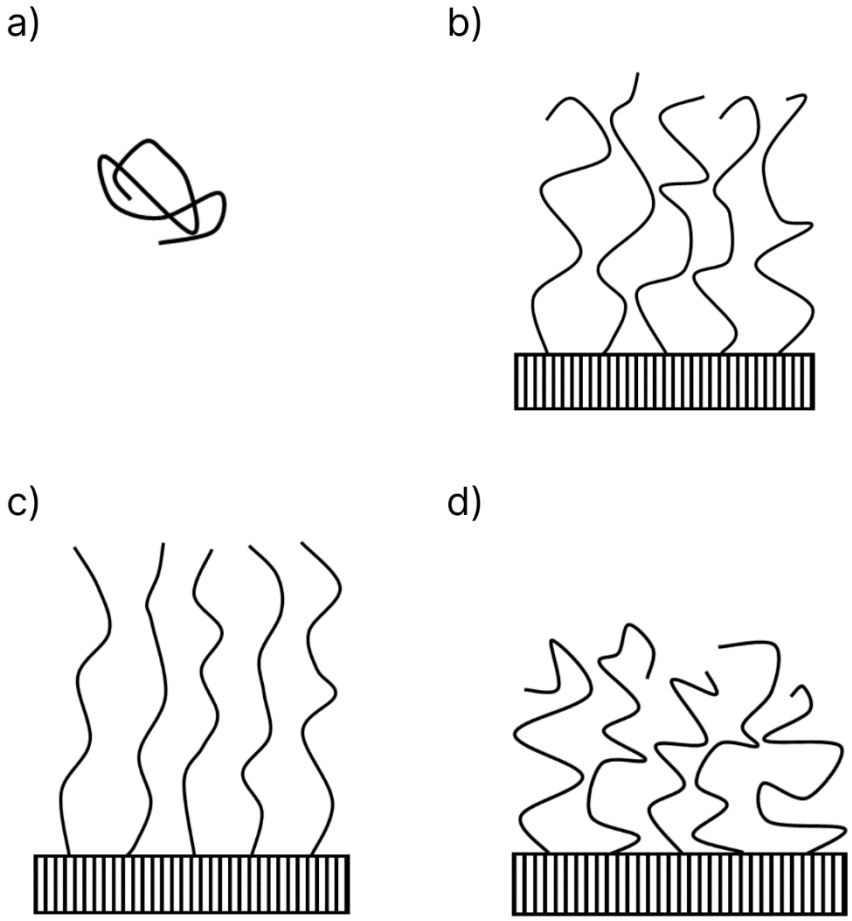


**Figure 1.1** Schematic representations of polymer chains in a) a coiled configuration b) grafted in a brush configuration, c) grafted in a swollen configuration and d) grafted in collapsed configuration.

The presence of charges significantly increases the responsive properties of PBs compared to those of uncharged PBs. For example, polyelectrolyte (PE) brushes and polyzwitterionic (PZ) brushes both display highly responsive behaviour in the presence of salt solutions.[3,4] PE brushes contain PE chains (charged chains) and PZ brushes consist of zwitterionic polymer chains. For both PE and PZ brushes, a change in ionic strength of the surrounding electrolyte solutions, for example, can induce a conformational collapse/swelling transition (Figure 1.1).[3,4,7,27–29]

In water, a PE brush will adopt a stretched configuration. Both electrostatic repulsion between the PE chains, along with the fully hydrated nature of the chains contribute to this swollen configuration.[3] In electrolyte solutions, particularly as the ionic strength of the electrolyte increases, a collapsed conformation is adopted. A decrease in the Debye screening lengths occurs which strengthens electrostatic screening, thus minimising electrostatic repulsions between PE chains.[3,6]

In contrast, PZ brushes typically demonstrate an "anti-polyelectrolyte effect" as the conformational behaviour observed is typically the opposite to that seen in PE brushes.[7,29] PZ brushes adopt a collapsed conformation in water. Low levels of hydration[28] have been observed within the brush due to electrostatic association between the PZ chains and within the PZ chains themselves.[27,29] In the high ionic strength regime, PZ brushes are swollen and the extent of hydration is increased as a rise in ionic strength weakens interchain/intrachain dipole-dipole interactions.[4,27]

Ionic effects beyond ionic strength of the surrounding electrolyte solution must also be considered to fully comprehend the properties of PE and PZ brushes. Hydration and conformation properties of both types of brushes are sensitive to, and can be adjusted by, the exact type of salt ions present,[8–10] specifically regarding their categorisation within the Hofmeister series.[11,30] This is known as the specific-ion effect (or the Hofmeister effect).[30]

## 1.2 The Specific-Ion Effect

Over 130 years ago, the specific-ion effect was reported by Franz Hofmeister and co-workers[30,31] who noted that certain salts were effective at precipitating egg-white protein from aqueous solutions, while others were less so. Ions in aqueous solution were consequently ranked based on their ability to precipitate the protein[31] and by investigating multiple different salts, two separate "Hofmeister series" for cations and for anions were constructed. Figure 1.2 shows the series for selected anions.


**Figure 1.2** Hofmeister series for selected anions. Kosmotropic anions are situated to the left of the Hofmeister series, with chaotropic ions positioned on the right. $Cl^-$ anions are known to be borderline kosmotropic.

These original studies[30,31] led to ions being classified as *kosmotropes* or *chaotropes* depending on the influence they exert on water networks (Figure 1.3a). Kosmotropic ions were said to have "structure making" properties and possess the ability to organise water molecules, even beyond their own hydration shells.[32] At the opposite end of the Hofmeister series are chaotropic ions, which can disrupt water networks and are described as "structure breaking".[19]

Since the concept of the specific-ion effect was proposed, there has been considerable disagreement in the literature[33–38] over the classifications and conclusions drawn by the original

study.[30,31] Firstly, an increasing number of investigations, both experimental[33,37] and theoretical,[38] suggest there is no significant long-range influence exerted by ions: only the immediate hydration layers are affected.[33–38] This challenges the structure making/breaking definition of kosmotropic and chaotropic ions; the structural effects of the ions in relation to water are generally proposed to affect bulk water (water molecules situated beyond the immediate hydration shells of ions). Moreover, the properties and behaviour of the hydrated solute are excluded from the original explanation, as only the properties of the ions themselves are considered.[30,31] It is now believed that it is not possible to explain specific-ion effects without fully considering the properties of all components within a studied system, and interactions between them.[19]

Currently, it is generally accepted that the two different types of ions, kosmotropes and chaotropes, exhibit distinct effects on the stability, solvation and conformation of proteins.[19] Specific-ion effects are also observed for many different species including synthetic PEs and PBs, particularly PE brushes and PZ brushes.[4,5,7,39] The Hofmeister series is also now more commonly seen as a ranking of the relative effects of ions on the physical behaviour of many aqueous processes. However, there are still no definitive explanations surrounding the molecular mechanism of specific-ion effects and those interactions between ions, water, and the solute within the system of interest. The mechanism of the specific-ion effect is now often proposed to centre around interactions between ions and the solute (Figure 1.3) and has been interpreted by several models.[40–44]

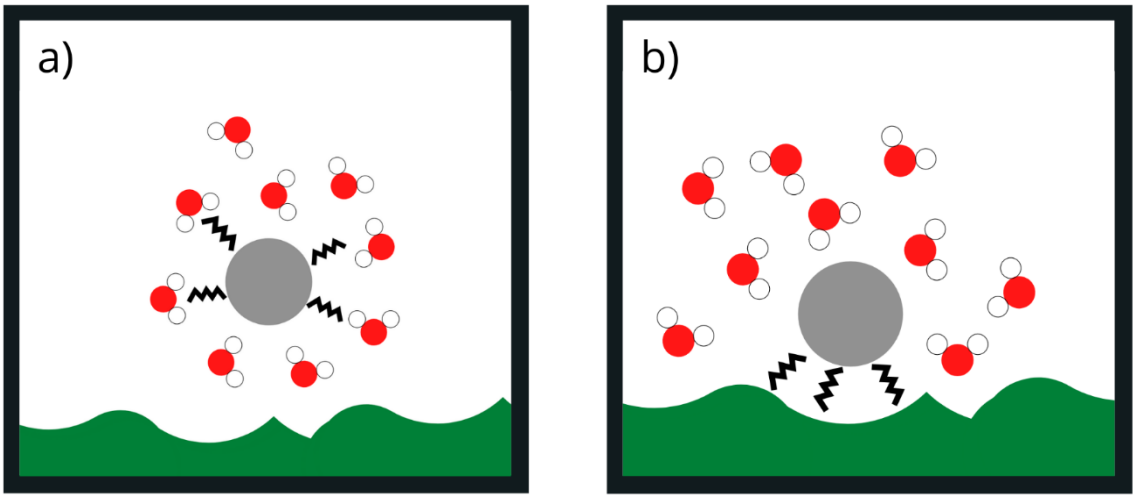


**Figure 1.3** Schematic representations of the main difference between the focus of the original theory and latest theories explaining the mechanism of the Hofmeister effect. a) Mechanism involved in the original theory, b) Mechanism involved in the latest explanations. The direct interactions are represented black zig zag lines, the ions are grey, the proteins are green, and the water molecules are red and white.

Specific-ion effects are believed to be linked to interactions (or lack of interactions) between ions and particular binding sites on the surface of the solute. It has been proposed that specific-ion interactions are dominated by the formation of ion pairs.[40,41] Collins' Law of Matching Water Affinities (LMWA)[40,45] proposes that an ion pair can only form between oppositely charged ions with similar hydration strengths (Figure 1.4). Ions with mismatched water affinities cannot form ion pairs as interactions between them are too weak. The ion dispersion theory[42] suggests that ion dispersion forces are an ever-present source of specific-ion effects. The polarisability of ions is considered to be the key factor involved, and determines if an ion pair can be formed or not.[42]

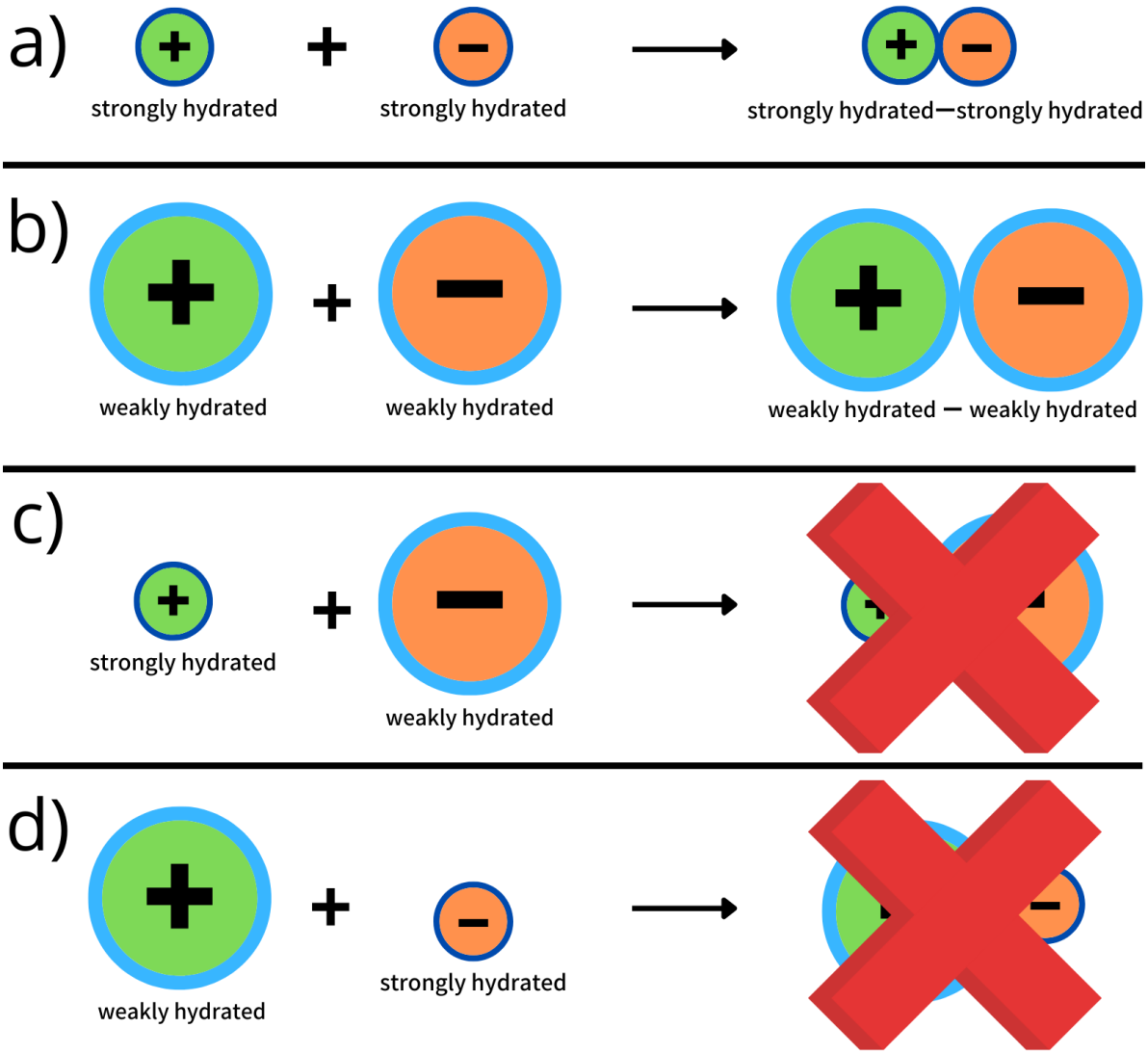


**Figure 1.4** Schematic representation of Collins' Law of Matching Water Affinity (LMWA): [40,45] a) an ion pair would form between a kosmotropic cation and a kosmotropic anion, b) an ion pair would form between a chaotropic cation and a chaotropic anion, c) an ion pair would *not* form between a kosmotropic cation and a chaotropic anion, d) an ion pair would *not* form between a chaotropic cation and a kosmotropic anion.

### 1.2.1 Ion pairs

An ion pair is a distinct chemical species[46] and is formed if two oppositely charged ions associate with each other together at a distance, *R*, for a time longer than that needed to diffuse over *R*.[46] An ion pair can be categorised in three different ways (Figure 1.5).[46,47] A contact ion pair (CIP) occurs when two ions are in direct contact, no solvent molecules are situated between the ions. When a single solvent layer is present between the two ions, a solvent-shared ion pair (SIP) occurs and when the first solvation shells of the two ions remain, a (double) solvent-separated ion pair (2SIP) is formed.

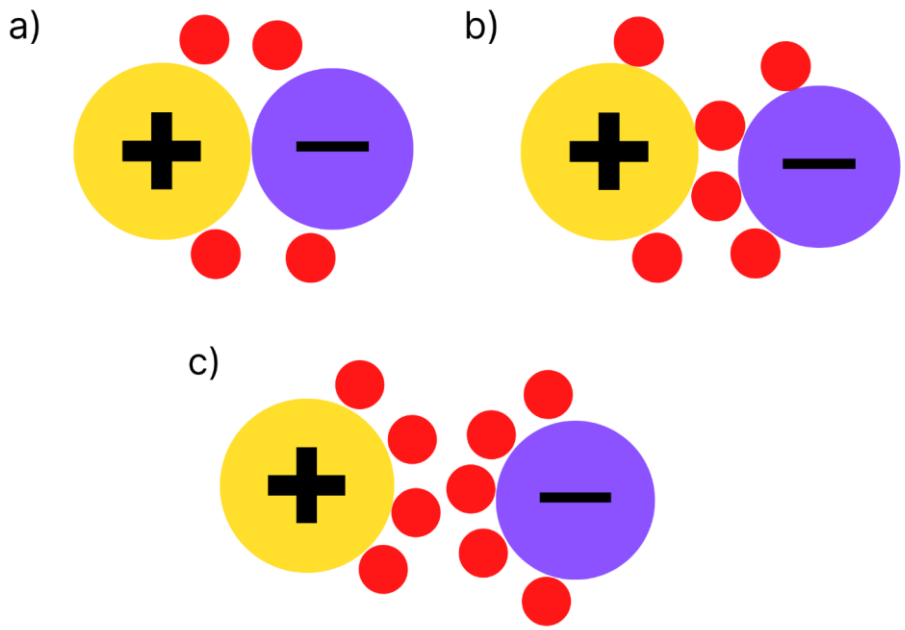


**Figure 1.5** Schematic representations of the three types of ion pairing interactions: a) contact ion pair (CIP), b) solvent-shared ion pair (SIP), and c) solvent-separated ion pair (2SIP), formed between an anion (purple), cation (yellow), and solvent molecules (red). The complete solvation shell is not illustrated.

Numerous experimental techniques have been employed to examine ion pair formation in low ionic strength electrolyte solutions.[48–52] Spectroscopic methods such as dielectric spectra

techniques[50,52] and ultrasonic relaxation[51] methods have studied dynamic properties of electrolyte solutions. These methods can provide information on the rotational timescales of dipolar species including CIP, SIP and 2SIP.[50–52] One of the limitations of these methods, however, is resolving ion pairing dynamics that occur on picosecond timescales.[47] This is important as many ion pairs have lifetimes on this timescale.[46] Furthermore, only a few studies have examined highly concentrated electrolyte solutions.[46] It is believed that further association may occur and the formation of ion triplets, ion quadruplets and even higher-order ion clusters can be observed as the ionic strength of an electrolyte solution is increased.[53,54] No studies, either experimental or computational, have been undertaken to examine dynamics, or conformations, of ion pairs or higher-order ion clusters within PBs. This is despite the widely believed significance of ion pairs on changes observed in the hydration and conformational behaviour of PBs.[4,8,39,55–57]

## 1.3 Specific-Ion Effects on Polymer Brushes

The formation of ion pairs has previously been hypothesised to underly the highly complex hydration and conformational behaviour displayed by PE and PZ brushes upon changes in salt type.[4,8,39,55–57] Experimental[4,8,39,55–57] and theoretical[5,56] research has been undertaken in recent years to explore the effects of ion pairs on PBs.

### 1.3.1 Polyelectrolyte Brushes

There are two classifications of PE brushes, strong and weak PE brushes. Strong PE brushes contain PE chains with permanent charges, such as poly (2-methacryloyloxy)-ethyl-trimethylammonium chloride (PMETAC) and poly (vinylbenzyl trimethylammonium chloride) brushes (chemical structures of monomers are shown in Figure 1.6). Whereas the charge density of weak PE brushes, like poly (dimethyl aminoethyl methacrylate), is regulated by the pH of the

surrounding solution. In this thesis, strong PE brushes have been studied due to their recorded responsiveness regarding specific-ion interactions.[6,8,11,58]

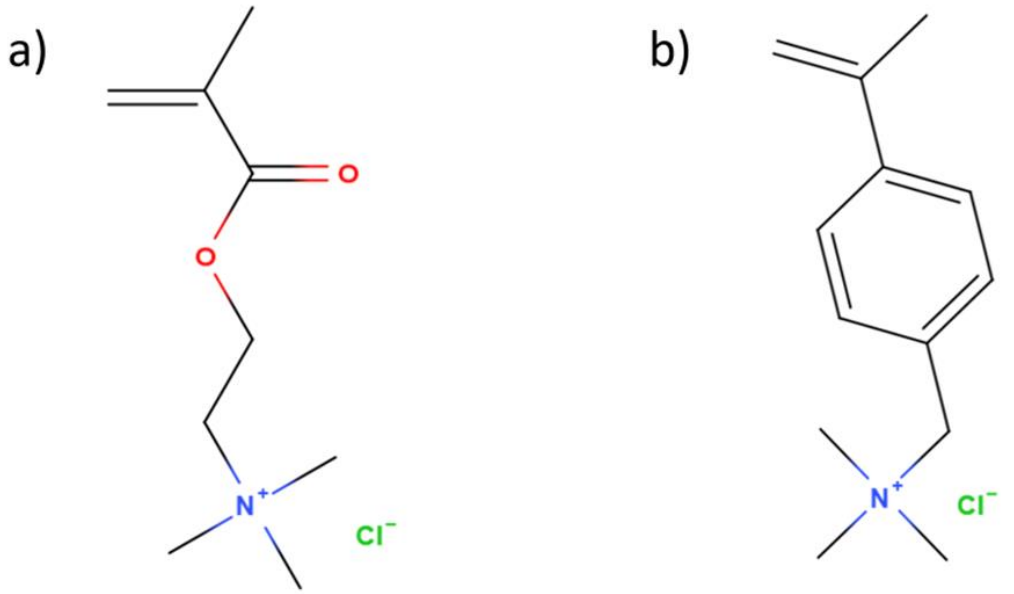


**Figure 1.6** Chemical structures of common strong basic monomers: a) (2-methacryloyloxy)-ethyl-trimethylammonium chloride, b) vinyl benzyl trimethylammonium chloride.

Specific-ion interactions with strong PE brushes have been widely examined[4–6,8,9,11,39] and the strong cationic PMETAC brush (Figure 1.6a), in particular, has been commonly studied.[4–6,8,9,11,39] This brush contains a permanent positive charge, a quaternary ammonium (QA) group within its monomeric unit.[4,6] Many other strong cationic PEs, such as poly (propyl trimethylammonium chloride), poly (vinylbenzyl trimethylammonium chloride) (Figure 1.6b) and poly [3-(methacryloylamino) propyl trimethylammonium chloride], contain the positively charged trimethylammonium chloride group present in PMETAC. Hence, results obtained while studying PMETAC brushes are potentially applicable to other cationic PE brush systems.

Kou *et al.*[8] examined PMETAC brushes in a range of sodium salt solutions (1 and 500 mM), some of which contained kosmotropic anions and others, chaotropic anions. As the concentration of each solution increased, the extent of brush collapse increased. Chaotropic anions induced a more pronounced collapse than kosmotropic anions, supporting previous research from Azzaroni *et al.*[11] and Wei *et al*.[58] This observation is believed to be due to the formation of ion pairs between the highly polarisable, but weakly hydrated chaotropic anions and the weakly hydrated chaotropic QA group of the PMETAC chains (illustrated in Figure 1.7).[6,8] It has been proposed that the presence of ion pairs leads to a decrease in the hydration of the anions which in turn, results in the reduced levels of solvation within the PMETAC chains.[8]

The behaviour of the PMETAC brush was considerably distinct in the presence of kosmotropic anions. The hydration levels within the PMETAC brush, together with the thickness of the brush, were only minimally affected by an increase in ionic strength of the sodium-kosmotropic anion solutions. Kou *et al.*[8] suggested that the mechanism involved in specific-ion interactions altered.[8] It was hypothesised that ion pairs did not form. Instead, the highly solvated nature of kosmotropic anions was suggested to introduce competition between the kosmotropic anions and QA groups for water molecules that are situated within the PMETAC chains (shown in Figure 1.7).[8] The extent of brush collapse across the studied salt solutions followed predictions made using both the LMWA theory[40,45] and the theory of ion dispersion.[42]

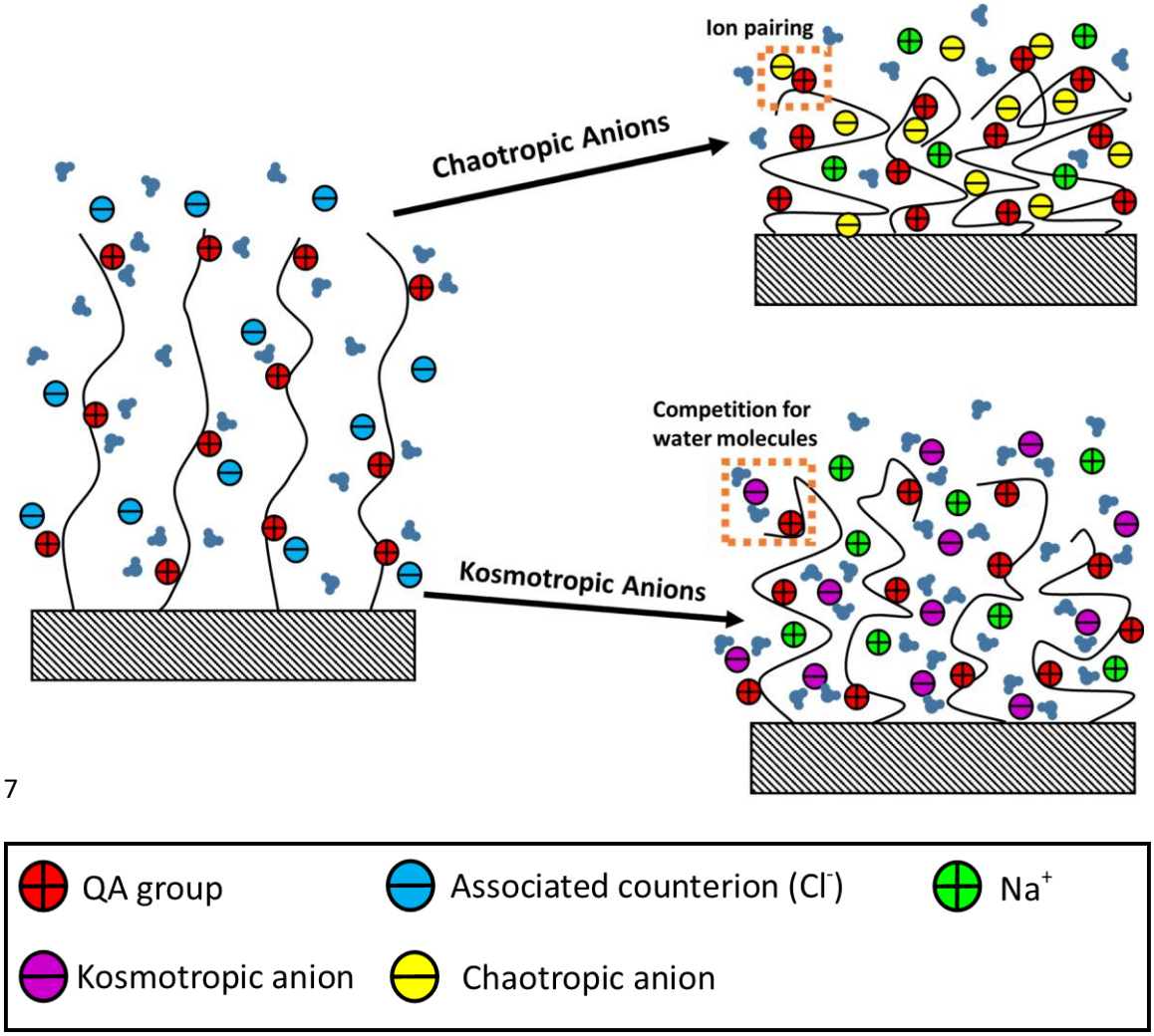


7

**Figure 1.7** Schematic representation of the conformational transition occurring upon the addition of chaotropic and kosmotropic ions in the high ionic regime. The suggested molecular mechanism involved in the specific-ion effects of PMETAC brushes is highlighted by orange dotted-line boxes.

Changes in hydration and conformational behaviour of PMETAC brushes, induced by different types of ions, have also been successfully reproduced using computational methods.[5] Atomistic MD simulations have been performed on a PMETAC brush in the presence of both chaotropic and kosmotropic anions and radial distribution functions (RDFs) were plotted for QA groups in the PMETAC brush with added ions.[5] It was reported that chaotropic $ClO_4^-$ anions are more likely to be found in close proximity to QA groups, rather than the kosmotropic $Cl^-$ or $SO_4^{2-}$ anions.[5]

This has been presented as evidence that chaotropic anions form strong ion pairs with QA groups in the PMETAC brush.

It is vitally important to understand the nature of ion pairs, as they have been found to significantly affect the macroscopic properties of PMETAC brushes.[5,6,11,58] Azzaroni *et al.*[11] explored how different electrolyte solutions influenced the hydrophobicity/hydrophilicity of a PMETAC brush. As the electrolyte anion was changed from a kosmotropic $PO_4^{3-}$ anion to the chaotropic $ClO_4^-$ anion, a considerable change in wetting properties of the surface of the brush occurred.[9,11] By measuring the contact angle of water on the PMETAC brush surface, it was reported that the hydrophobicity of PMETAC brushes increased in the presence of chaotropic anions.[11] The hydrophobicity of PMETAC brushes is therefore controlled by the hydrophobicity/hydrophilicity of the newly formed ion pair between QA groups and counterions.[9,11] The ability to control the hydrophobicity of a PE brush has major implications for current and potential applications. For PE brushes in their application as bio-lubricants on artificial joints, the hydrophilicity of the brush plays a valuable role in the reduction of wear.[11,15,59]

### 1.3.2 Polyzwitterionic Brushes

Unlike PE brushes, only a few investigations have been undertaken to study how chaotropic and kosmotropic ions affect the hydration and conformational behaviour of PZ brushes.[7,27,60] Moreover, the mechanism responsible for specific-ion interactions, and how they influence the properties of PZ brushes, still requires further research.

Poly (sulfobetaine methacrylate ammonium) (PSBMA) brush (chemical structure of monomer is shown in Figure 1.8) is an example of a typical PZ brush and has been found to display specific-ion effects.[7,27] In low ionic strength regimes (< ~ 0.1 M), anions were found to enhance the hydration of the PSBMA brushes following the trend: $Cl^-$ < $Br^-$ < $ClO_3^-$ < $SCN^-$ < $ClO_4^-$ in accordance with the Hofmeister series (Figure 1.2). It was suggested that anions which are more effective at weakening interchain/intrachain interactions within the PSBMA brush, result in stronger hydration.[7] It is believed that chaotropic anions form the strongest ion pairs with QA groups along the PSBMA chains. Interchain/intrachain interactions are, consequently, disrupted and the PSBMA brush swells.

For PSBMA brushes in highly concentrated electrolyte solutions (> ~ 0.1 M), however, it was observed that the anion trend almost completely reversed, $SCN^-$ < $ClO_4^-$ < $ClO_3^-$ < $Br^-$.[7] Wang *et al.*[7] proposed that in the high ionic regime, there may be dissociation of ion pairs between the QA groups and anions, subsequently, the newly free dipoles on the PSBMA grafted chains may not reform interchain/intrachain associates. Ion pair dissociation leaves QA groups free to bind with water molecules and the hydration levels within the brush increase. A stronger ion pair (i.e., a more chaotropic anion in contact with a QA group) finds it more difficult to disassociate, therefore resulting in lower brush hydration.

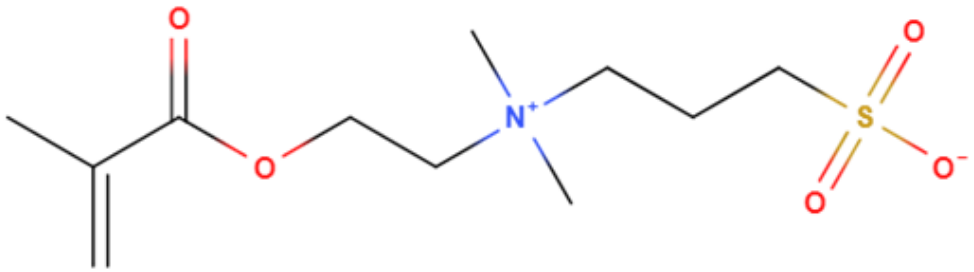


**Figure 1.8** Chemical structure of the sulfobetaine methacrylate monomer.

PZ brushes are important to study as their applications in protein resistant surfaces are a critical field. It is widely known PZ brushes have strong protein resistance properties due to strong electrostatically induced hydration.[4,61–65] Chaotropic anions have been observed to enhance the protein resistance of PZs.[7,27] The level of hydration is dependent on what type of anion is added, therefore protein desorption and adsorption is also dependent on specific-ion effects.[4,7]

## 1.4 Scope of Thesis

Our understanding of PBs and their specific-ion interactions has evolved via both experimental and computational methods. Experimentally, the hydration and conformational behaviour of PE and PZ brushes in different types of electrolyte solutions, have been investigated.[7,66–68] A variety of techniques, such as spectroscopic ellipsometry (SE),[1,4,26,67,69] surface plasmon resonance (SPR)[7,67], neutron reflectivity (NR)[68] and atomic force microscopy (AFM)[66] have been employed.

Quartz-crystal microbalance with dissipation (QCM-D) is a commonly used experimental method.[1,4,26,67,69] Resonance frequency, *f*, can be monitored as a function of time and is known to be dependent on the mass of PBs. QCM-D can be used, therefore, to analyse hydration levels

within PBs by reporting variations in *f* relating to changes in the quantity of water molecules coupled to the PB.[76] Moreover, changes in dissipation can be measured reflecting differences in the mechanical properties of PBs.[1,4,26,67,69] The use of QCM-D as an experimental technique successfully captures the loss or gain of water within PBs as well as changes in conformation.[1,4,26,67,69]

Many of the macroscopic properties measured by the techniques mentioned above can be linked to the effects of forming ion pairs.[1,4,26,67,69,70] The conformation and dynamics of ion pairs forming within PB systems is, however, somewhat challenging to investigate fully via experimental means. As mentioned previously, spectroscopic methods[50–52] can only resolve ion pairing dynamics that occur on nanosecond (or larger) timescales.[47] It would be valuable to enhance our understanding of ion pairs hypothesised to form in PBs as they are generally cited as the principle reason for specific-ion effects observed in PB systems.[1,4,26,67,69,70]

Computational techniques are ideally suitable for the study of PBs; not only shedding light on the hydration and conformational behaviour of the PBs, but also allowing for the exploration of the microscopic dynamics of ion pairs. Computational techniques enable analysis even at femtosecond timescales. Thus, it is possible to assess the validity of the hypothesis offered by experimentalists to explain the driving force involved in changes of conformation and hydration levels within PBs. Furthermore, the use of computational techniques affords the opportunity to test a great variety of systems and observe new interactions, properties, and behaviours. Future experimental chemists can utilise this new information to select the right technique to better observe PBs and their specific-ion interactions.

Thus far, extensive computational studies have been carried out on the properties of PBs using continuum models based on scaling[71,72] and self-consistent field theories.[73–75] These methods, although able to provide fundamental insights, only offer a limited account of responsive behaviours due to the non-atomic description of the chemical structure of PBs. Alternatively, MD simulation is an attractive computational method which can be used to analyse PBs. The thermodynamic and structural properties of PBs have been examined by combining MD simulations with different levels of coarse-grained models.[76–85] Bead-spring type models are commonly used to study PB systems[76,83] due to their ability to provide an understanding of general dependencies, for example, on grafting density or on the length of polymer chains.[77] However, these types of coarse-gained models do not contain chemical specificity and it is, therefore, difficult to compare directly with experimental results.

Atomistic MD simulations are a promising alternative. Via such methods, it is possible to extract information on the conformation and hydration levels within PBs as well as associated specific-ion interactions from one simulated trajectory. Until recently, atomistic MD studies only tended to focus on PB systems with a few very short (6-30 monomers long) oligomer-like chains.[57,86] It was too computationally expensive to simulate a "realistic" PB owing to the complexity of the system and its size. In recent years,[87] the highly parallelised nature of MD simulations programmes means it is increasingly possible to simulate a PB system more representative of experimental size.[5]

In this thesis, the large-scale atomic/molecular massively parallel simulator (LAMMPS)[88,89] has been employed to perform atomistic MD simulations. A brush thickness comparable to synthesised PBs was simulated in the atomistic models of PMETAC and PSBMA brushes using

AMBER force fields.[90] The aim of the research in this thesis, is to use atomistic MD simulations to further understand molecular mechanisms involved in specific-ion effects, specifically how the formation of ion pairs influences hydration levels and conformational properties of PE and PZ brushes.

Firstly, ion pairs and clusters within PMETAC brushes consisting of two modelled polymer chains, in the presence of chaotropic anions, perchlorate ($ClO_4^-$), and thiocyanate ($SCN^-$), are studied extensively. These results are further supported by performing simulations on larger models of PMETAC brushes containing eight polymer chains within the finite simulation cell. Next, a PSBMA model containing two polymer chains is simulated in the presence of $ClO_4^-$ and $SCN^-$ and the findings are compared with results from the PMETAC brush. The results from simulations of a strongly kosmotropic anion, sulphate ($SO_4^{2-}$), on the PB models are then discussed.

The final chapter investigates the hydration and conformational behaviour of two different types of di-ions, in which the two distinct charge centres are separated by a flexible, hydrophobic alkyl $(CH_2)_m$ chain. Global optimisation techniques are utilised to examine di-ions in unhydrated, implicitly, and explicitly solvated conditions. This chapter is based on the paper, "Effects of Hydration on the Conformational Behaviour of Flexible Molecules with Two Charge Centres" published in the Journal of Physical Chemistry A in 2020.[91]

# CHAPTER 2: METHODOLOGY

The characteristics and behaviours of polymer brushes (PBs) can be altered upon the addition of electrolyte solutions.[3,6–10] Interactions between salt ions and grafted polymer chains of a PB are said to induce changes within the structure of PBs via the formation of ion pairs.[5,7,8,11,27,58] These ion pairing interactions occur on femtosecond to nanosecond timescales[47] and can be, therefore, challenging to visualise via experimental techniques.[46,47] Molecular dynamics (MD) can shed light on the microscopic dynamical behaviour of ion pairing interactions,[87] enabling analysis at appropriate timescales, and allowing for the potential elucidation of mechanisms underlying specific-ion interactions.[5,56] As such, the validity of hypotheses suggested by experimentalists explaining driving forces accountable for the responses of PBs to external stimuli, discussed throughout Chapter 1: Section 1.3, can be explored and validated. Furthermore, experimental researchers can utilise results from MD simulations, not only to better interpret experimental findings, but also to guide future studies, for example by selecting appropriate techniques to observe ion pairing interactions within PBs.

## 2.1 Molecular Dynamics Simulations

MD can be used to produce a dynamical trajectory showing how particles within a particular system evolve in time. This is achieved by the integration of Newton's equations of motion. Initial positions and velocities of each particle within the system of interest are required. The classical equation of motion (equation 2.1) can then be solved:[92,93]

$$m_i \frac{d^2\mathbf{r}_i}{dt^2} = \mathbf{F}_i \qquad (2.1)$$

Where $t$ is time, the position and mass of the $i$-th particle is represented by $\mathbf{r}_i$ and $m_i$ respectively and the force acting upon the particle is $\mathbf{F}_i$. $\mathbf{F}_i$ can also be represented by the negative gradient of the potential:[92,93]

$$\mathbf{F}_i = -\frac{\partial}{\partial \mathbf{r}_i} U(\mathbf{r}_1, \mathbf{r}_2, \ldots, \mathbf{r}_N) \tag{2.2}$$

Where the potential energy, $U(\mathbf{r}_1, \mathbf{r}_2, \ldots, \mathbf{r}_N)$, is dependent on the coordinates of $N$ particles. Force fields can be used to estimate this in MD simulations.

### 2.1.1 Force Fields

To effectively and accurately simulate PBs and their specific-ion interactions, an appropriate model representing the interatomic forces and interactions within PB systems is required.[92,93] Ideally, the forces on each and every atom within the system of interest would be calculated by solving the electronic structure for a particular configuration of each nuclei.[94] Although there has been significant progress in techniques using these first principles, such as *ab initio* MD simulations and density functional theory (DFT), the size and complexity involved in PB systems, as well as the desired timescales for simulations within this thesis, mean that such methods would be excessively computationally expensive. As a result, to achieve the simulation of PBs containing several hundreds of thousands of atoms on nanosecond timescales, it is necessary to use a higher level of approximation.[94]

Empirical force field-based methods were, therefore, employed throughout this work. Empirical methods use both experimental results from related systems and quantum chemical data to

approximate elements of the underlying theory.[94] An empirical force field is a mathematical expression of the interatomic potential energy and a set of parameters entering this form. Many force fields exist, each specialised to describe different kinds of system and each with varying degrees of complexity.[95,96]

*AMBER force fields*

The Assisted Model Building with Energy Refinement (AMBER)[97] package provides a set of force fields. The functional form of the AMBER force fields comprises of the following terms:[98]

$$U_{tot} = U_{bond} + U_{angle} + U_{torsional} + U_{vdw} + U_{elec} \quad (2.3)$$

The bond potential, $U_{bond}$, represents the energy between all atom pairs that are covalently bonded (indexed as *i* and *j* in equation 2.4), and the stretching movement involved in this. It is represented with a simple harmonic function and is defined as:[98]

$$U_{bond} = \sum_{bonds} K_r \left(r_{ij} - r_{ij}^0\right)^2 \quad (2.4)$$

Where $K_r$ is the force constant of the bond between atoms *i* and *j*, the instantaneous length of the bond is $r_{ij}$ and $r_{ij}^0$ is the equilibrium bond length.

The harmonic angle potential describes the angle between three atoms; *i*, *j* and *k*:[98]

$$U_{\text{angle}} = \sum_{\text{angles}} K_{\theta} \left(\theta_{ijk} - \theta^{0}_{ijk}\right)^2 \quad (2.5)$$

Where $K_\theta$ is the force constant of the angle between atoms *i*, *j* and *k*, the angle between the three atoms is $\theta_{ijk}$ and $\theta_{ijk}^{0}$ is the equilibrium angle.

The torsional potential represents the energy for twisting a bond due to bond order and neighbouring bonds or lone pairs of electrons. It is defined by:[98]

$$U_{\text{torsional}} = \sum_{\text{torsions}} \frac{V_n}{2} \left[1 + \cos\left(n\emptyset_{ijkl} - \gamma\right)\right] \quad (2.6)$$

Where $V_n$ is the energy barrier involved, $\emptyset_{ijkl}$ and γ are the torsion angles for the atoms *i*, *j, k* and *l* and *n* accounts for the preferred symmetry of the molecule.

The next term within the AMBER potential,[98] $U_{\text{vdw}}$, is representative of the balance between repulsive and attractive forces between atoms, *i* and *j*, which give rise to van der Waals forces. The Lennard-Jones potential represents the van der Waals interactions between atoms and is defined by equation 2.7:[98]

$$U_{\text{vdw}} = U_{\text{LJ}} = \sum_{j>i} \left(\frac{A_{ij}}{R_{ij}^{12}} - \frac{B_{ij}}{R_{ij}^{6}}\right) \quad (2.7)$$

Where the separation distance of the two particles is defined as $R_{ij}$ and the coefficients, A and B, are parameters specific to the atoms of *i* and j. The first part of of the Lennard-Jones potential

(equation 2.7) defines repulsive forces where electron clouds of non-bonded particles overlap at short distances causing a steep repulsion. The second part represents attractive forces acting between particles.

Polyelectrolyte (PE) and polyzwitterionic (PZ) brushes contain charged molecules, therefore, it is important to take electrostatics into account. The Coulombic component of equation 2.8 describes the electrostatic interaction energy between two particles' charges ($q_i$ and $q_j$).

$$U_{\text{elec}} = U_{\text{Coulomb}}\left(r_{ij}\right) = \sum_{j>i} \frac{q_i q_j}{4\pi\varepsilon r_{ij}} \tag{2.8}$$

A system specific dielectric constant is represented by $\varepsilon$ and the distance between the charged particles $i$ and $j$ is $r_{ij}$.

*Choice of Force Fields*

The standard parameters found in the ff14SB atomistic force field[99] and the General Amber force field (GAFF),[100] within the AMBER simulation package[90] were selected to model the PBs of interest throughout this work. The ff14SB force field[99] is one of AMBER's primary protein model, whereas GAFF[100] is a more complete and general force field.

Within AMBER force fields, parameters are expressed in terms of atom types. Varying values for bond strengths and equilibrium bond lengths (required for equation 2.4) arise for atoms of the same element upon forming bonds in different chemical environments. For example, the

carbon-carbon bonds present in the two molecules, ethane and benzene, will have different lengths and strengths despite both connecting two carbon atoms. This is due to different types of hybridisation. The carbon atoms are $sp^3$ hybridised in ethane but are $sp^2$ hybridised in the benzene ring. Within the work presented throughout this thesis, both ff14SB and GAFF parameter sets were required to model the PB systems. ff14SB[99] was not able to represent all atom types within the PBs of interest. These force fields are compatible and are often used in combination. They have been previously used in the simulation of polymer[101] and protein systems.[102,103]

### 2.1.2 Numerical Integration Methods

The main step of MD is the integration Newton's equations of motion (Equation 2.1). An integration algorithm is used to numerically solve the equations over small time steps. There are many different integrators including Verlet[104] and velocity Verlet,[105] each algorithm having advantages and disadvantages to consider.

#### *Verlet Algorithm*

In order to find the position of a particle at the next timestep, $\mathbf{r}(t + \delta t)$, the Verlet algorithm[104] utilises the positions of the particles from the preceding step, $\mathbf{r}(t - \delta t)$. An expression is approximated for both $\mathbf{r}(t - \delta t)$ and $\mathbf{r}(t + \delta t)$ using a Taylor expansion about $\mathbf{r}(t)$:

$$\mathbf{r}(t + \delta t) = \mathbf{r}(t) + \delta t\, \mathbf{v}(t) + \left(\frac{1}{2}\right) \delta t^2 \mathbf{a}(t) + \ldots \tag{2.9}$$

$$\mathbf{r}(t - \delta t) = \mathbf{r}(t) - \delta t\, \mathbf{v}(t) + \left(\frac{1}{2}\right) \delta t^2\, \mathbf{a}(t) - \ldots \tag{2.10}$$

The new positions at time ($t + \delta t$) can be calculated by the addition of the Equations 9 and 10 to generate the Verlet algorithm (ignoring the local error, $O(\delta t^4)$):

$$\mathbf{r}(t + \delta t) = 2\mathbf{r}(t) - \mathbf{r}(t - \delta t) + \delta t^2 \mathbf{a}(t) \tag{2.11}$$

During the addition of Equations 2.9 and 2.10, however, the velocities are cancelled out. This is an inconvenience because, in order to calculate the kinetic energies and, therefore, the total energy of the system is to be computed, velocities of each particle are required. An extra step must be carried out to calculate the velocity of each particle:

$$\mathbf{v}(t) = \frac{\mathbf{r}(t + \delta t) - \mathbf{r}(t - \delta t)}{2\delta t} \tag{2.12}$$

One of the advantages of the Verlet method its simplicity. The algorithm's handling of velocities, however, is somewhat awkward as velocities can only be calculated if the updated positions have already been collected. Furthermore, values calculated for velocities are subject to errors of the order $\delta t^2$.

*Velocity Verlet Algorithm*

The Velocity Verlet algorithm[105] improves upon the Verlet algorithm. The velocities, positions, and accelerations of the particles at time, $t$, are all stored simultaneously, and the round-off error is minimised. The first step involves the calculation of the new positions followed by the

computation of velocities at the mid-step and finally the evaluation of the new accelerations and forces. The algorithm can be represented by:

$$\mathbf{r}(t + \delta t) = \mathbf{r}(t) + \delta t\ \mathbf{v}(t) + \frac{1}{2}\delta t^2\ \mathbf{a}(t) \tag{2.13}$$

$$\mathbf{v}(t + \delta t) = \mathbf{v}(t) + \frac{1}{2}\delta t\ [\ \mathbf{a}(t) + \mathbf{a}(t + \delta t)] \tag{2.14}$$

The minimisation of errors, the convenience and the simplicity of this method means that the Velocity Verlet method is one of the most attractive integration methods to use. Although variations of the velocity Verlet algorithm, such as the Beeman's algorithm,[106] have been developed they are usually more computationally expensive. Consequently, these newer algorithms are inappropriate to use on the large and complex PB systems studied in this work.

### 2.1.3 Ensembles

An ensemble is defined as a collection of particles which have different microstates (for example, atomic positions) but the same thermodynamic state. A Canonical (*NVT*) Ensemble is used throughout this work and is more indicative of experimental conditions than other commonly ensembles in statistical mechanics (like the microcanonical ensemble, *NVE*). The number of particles in a system (*N*), volume (*V*) and temperature of the system (*T*) remains unchanged throughout the simulations. The canonical ensemble, therefore, requires the temperature to be controlled. Temperature is defined as the average kinetic energy (*K*) of all the particles in a system:

$$T = \frac{2}{3}\frac{\langle K \rangle}{Nk_b} \quad (2.15)$$

$k_b$ is the Boltzmann constant, and the angular brackets represent the average value taken over the ensemble. During the simulations, velocities of the particles fluctuate therefore it is impossible to keep the kinetic energy and hence the temperature of the system constant. Energy is added or removed from the system using a thermostat to maintain a constant temperature. The Nosé-Hoover thermostat[107] was used in this thesis. In this thermostat, fictitious variables for the heat bath are included in the equations of motion, thus considering the heat bath as an integral part of the system. A value of mass is associated with the additional variable and its magnitude controls the strength of the coupling.

### 2.1.4 Periodic Boundary Conditions

The use of periodic boundary conditions in MD simulations provides a computationally efficient means for calculating the bulk properties of a system.[92,93] An infinite lattice is formed by replicating the original simulation box through all directions in space. These conditions eliminate surface and edge effects; when a particle leaves the original box, an identical one will enter through the opposite face of the box. This is due to the position of the particle being updated in all the boxes. Each individual particle interacts with their nearest image of all the remaining particles within the system because of the minimum image convention.[92,93]

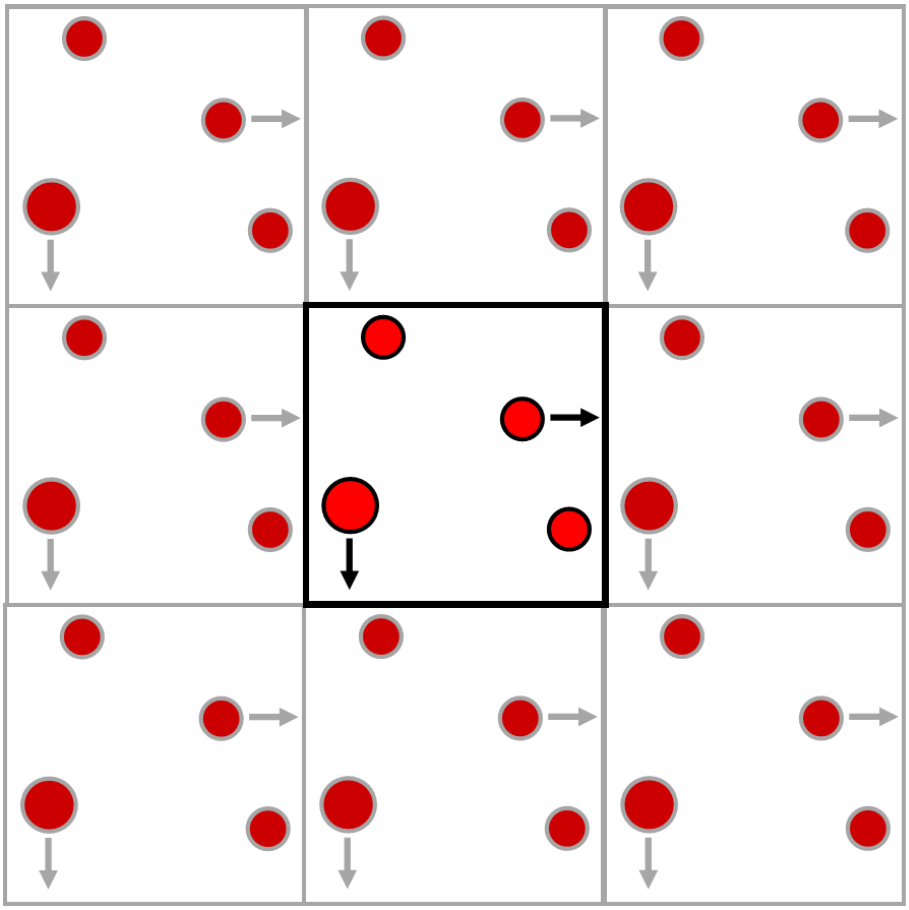

**Figure 2.1** Schematic representation of periodic boundary conditions in a two-dimensional (2D) system.

### 2.1.5 Long-range Interactions

The computation of forces that result from electrostatic interactions use up most of the central processing unit (CPU) time during MD simulations. To reduce computational time, methods that use approximations are employed, such as the Ewald method[108] or, in this work, the particle-particle particle mesh (pppm) method.[109]

*Ewald Summation*

Ewald Summation is a commonly used method in MD simulations to compute long-range interactions in periodic systems. In a periodic system, the total electrostatic energy with *N* point charges is defined as:

$$U_{\text{Elec}} = \frac{1}{2}\sum_{|n|=0} \sum_{i,j=1}^{N} \frac{q_i q_j}{|r_{ij} + nL|} \tag{2.16}$$

Where *L* is length of simulation box and *n* is the cell image vector.

*Particle-Particle Particle-Mesh Method*

The pppm algorithm[109] is an alternative method used for modelling long-range electrostatic interactions in MD simulations. This technique can be described in three steps:

1. Charges are assigned to a finely spaced mesh within the simulation box to approximate the charge density of the fluid.
2. Poisson's equation for the electrostatic potential is solved using the fast Fourier transform technique.
3. The potential at each mesh point is numerically differentiated to calculate the field, from which, the force on the particle can be calculated by interpolation.

The pppm method was chosen over the Ewald Method (and other methods) due to its more efficient handling of long-range interactions commonly present in large molecular systems, such as the PB systems in this project. The time taken to complete the pppm method is proportional to the number of particles within the system as opposed to the square of number of particles as in the Ewald Method.[108]

### 2.1.6 Solvent Models

Water plays a crucial role in the structural changes observed in PBs upon the addition of electrolyte solution. As discussed in Chapter 1, different salt solutions can trigger dehydration or hydration processes within PBs leading to a conformational transition. Therefore, the effect of water must be properly considered to accurately simulate the behaviour of PBs in aqueous salt solutions.

Explicit solvent models treat water as individual molecules thus accounting for interactions between each water molecule and the solute within the system of interest, along with other simulated water molecules. While increasing the accuracy of the simulation, there is a high computational cost accompanying the implementation of this model. Furthermore, the model of water can further affect the computational expense.

*$TIP_nP$ water models*

Three versions of TIP (transferrable intermolecular potential) models are regularly used to explicitly represent water. TIP3P[110] is a three-site model in which the oxygen and two hydrogens of water are modelled. Due to the simplified (or perhaps oversimplified) nature of this model, simulated properties, such as temperature of maximum density (TMD),[111] have been reported to be far from known experimental values.[111] The TIP4P[110] water model is more accurate. This model contains a pseudoatom which represents the lone pair on the oxygen atom, fixed at 0.15 Å from the O atom, along the H-O-H bond angle bisector, and is the site of the oxygen's charge.[110,112]

Finally, the TIP5P[113] model positions the negative charge on two virtual, massless atoms (**L**) thus resulting in a more tetrahedral water structure. Compared to TIP3P[110] and TIP4P[110], the TIP5P[113] model better reproduces the TMD of water, along with other experimental properties. A disadvantage, however, is that the use of this water model is more computationally expensive and, consequently, slows down simulations.

*Simple Point Charge Models*

The simple point charge water model (SPC)[114] is a rigid 3-site model. Each site has a point charge and Lennard-Jones parameters. The H-O-H angle is 109.47° and is based on the ideal tetrahedral shape. The rigid SPC/E[115] (extended) model was used to explicitly represent water molecules throughout the investigations of PBs using atomistic MD simulations. The SPC/E water model[115] is the same as the SPC water model, except for the magnitude of the partial charges. An average polarisation correction is added to the potential energy function. The values for the density and diffusion constant of water is more accurate when calculated via the SPC/E model rather than the SPC.[110] Furthermore, upon comparison with the 3-site TIP3P model, SPC/E has been found to more accurately reproduce bulk water dynamics and structure measurements.[116]

**Table 2.1** Parameters for SPC[114] and SPC/E[115] water models.

| **Parameters and Units** | | **SPC** | **SPC/E** |
|---|---|---|---|
| $q^{O}$ | e units | -0.820 | -0.8476 |
| $q^{H}$ | e units | 0.410 | 0.4238 |
| $r_0^{OH}$ | Å | 1.0 | 1.0 |
| $\theta^{HOH}$ | ° | 109.47 | 109.47 |

## 2.2 Methods for Data Analysis

### 2.2.1 Configuration of Polymer Chains

To describe the conformation of the polymer chains in a PB computationally, it is necessary to know the location in space of each atom. MD simulations provide the opportunity to gather the cartesian coordinates of each atom within the PB of interest. The simplest measure of the configuration of a polymer chain is the end-to-end brush height (< $z_e$ >). This is defined in this thesis as the distance of between the sulfur atom acting as the initiator (SI) on the PB surface and the carbon of the methyl end group ($C_{Me}$).

$$\langle z_e \rangle = r_{C_{Me}} - r_{SI} \tag{2.17}$$

The mean of the brush height values over the simulated polymer chains and trajectory is reported throughout the thesis and is represented by $\langle\ \rangle$.

Another measurement used to characterise the configuration of the polymer chains is the radius of gyration, $R_g$. This is defined for a polymer chain containing $N$ atoms as:

$$R_g^2 = \frac{1}{M} \sum_i^N m_i (r_i - r_{cm})^2 \tag{2.18}$$

The total mass of the polymer chain is defined as $M$, $r_{cm}$ is the centre of mass of the polymer, and $m_i$ and $r_i$ are the mass and position of the $i$ th atom, respectively.

Although the radius of gyration tends to be a more precise measurement as it uses more than just the end groups of the polymer chains, the end-to-end brush height is more frequently reported throughout the thesis. End-to-end brush height values are an effective way of measuring conformational transitions and can be compared to experimental brush thickness measurements.

### 2.2.2 Grafting Density

An important feature to consider, when modelling any PB system, is the overlap grafting density, as the nature of PBs can be dramatically altered by changing the grafting density.[3] If the grafting density is below a critical value (to be explained later), a "pancake-like" conformation is observed if the polymer chains have an affinity to get adsorbed onto the interface and a "mushroom-like" conformation is seen if the chains are not likely to be adsorbed (Figure 2.2).[3] A brush type configuration is not achieved because the neighbouring grafted chains have very little effect on each other.

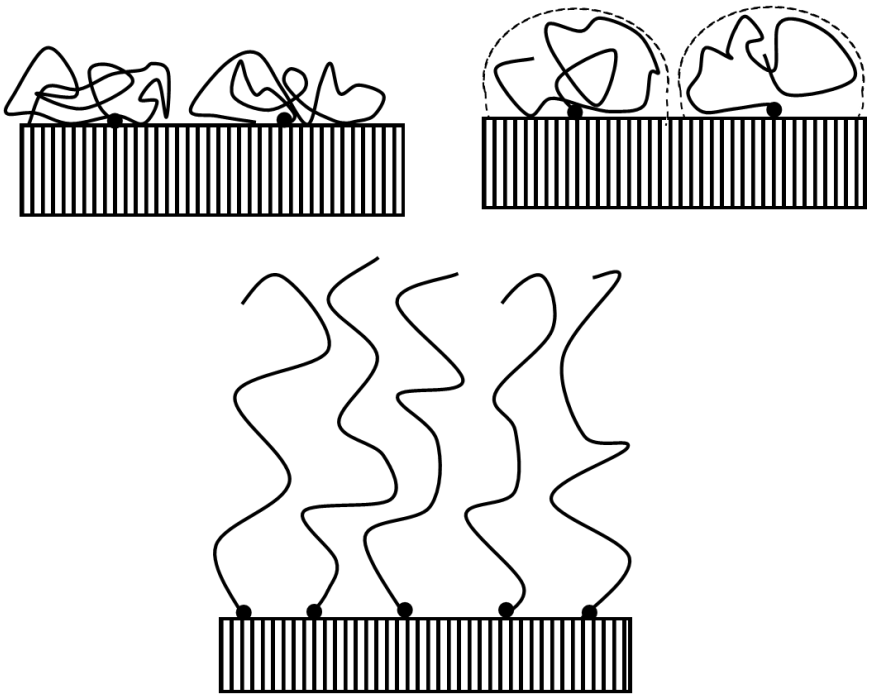

**Figure 2.2** Schematic representation of the "pancake" conformation (top row, left), the "mushroom" conformation (top row, right) and the brush configuration (bottom) that grafted polymers can adopt.

If the overlap grafting density is above a critical value, a brush configuration is adopted.[3] This occurs when the spacing between the anchor points of the grafted polymer chains is smaller than the chain's radius of gyration. Overlap grafting density, $\sigma^*$, is often used to prove a system is in the brush regime and is defined as:[117–119]

$$\sigma^* = \pi R_g^2 \Sigma \tag{2.19}$$

The experimental grafting density (chains per area) is expressed as $\Sigma$. $R_g$ is the radius of gyration calculated from MD simulations of free polymer solutions.

When $\sigma^* > 1$, the neighbouring chains are restricted to less area than they would occupy in solution and are forced to interact with each other, thus proving the system is in the brush configuration. The mushroom or pancake regime is adopted when $\sigma^* < 1$ as the chains do not have significant lateral interactions.[117–119]

The upper limit of experimental grafting density possible to attain with "grafting from" synthesis techniques, such as Atom Transfer Radical Polymerisation (ATRP), is ~ 0.700 chains $nm^{-2}$, [120] and was considered during the construction of the PBs atomistic models. The separation distance between two grafted polymer chains is defined as:[3]

$$r = \Sigma^{\frac{-1}{2}} \tag{2.20}$$

Table 2.2 shows the values of the studied PB systems. The value of experimental grafting density, 0.1 chains $nm^{-2}$, was taken from the literature.[5] MD simulations on the free PMETAC and PSBMA polymer solutions were performed to extract the $R_g$ value. A brush configuration was, therefore, observed due to the overlap grafting density value being greater than one.

**Table 2.2** Details of the polymer brush (PB) systems studied.

| Name of PB | Degree of Polymerisation | Experimental Grafting Density, $\Sigma$ (chains nm$^{-2}$) | Radius of Gyration (free polymer solution), $R_g$ (nm) | Overlap grafting density, $\sigma^*$ | Separation Distance, $r$ (nm) |
|---|---|---|---|---|---|
| **PMETAC** | 100 | 0.100 | 7.64 | 18.4 | 3.162 |
| **PSBMA** | 100 | 0.100 | 4.18 | 5.5 | 3.162 |

### 2.2.3 Radial Distribution Function

The radial distribution function (RDF) can be used to analyse the spatial arrangement of the PB systems. The probability of finding of a particle at a particular distance away from a reference particle is measured and averaged over all particles in the systems along the simulated trajectory. The probability function, $g(r)$, is represented by:

$$g(r) = \frac{N_S}{V_S \rho} \tag{2.21}$$

$$V_S = \frac{4}{3}\pi ( r + dr)^3 - \frac{4}{3}\pi r^3 \tag{2.22}$$

The probability function, $g(r)$, is the probability of finding a particle in a shell with thickness, $dr$, at a distance, $r$. The number of particles in the shell is $N_S$, $V_S$ is the volume of the shell, and the density of the system is $\rho$.

### 2.2.4 Change in Water Molecules in Polymer Brushes

The change in water molecules present in each PB was investigated. To achieve this, the space occupied by the polymer chains at each frame of the trajectory was defined and the number of water molecules within that space was calculated. The number of water molecules within the brush was subsequently averaged over the trajectory. A comparison was made between the average number of water molecules in the PB in a) a salt solution and b) water. The percentage change was then reported.

## 2.3 Global Optimisation

The final chapter of this thesis investigates the hydration and conformational effects of adding molecules of water to alkyl diammonium di-cations and alkyl dicarboxylate di-anions. Global Optimisation is the process of finding local minima and eventually the global minimum of a system.[121]

### 2.3.1 The Basin-Hopping Technique

The basin-hopping (BH) global optimisation technique is a well-known and well-established system used to explore the potential energy and optimise the structure of finite cluster systems. In this technique (illustrated in Figure 2.3), a random, initial configuration is generated and minimised, giving the first entry into a Markov chain.

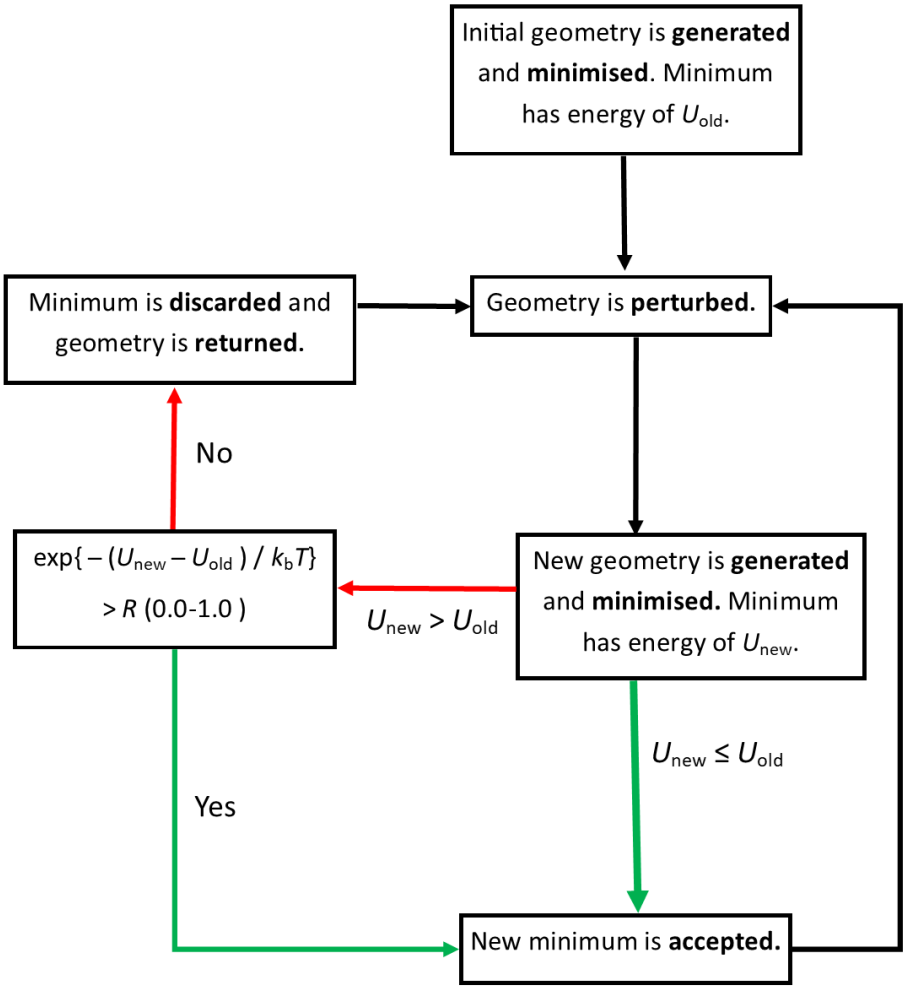


**Figure 2.3** A flow chart representing the operations occurring during the basin-hopping Monte Carlo technique, where the starting conformation is $U_{old}$ and the locally minimised structure is defined as $U_{new}$, $k_b$ is the Boltzmann constant, $T$ is an arbitrary temperature and $R$ is a random number between 0 and 1.

Following minimisation, the next step involves the random displacement of the translational and rotational coordinates of the latest entry to the Markov chain to generate a new configuration, which is then further minimised. The BH technique relies on a transformation of the potential energy surface (PES) to form a catchment basin, associated with each local minimum. The energy

of each local minimum becomes the potential energy for every point in the basin (Figure 2.4). Catchment basins divide all of configurational space, which means that the potential energy can only vary in discrete steps as the geometry moves from one basin to another during global optimisation.[122]

A comparison of the energies between the starting conformation ($U_{old}$) and the locally minimised structure ($U_{new}$) then takes place. This minimised conformation is then put through the Metropolis criterion:

If $\Delta U < 0$, or $R > e^{\frac{-(U_{new} - U_{old})}{k_b T}}$, the new conformation is accepted.

If $\Delta U > 0$, and $R < e^{\frac{-(U_{new} - U_{old})}{k_b T}}$, the new conformation is rejected.

If the new conformation is accepted, based on the Metropolis criterion, then this is placed into the Markov chain and acts as the new starting point in the next cycle of random structural perturbations. If it is rejected, the previous starting conformation is perturbed again, and the cycle begins again.

In a BH run, this cycle is repeated for a chosen number of steps and several low energy minima visited during the run are saved. To escape the basin of attraction of the starting structure and effectively explore the PES, the Monte Carlo moves need to be appropriately large.

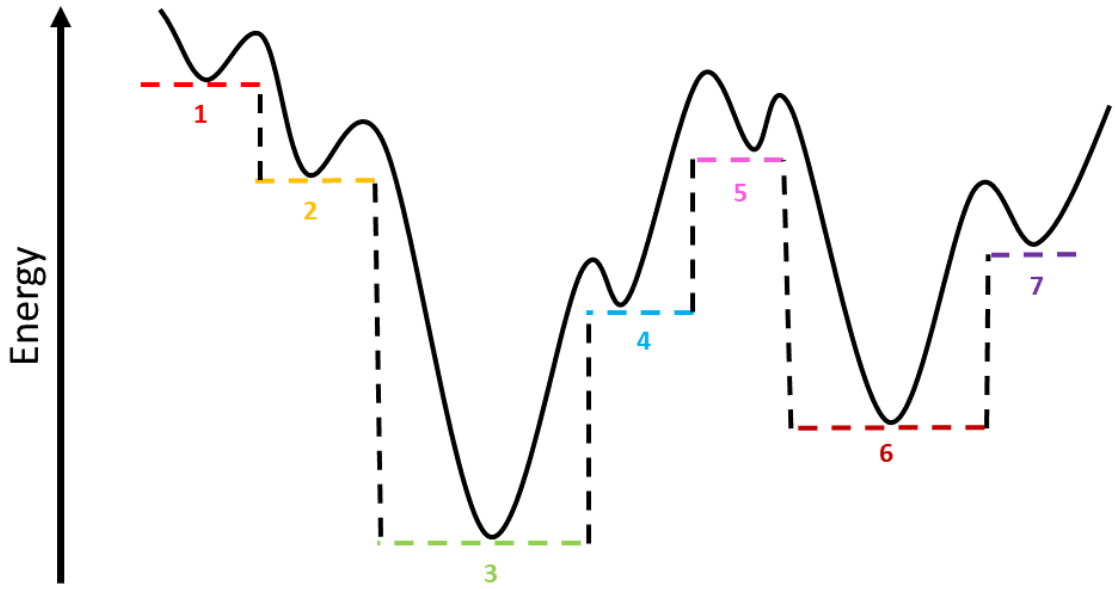


**Figure 2.4** A schematic representation, illustrating how the basin-hopping (BH) global optimisation (GO) technique transforms the potential energy surface (PES) to a set of basins. Basins are represented by coloured dashed lines and are numbered 1-7. Basin 3 is representative of the global minimum (GM) of this PES. The other basins (1, 2, 4-7) are local minima.

# CHAPTER 3: ION PAIRING AND HIGHER-ORDER ION CLUSTERING IN A TWO CHAIN ATOMISTIC POLYELECTROLYTE BRUSH MODEL.

## 3.1 Introduction

Polyelectrolyte (PE) brushes contain PE chains densely grafted to a surface.[3] These types of brushes have many promising applications, for example in bio-sensing,[123–126] drug delivery,[2,125,126] and biomechanical devices.[11,15,59,126] To optimise PE brushes for use in these practical applications requires a thorough understanding of their nanoscale structure and responsiveness to external stimulii.[6] It is well-known, for example, that the hydration levels and structural properties of PE brushes can be modulated by the addition of different types of electrolyte solutions,[8–10] depending on the categorisation of electrolyte ions within the Hofmeister series.[11] The tuneable properties of PE brushes by Hofmeister effects, otherwise known as specific-ion effects can, therefore, influence the suitability of PE brushes in potential industrial applications.

Specific-ion effects observed in PE brushes have been explained using Collins' "Law of Matching Water Affinities" (LMWA) (Figure 1.4).[40,45] This theory proposes that specific-ion interactions are dominated by a distinct chemical species,[46] ion pairs. According to LMWA, an ion pair can only form between oppositely charged ions with similar water affinities.[40,45] The formation of ion pairs is believed to heavily influence the hydration and conformation of PE brushes.[8,39]

The positively charged poly (2-(methacryloyloxy) ethyl trimethylammonium chloride) (PMETAC) brush (monomer shown in Figure 3.1) has been widely used as a model to study the effects of salt concentration and type of ion on the behaviour and properties of strong PE brushes.[4–6,8,39,55,127] Experimentally[5,8,39] and theoretically,[5] chaotropic anions have been found to induce a

strong dehydration and collapse within PMETAC brushes. Ion pairs are believed to form between chaotropic salt anions and the chaotropic, positively charged, quaternary ammonium (QA) groups situated along the grafted PMETAC chains. Ion pairing is reported to alter the osmotic pressure within the brush as well as the hydrophobicity of the chains which therefore leads to a collapse in PMETAC chains.[4,6,8,39,127]

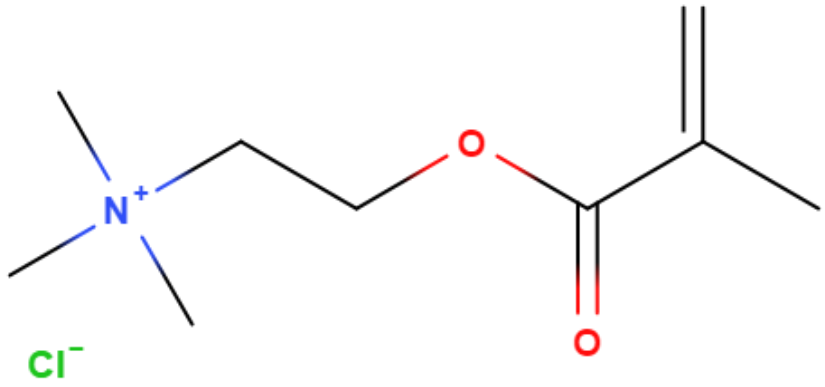


**Figure 3.1** Chemical structure of the 2-(methacryloyloxy) ethyl trimethylammonium chloride (METAC) monomer.

There is no standard procedure for identifying ion pairs within PE brushes or examining their conformations and lifetimes. This chapter aims to address this and further link ion pairing to the responsiveness displayed by PE brushes in salt solutions. Interactions between salt ions and the PMETAC brush can be defined as ion pairs if two oppositely charged ions stay together at a distance, *R*, for a time longer than that needed to diffuse over such a distance.[46] Any ions with a separation larger than *R* are considered as free.[46] There are numerous different theories suggesting how to specify the value of *R* and it is dependent on the type of ion pair under

investigation.[46] *R* is defined, in this chapter, as the radius of the first coordination shell of QA groups within the PMETAC brush, in order to focus on contact ion pairs (CIP) (Figure 1.5a).

Equation 3.1 is adapted from the mean squared displacement equation. This chapter's definition of *R* is included:

$$t = \frac{R^2}{2D} \tag{3.1}$$

The time is dependent on the diffusion coefficient of the mobile anion, and determines the time required for the anion to translate over distance, *R*. However, it is important to not only consider the diffusion coefficient in a bulk solution, as this will not take into account effects of confinement of ions within PE brushes. The brush-induced confinement along with the large brush-ion electrostatic attraction/repulsion has been previously found to substantially reduce the mobility of ions within PE brushes and hence affect the rate of diffusion, even for those ions that are not involved in ion pairing.[128]

In this chapter, atomistic MD simulations are used to study the influence of highly concentrated salt solutions, specifically 0.5 M $NaClO_4$ and 0.5 M NaSCN solutions, interacting with a PMETAC brush. Sodium was used as a common counterion within the salt solutions to concentrate on the differences between the effects of $ClO_4^-$ and $SCN^-$ anions. According to the Hofmeister Series (Figure 1.2) both $ClO_4^-$ and $SCN^-$ anions are known to be chaotropic anions, with stronger chaotropic effects observed for $ClO_4^-$ anions. It is expected that $ClO_4^-$ and $SCN^-$ anions will form ion pairs with QA groups within the PMETAC brush. The variation of brush height and hydration properties with the different salt solutions are examined. Subsequently, ion pairs within the

PMETAC brush are studied whereby a focus is on quantifying the lifetimes and conformations of newly formed ion pairs. Understanding the structure and arrangement of ions within PE brushes gives valuable insights into brush properties and is important for both current and future applications. The results in this chapter provide an atomistic-level elucidation of the PMETAC brush properties along with previously unknown quantitative findings about interactions between the functional groups within the PE brush and strongly chaotropic salt anions.

## 3.2 Methodology

### 3.2.1 System Description

Atomic coordinates for the initial configurations of the two modelled PMETAC chains each consisting of 100 monomers were built using the TopoTools plugin for Visual Molecular Dynamics programme (VMD)[129] and in-house codes. Each chain was tethered with the distance between the grafting points as 3.162 nm. PMETAC chains were initially built as fully stretched rod-like chains perpendicular to the surface (defined using LAMMPS[88] intrinsic functions) consisting of four layers of sulfur atoms that remained fixed throughout the simulation. The initial configuration of the PMETAC brush consisted of an array of chloride counterions.

A combination of two AMBER[90] force fields, ff14SB[99] and the General Amber force field (GAFF),[100] were used to model the PE chains, thiol initiators and surface. The three-site SPC/E model was used to explicitly represent water molecules.[115,116] The chloride counterions of PMETAC were modelled using Joung and Cheatham's set of parameters specific for use with the SPC/E water model.[130] The atomic charges for the polymer chains and thiol initiators were calculated with the Hartree−Fock self-consistent field theory and the 6-31G* basis as described in restrained electrostatic potential (RESP) methodology.[131]

The PMETAC chains were orientated in the simulation box in such a way that the PE chains were parallel to the *y*-axis and normal to the *xz*-plane. Periodic boundary conditions (PBCs) were set in the *x*, *y* and *z* directions. Interactions between the top of the PMETAC chains and the periodic image of the surface in the *y*-direction were prevented because the simulation box was larger than the fully stretched chains of the PMETAC combined with the non-bonded interaction cut-off distance.

### 3.2.2 Simulation Details

Atomistic MD simulations were performed using LAMMPS.[88] The Velocity Verlet algorithm[105] was used, with a time step of 2 fs to integrate Newton's equations of motion. Initial velocities were taken from a Maxwell distribution at 298 K and 1 atm. Energy minimisation, using the conjugate gradient method, was performed for all the systems until a mean force of less than $1.0 \times 10^{-6}$ kcal $mol^{-1}$ $Å^{-1}$ was achieved. Equilibrium runs were then performed on the PMETAC brush systems in a canonical ensemble (NVT) at 500 K for 35 ns. The system was then cooled to 298 K and simulated for a further 30 ns.

Following this, production runs were executed in the same conditions as the equilibrium run for 4 ns using the last snapshot of the equilibration process as the initial configuration. In both the equilibration and production steps the Noose-Hoover thermostat[107] was employed. The SHAKE algorithm[132] was used to constrain the bond lengths and bond-bending angles of water molecules. The cut-off for the interatomic potential is set at 11.0 Å with long-range electrostatic interactions between charged species handled using the particle−particle particle-mesh (pppm) method[109] with a root-mean accuracy of $10^{-6}$.

Analysis of the trajectories were performed by a combination of LAMMPS[88], MDAnalysis and in-house codes. Analysis has been achieved considering the last 4 ns of each of the simulations.

## 3.3 Results

### 3.3.1 Conformation and Hydration of PMETAC Brush

Atomistic MD simulations were performed for PMETAC brush systems in water, 0.5 M $NaClO_4$ and 0.5 M NaSCN solutions. The starting configuration of the PMETAC chains were fully stretched with anisotropic values of 1 for all chains. A rapid collapse, as can be observed in Figure 3.2, was almost instantaneous and the rate of collapse for the PMETAC chains was similar across the simulated systems under investigation.

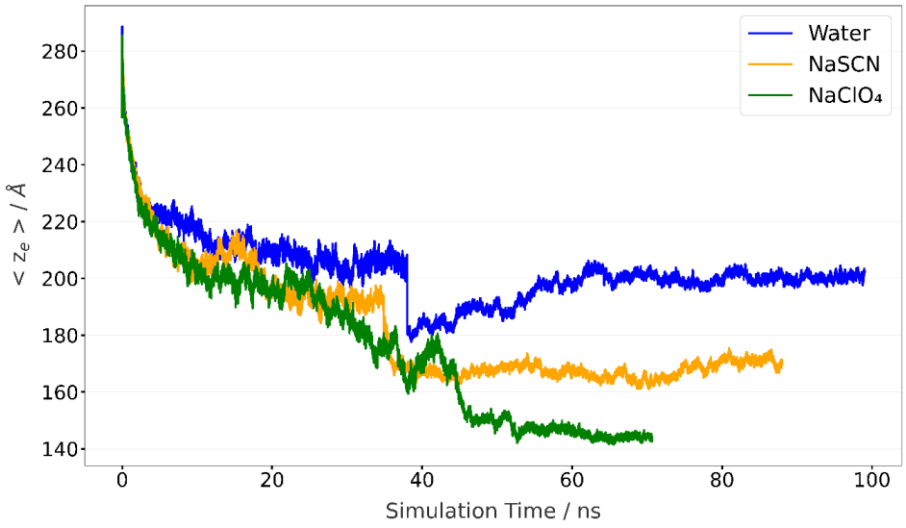


**Figure 3.2** Plot of the time evolution of the maximum height of brush averaged over the two PMETAC chains in the presence of water (blue), 0.5 M NaSCN (orange) and 0.5 M $NaClO_4$ solution (green). The cooling of the system from 500 K to 298 K occurred between 38-40 ns.

The final configurations for the PMETAC brush systems in water, 0.5 M $NaClO_4$ and 0.5 M NaSCN solutions are shown Figure 3.3. It can be seen that the salt ions are distributed throughout the simulation box.

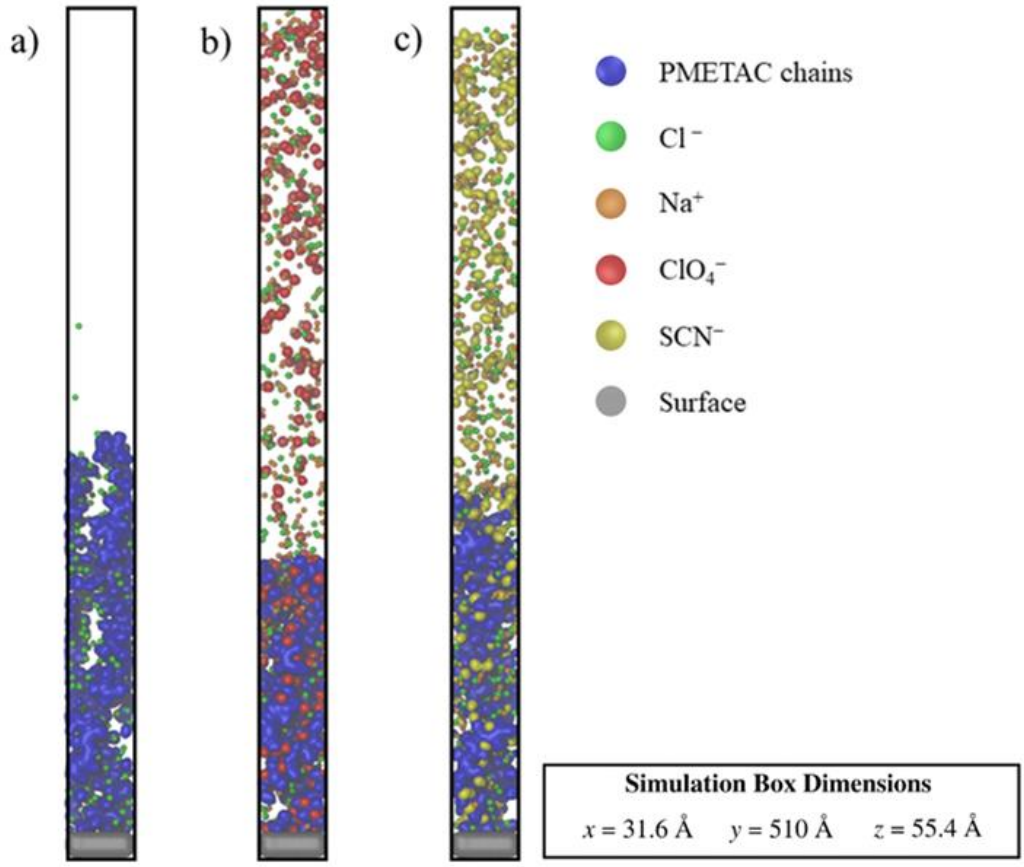


**Figure 3.3** Final configurations illustrating the modelled PMETAC chains in the presence of a) water, b) 0.5 M $NaClO_4$ and c) 0.5 M NaSCN. PMETAC chains are shown in blue. $Cl^-$ are green. $Na^+$ are orange, $ClO_4^-$ are red, and $SCN^-$ are yellow. Water molecules are not displayed for clarity.

In the presence of the salt solutions under investigation, a visible difference in the conformation of the PMETAC chains (Figure 3.3) was displayed. This was further illustrated by a significant decrease in the average end-to-end brush height (< $z_e$ >) of the PMETAC chains (Figure 3.4). The decrease in brush height was more prominently observed in the presence of $ClO_4^-$ than $SCN^-$ anions.

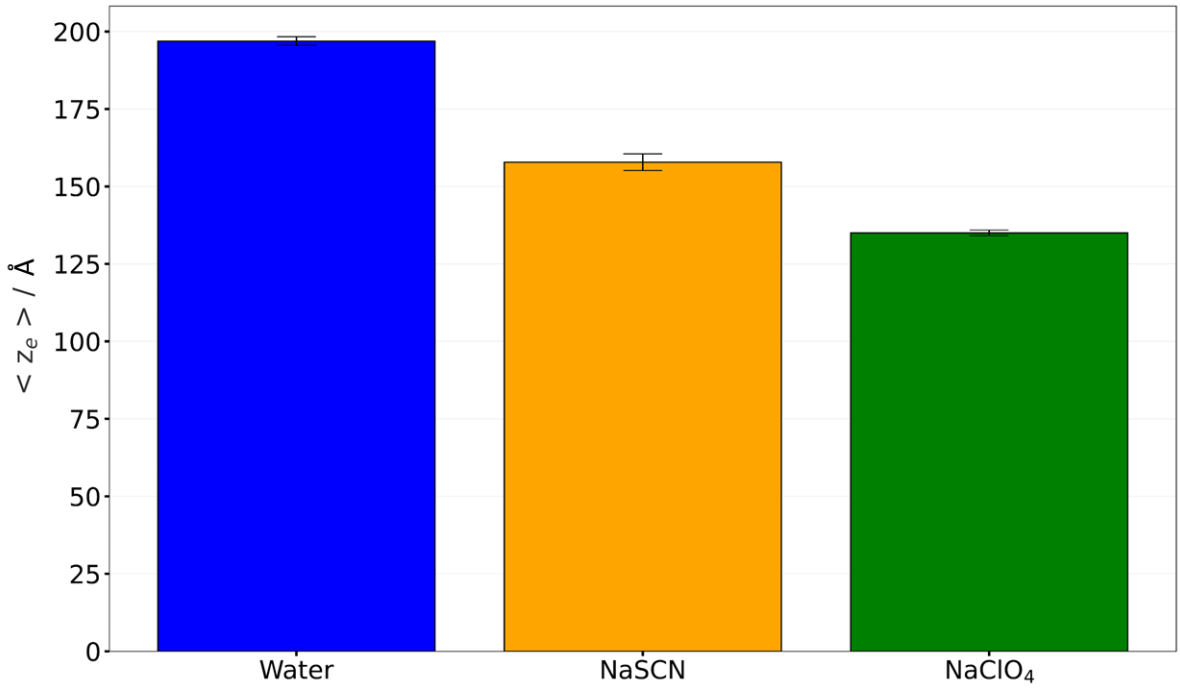


**Figure 3.4** Plot of the variation in the average end-to-end brush height (< $z_e$ >) of the PMETAC chains in the presence of water (blue), 0.5 M NaSCN (orange) and 0.5 M $NaClO_4$ solution (green). Error bars are shown representing the standard deviation of the set of end-to-end brush height values per PMETAC system.

The decrease in the height of the PMETAC brush upon the addition of NaSCN and $NaClO_4$ solutions was accompanied by a dehydration of the PMETAC chains. The loss of water situated

within the PMETAC chains (Figure 3.5) was calculated and less water molecules were situated within the PMETAC brush in the presence of $ClO_4^-$ than $SCN^-$ anions.

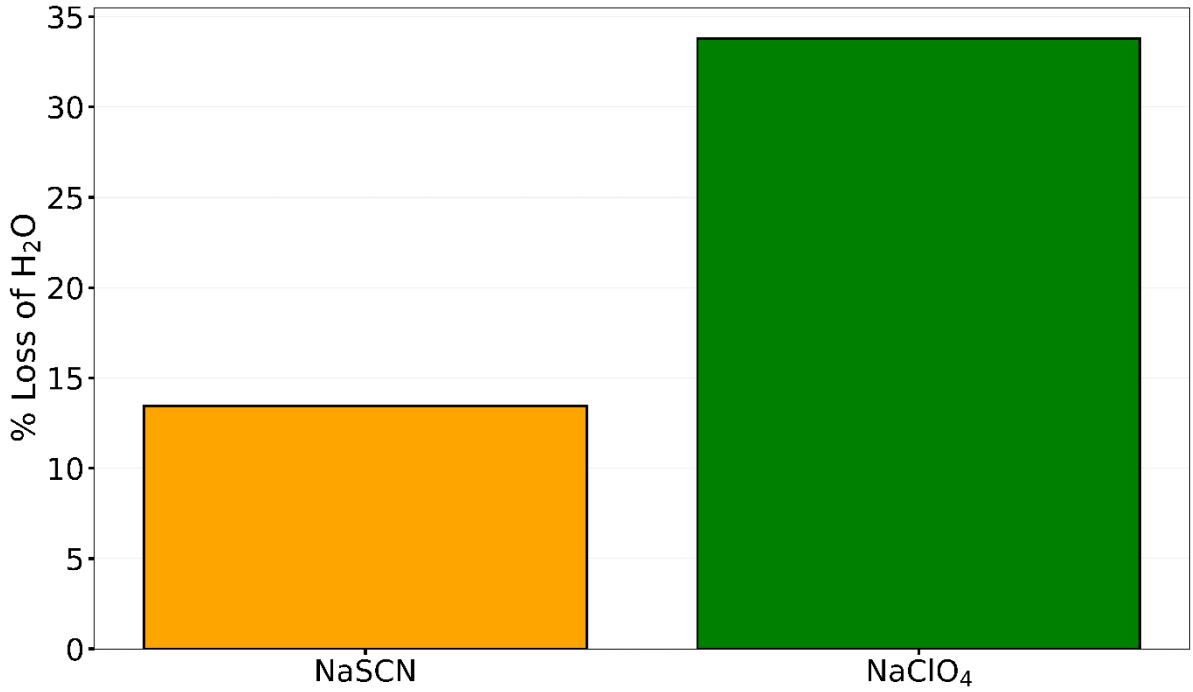


**Figure 3.5** Plot of the percentage loss of water molecules within the PMETAC brush in the presence of 0.5 M NaSCN solution and 0.5 M $NaClO_4$ solution. Values are recorded in Appendix 4: Table A.4.1.

### 3.3.2 Specific-Ion Interactions

The $N_{QA}$- $CA_{anion}$ radial distribution functions (RDFs), where $N_{QA}$ represents the nitrogen of QA groups of the PMETAC chains and $CA_{anion}$ represents the central atom of $ClO_4^-$ and $SCN^-$, are plotted in Figure 3.6. The intensity of the first peak for the $ClO_4^-$ anions is larger compared to that observed for the $SCN^-$ anions, thus implying a greater proportion of the $ClO_4^-$ anions were associating with QA groups within the PMETAC brush.

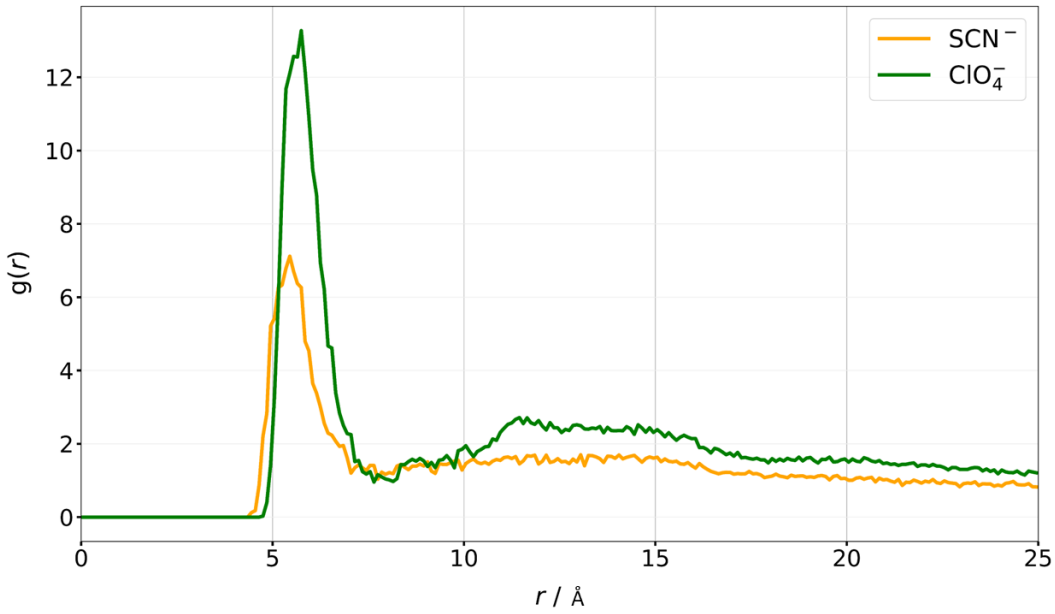


**Figure 3.6** Plot of the radial distribution functions (RDFs) of the nitrogen in the QA group ($N_{QA}$) of the PMETAC chains with the $CA_{anion}$ of the $SCN^-$ anions (orange) and the $CA_{anion}$ of the $ClO_4^-$anions (green)

From the RDF in Figure 3.6, the radius of the first coordination shell of QA groups was approximated to be 8.15 Å in the PMETAC brush systems. Graphs displaying the distribution of lifetimes for $ClO_4^-$, $SCN^-$ anions and the intrinsic $Cl^-$ counterions within 8.15 Å of the QA groups were generated and are plotted in Figure 3.7. For the PMETAC brush systems in the studied salt solutions, a proportion of $ClO_4^-$ and $SCN^-$ anions reside in the first coordination shell of the QA groups for the entire simulated trajectory (4000 ps). The $Cl^-$ counterions have shorter lifetimes than $ClO_4^-$ and $SCN^-$ anions. The graphs shown in Figure 3.7 demonstrate there is a distinct difference in the behaviour of $Cl^-$ counterions in close contact with the QA groups and studied salt anions, $SCN^-$ and $ClO_4^-$.

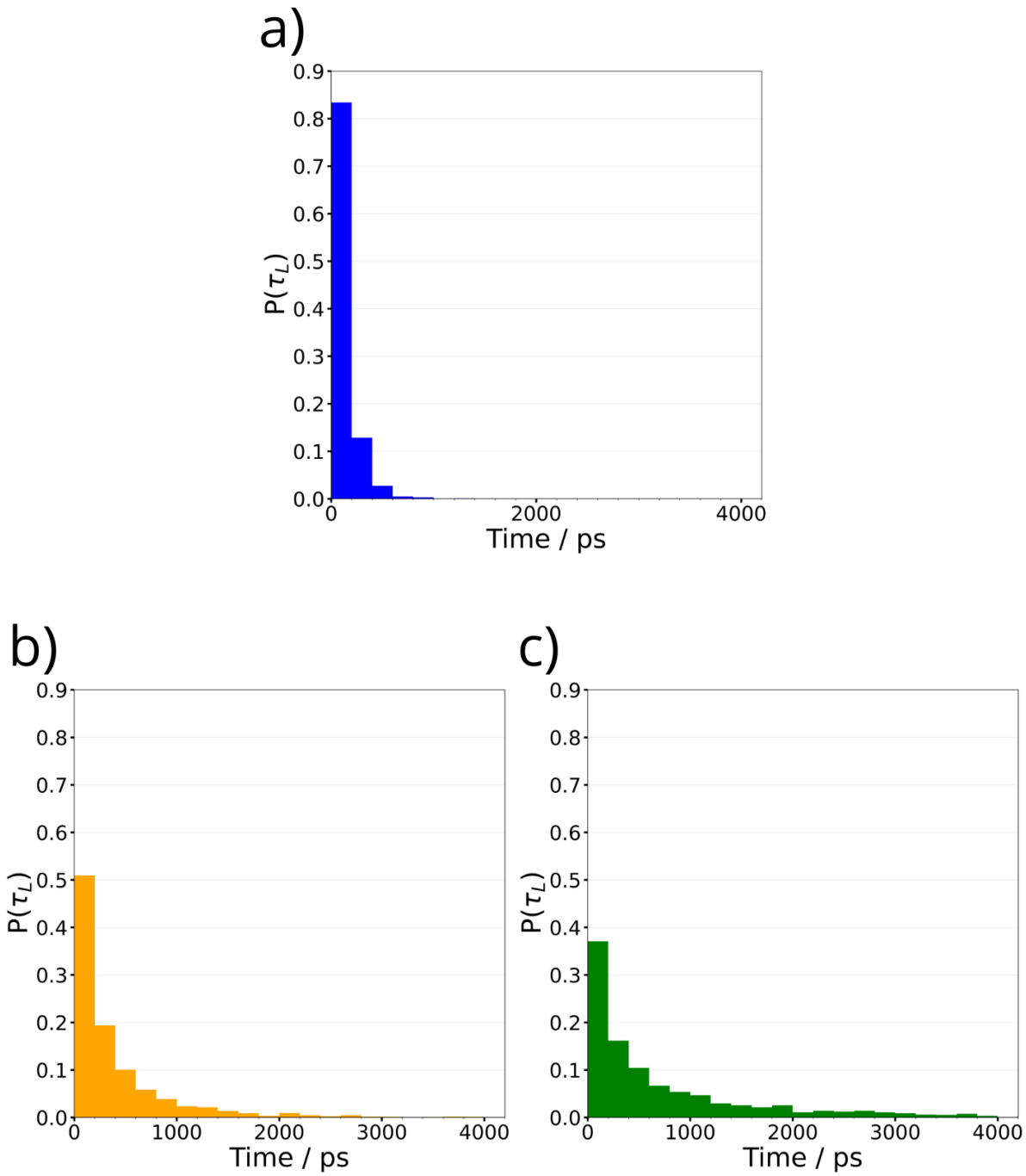


**Figure 3.7** Plots of the normalised distribution of lifetimes for the a) $Cl^-$ counterions within 8.15 Å of the nitrogen in the QA group ($N_{QA}$) of the PMETAC brush in the presence of water, b) $SCN^-$ anions within 8.15 Å of the nitrogen in the QA group ($N_{QA}$) of the PMETAC brush and c) $ClO_4^-$ anions within 8.15 Å of the nitrogen in the QA group ($N_{QA}$) of the PMETAC brush.

## 3.4 Discussion

### 3.4.1 Conformation and Hydration of PMETAC Brush

Both the hydration and conformational behaviour of the modelled PMETAC chains have been observed to vary in the presence of water, 0.5 M NaSCN and 0.5 M $NaClO_4$ solutions. The chains were fully extended in water, and perpendicular to the surface with no observed layering over the surface as displayed in Figure 3.8a. This is due to the high grafting density (Table 2.2) considered in this study and can be attributed to both the electrostatic repulsion between the charged chains and to the fully hydrated chains. The addition of the salt solutions under investigation caused a decrease in the height of the brush (Figure 3.4) and a less swollen configuration was observed (Figure 3.8b and 3.8c), thus successfully capturing the well-known conformational response that occurs when salt solutions are added to PE brushes.[3,6]

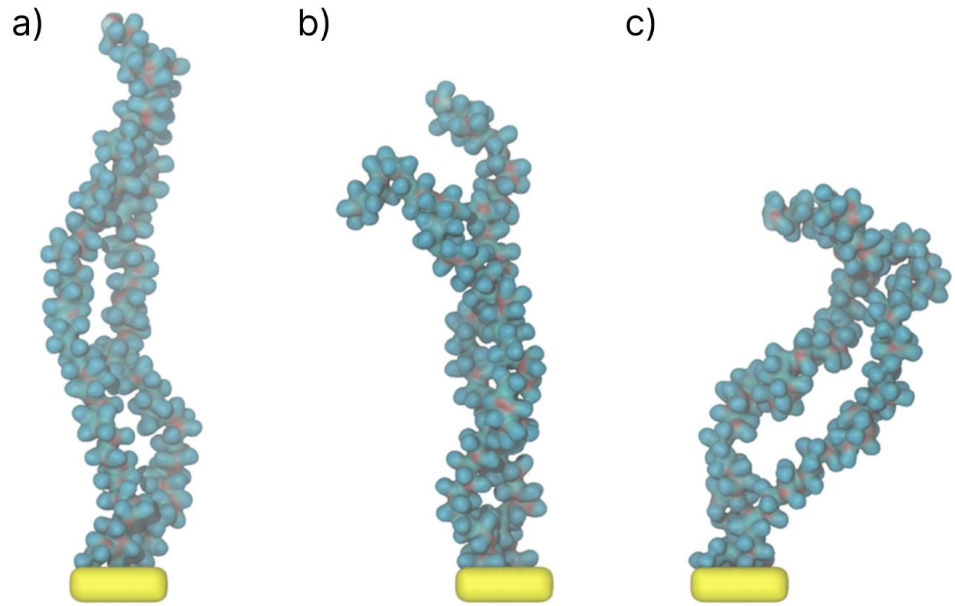


**Figure 3.8** Final configurations of PMETAC chains upon the addition of a) water, b) 0.5 M NaSCN solution, c) 0.5 M $NaClO_4$ solution. Water molecules, hydrogen atoms and ions are not displayed for clarity.

According to polymer brush (PB) literature, the observed collapse is due to the presence of highly mobile salt anions within the PMETAC brush. This causes a decrease in the Debye screening lengths accompanied by a strengthening of electrostatic screening of the QA groups.[3,8] Electrostatic repulsions between the chains are, therefore, minimised and a collapsed conformation is adopted.[3] Although, it must be noted that this "electrostatically-driven collapse" theory[3,8] does not explain why the collapse is more prominent in the presence of $ClO_4^-$ than $SCN^-$ (Figures 3.3, 3.4 and 3.8) as reported from the simulations in this study. The two studied anions have the same charge and, therefore, the collapse observed in both salt solutions should be equal.

Findings in this thesis, however, have demonstrated that the decrease in the height of the PMETAC brush (Figure 3.4) and decrease in the number of water molecules within the brush (Figure 3.5) was more prominently observed in $NaClO_4$ than NaSCN. The subtle differences observed between the two chaotropic anions, $ClO_4^-$ and $SCN^-$ regarding hydration and conformational behaviour of PMETAC, has previously been reported by Kou *et al.*[39] and support the results from the simulations in this thesis. Kou *et al.*[39] found that $ClO_4^-$ had a more pronounced effect not only on the conformation of the PMETAC brush, but also the observed dehydration process.[39] To understand the difference in the behaviour of the brush in the presence of $ClO_4^-$ and $SCN^-$, it is important to appropriately consider the formation of distinct chemical species such as ion pairs.

### 3.4.2 Detecting Ion Pairing

Two different types of ion binding states have been observed in the PMETAC system as indicated by differences in the lifetimes of $ClO_4^-$ and $SCN^-$ anions and the intrinsic $Cl^-$ counterions, shown

in Figure 3.7. The distribution of lifetimes for $ClO_4^-$ and $SCN^-$, along with $Cl^-$ counterions (Figure 3.7) within 8.15 Å of QA groups show that $Cl^-$ counterions have short lifetimes compared to $ClO_4^-$ and $SCN^-$ anions. This observation, along with LMWA theory,[40,45] ion dispersion theory[42] and previous investigations,[5,8,9] suggests that $ClO_4^-$ and $SCN^-$ anions are forming ion pairs with QA groups in the PMETAC chains, whereas $Cl^-$ counterions are not.[5,8,9]

To detect ion pairs within each PMETAC brush system, equation 3.1 was used. As discussed, *R* is approximated to be 8.15 Å, the first coordination shell of QA groups along the PMETAC chains (Figure 3.6). Effects of confinement were estimated by calculating the diffusion coefficient of $Cl^-$ counterions which are confined within the brush but are not involved in ion pairing (Figure 3.7). The diffusion coefficient of $Cl^-$ counterions from the PMETAC system in water was calculated to be $0.547 \times 10^{-9}$ $m^2$ $s^{-1}$, using the diffusion coefficient plug-in[133] in VMD,[129] which in turn, uses the mean squared deviation of the $Cl^-$ anions and Stokes-Einstein Equation.[129,133]

It was, therefore, proposed that an ion pair forms when an anion resides for longer than 600 ps, within 8.15 Å of a QA group. Graphs showing the distribution of lifetimes are shown in Figure 3.9. Very few $Cl^-$ counterions show evidence of ion pairing in the PMETAC brush systems in water (Figure 3.9), NaSCN and $NaClO_4$ solutions (Appendix 3: Figure A.3.1 and A.3.2). In contrast, a large proportion of $ClO_4^-$ and $SCN^-$ anions are involved in ion pairing. These findings (Figure 3.9) are consistent with the previously reported chaotropic nature of $ClO_4^-$ and $SCN^-$ anions and the borderline kosmotropic nature of $Cl^-$ counterions.[5,8,9]

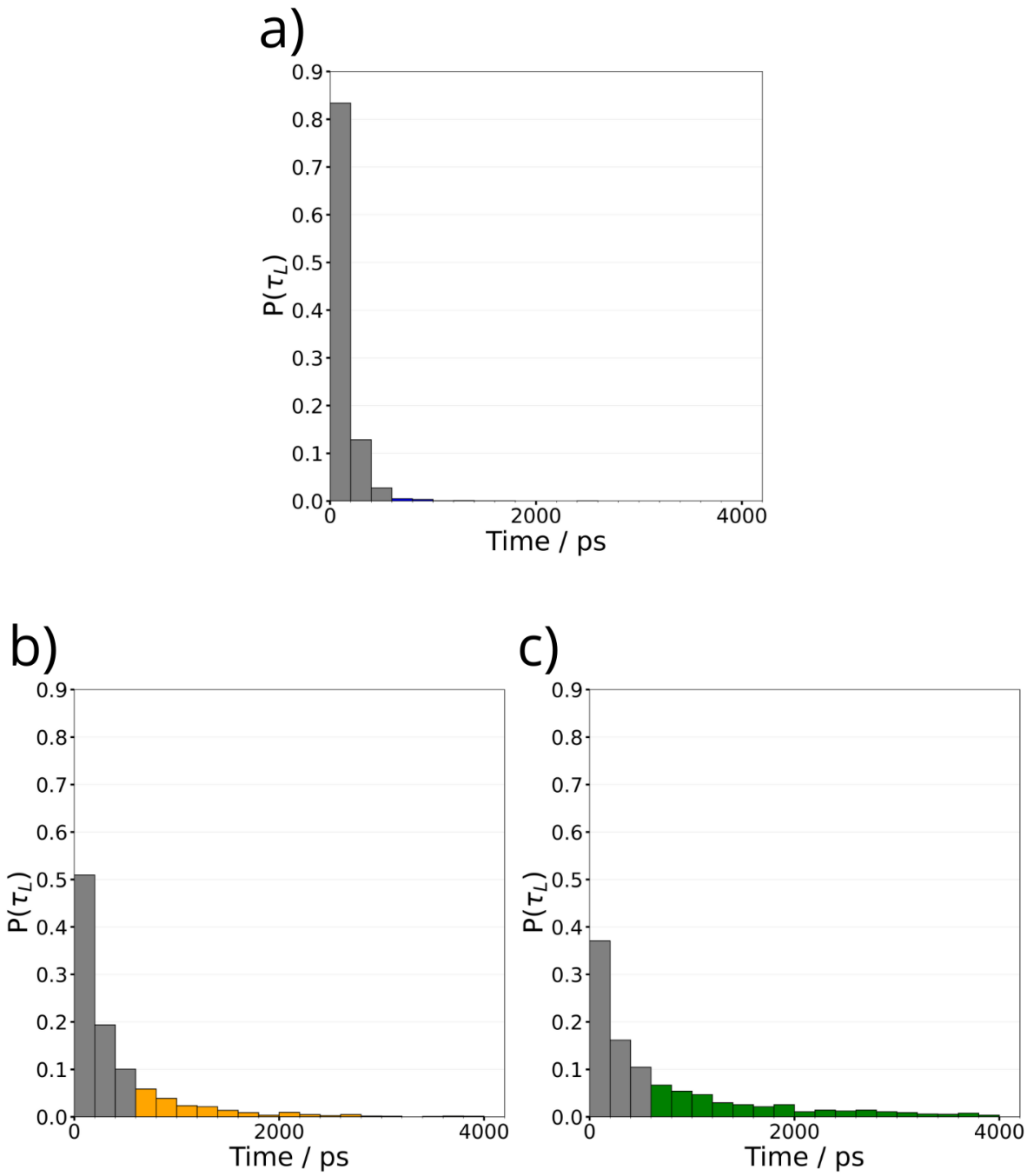


**Figure 3.9** Plot of the normalised distribution of lifetimes for the a) $Cl^-$ counterions within 8.15 Å of the nitrogen atoms of the QA groups ($N_{QA}$) along the PMETAC chains in water, b) the $SCN^-$ anions within 8.15 Å of the nitrogen atoms of the QA groups ($N_{QA}$) along the PMETAC chains and c) for the $ClO_4^-$ anions within 8.15 Å of the nitrogen atoms of the QA groups ($N_{QA}$) along the PMETAC chains. Only ion paired anions are displayed ($t \geq 600$ ps) in colour.

Ion pairing is observed between QA groups and the $ClO_4^-$ and $SCN^-$ anions in the PMETAC brush systems. 11 % of QA groups in the PMETAC brush system (Figure 3.10) are paired to one $ClO_4^-$ anion (illustrated in Figure 3.11a) and significantly more, 44 % of QA groups (Figure 3.10) are paired to one $SCN^-$ anion (illustrated in Figure 3.11c).

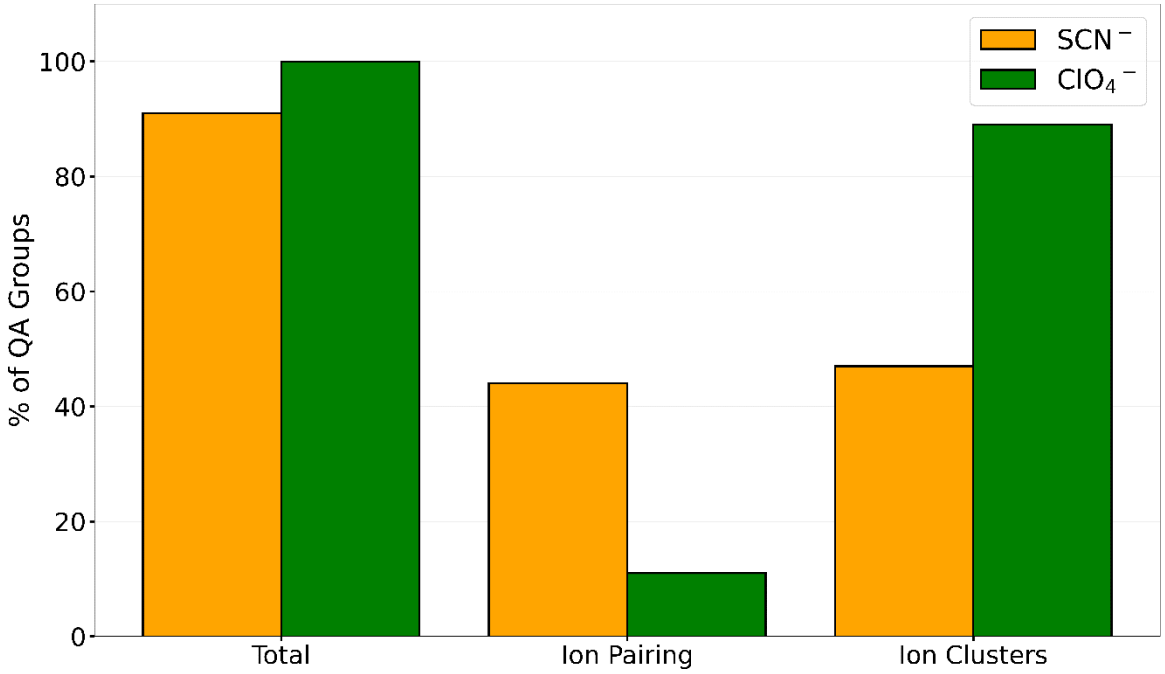


**Figure 3.10** Plot of the percentage of QA groups on the PMETAC chains bound to the $SCN^-$ and $ClO_4^-$ anions, ion pairs and higher-order ion clustering over the trajectory. Values are recorded in Appendix 5: Table A.5.1

However, the nature of the interactions and structures formed between the $ClO_4^-$ and $SCN^-$ anions and QA groups in the PMETAC chains seem to be more complex than the accepted term "ion pairing" initially suggests. Evidence from simulations in the present study indicates that a significant proportion of QA groups are involved in interacting with multiple salt anions for at

least 600 ps, leading to the formation of higher-order ion clusters. The presence of $ClO_4^-$ anions favours this type of ion interaction with 89 % of QA groups (Figure 3.10) involved in higher-order ion clustering (illustrated in Figure 3.11b) compared to 47 % of QA groups being involved in higher-order ion clustering with $SCN^-$ anions (illustrated in Figure 3.11d).

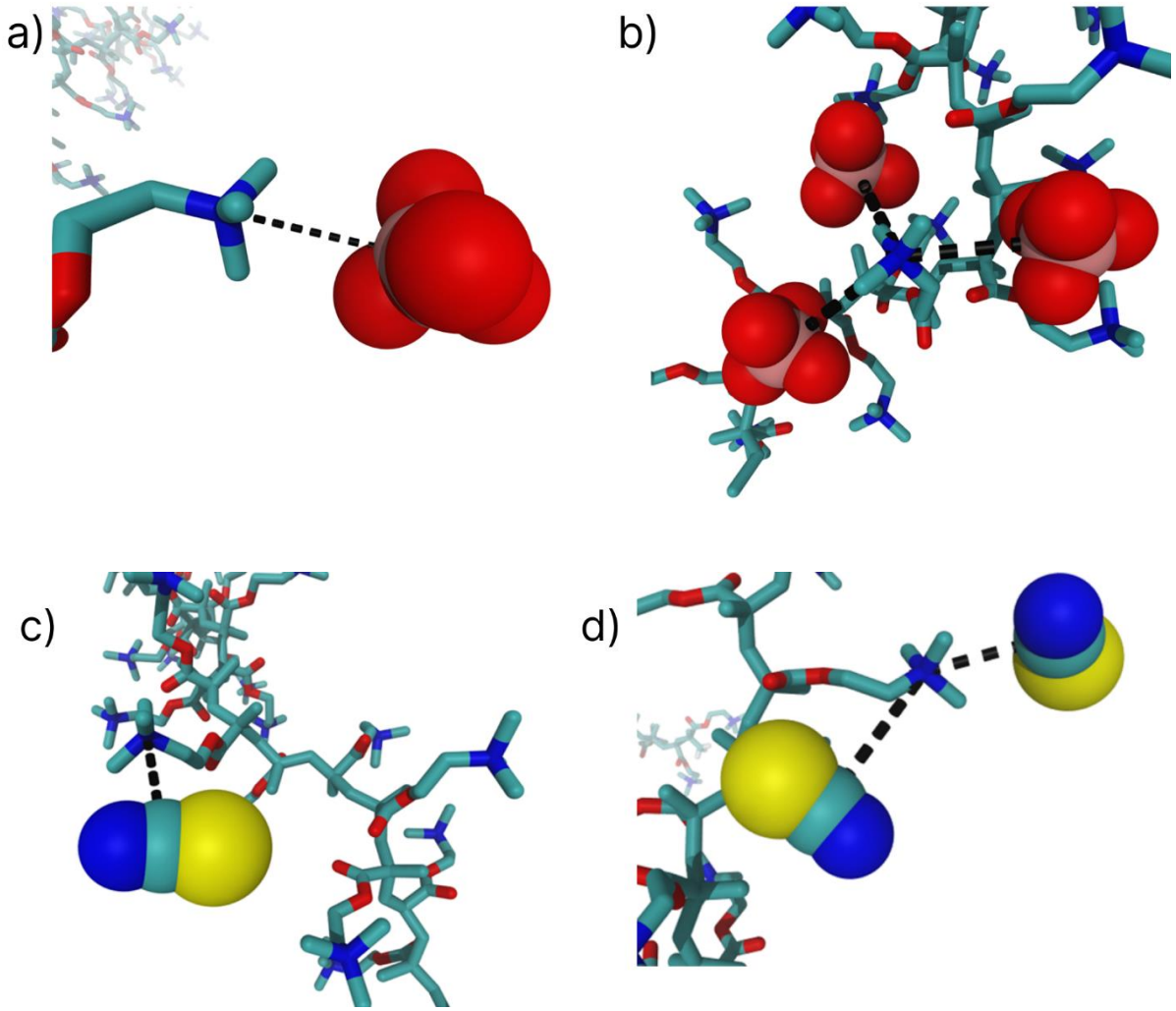


**Figure 3.11** Configurations showing examples of ion pairs and higher-order ion clusters forming with a QA group along the PMETAC chains and a) one $ClO_4^-$ anion, b) three $ClO_4^-$ anions, c) one $SCN^-$ anion and d) two $SCN^-$ anions. Only relevant anions are displayed and water molecules along with hydrogen atoms are not shown for clarity. Carbon atoms are cyan, sulfur atoms are yellow, nitrogen atoms are blue, oxygen atoms are red and chlorine atoms are pink. Representations of specific-ion interactions have been added as dashed lines, to better demonstrate ion pairing or higher-order ion clustering in each system.

It is important to note that ion pairing tends to be overestimated in MD simulations using simple force fields.[134] Force fields are only estimates of interactions between particles and the quality

of that estimate is dependent on the exact scenario which those particles are in. By including electronic polarisation effects or by using *ab initio* MD, results could be significantly improved. However, the computational cost of including an explicit polarisation effect rises considerably. The computational expense of building and running a PB system simulation is already substantial so the additional cost of polarisability effects may be unfeasible.[5,134] A significant compromise in the size of the simulated PB would have to be made which may affect the reproducibility of results experimentally. Recently, progress has been made in machine learning potentials for complex aqueous systems[135] and may be applicable to the PB systems studied throughout this thesis.

Despite the recorded drawbacks in using non-polarisable force fields, the experimentally observed and complex conformational responses of PMETAC brushes[5,8,39] were reproduced by the simulations in this thesis. Hence, showing that the chosen atomic parameters have captured the specific-ion behaviour of a PMETAC brush in the presence of highly concentrated chaotropic anions, $ClO_4^-$ and $SCN^-$.

### 3.4.3 Influence of Ion Pairs and Higher-Order Ion Clusters

Thus far, it has been shown that the hydration levels of PMETAC brushes are decreased in NaSCN and $NaClO_4$ solutions (Figure 3.5). Upon closer inspection, it is clear there is also a decrease in water molecules in the first hydration shell of QA groups in the presence of the studied salt solutions, as indicated by the relative heights of peaks in the RDFs plotted in Figure 3.12. This observation, along with percentage values of water molecules lost from the PMETAC brush (Figure 3.5), indicates that the newly formed ion pairs and higher-order ion clusters are hydrophobic, particularly those formed between the QA groups and the $ClO_4^-$ anions. An overall

shift in the chemical properties of the PMETAC chains may, therefore, be occurring, thus leading to a "hydrophobic collapse",[9] similar to hydrophobic driven protein folding mechanisms.[136] Consequently explaining, in part, the decreased height of the PMETAC brush in the salt solutions under investigation, which is more prominently observed in $NaClO_4$ solution.

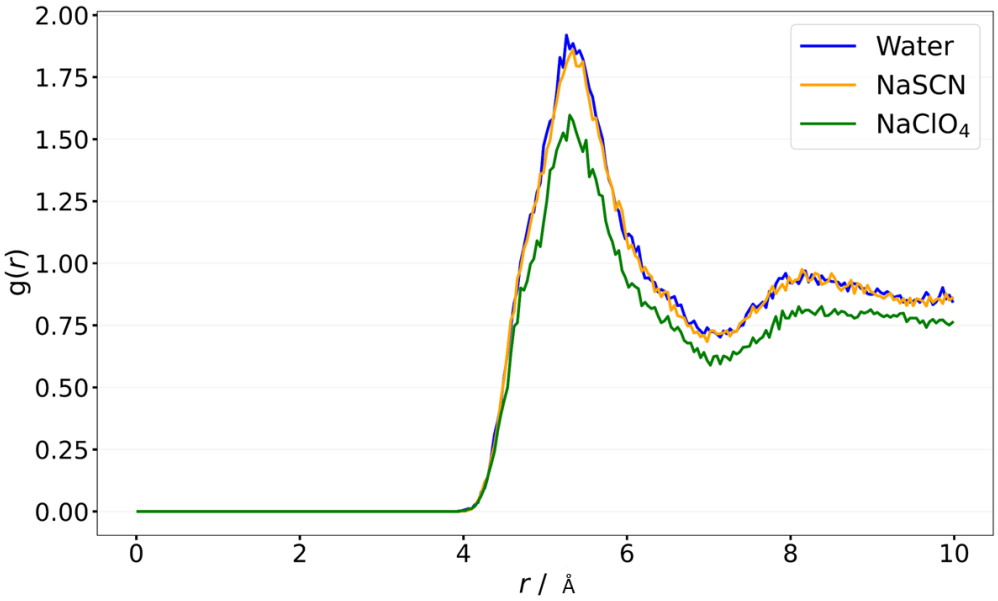


**Figure 3.12** Plot of the radial distribution functions (RDFs) of the nitrogen of QA groups ($N_{QA}$) of the PMETAC chains with the oxygen of water molecules ($O_W$) in water, 0.5 M NaSCN solution and 0.5 M $NaClO_4$ solution.

The decrease in PMETAC brush height in NaSCN and $NaClO_4$ solutions can be further explained by considering the frequency and conformations of higher-order ion clusters. The conformation of the PMETAC brush is more entangled and disordered in the presence of $ClO_4^-$ and $SCN^-$ anions (Figure 3.8), compared to the chains in water, owing to the formation of higher-order ion clusters and ion pairs. Additionally, only higher-order ion clusters consisting of multiple anions interacting with one QA group have been discussed up to now. However, conformations within

the PMETAC chains indicates the formation of ion pockets around chaotropic anions, where several QA groups simultaneously associate with one $ClO_4^-$ anion or $SCN^-$ anion for at least 600 ps (illustrated in Figure 3.13). Ion triplets (two QA groups surrounding the anion), ion quadruplets (three QA groups surrounding the anion), ion quintuplets (four QA groups – one anion) and on rare occasions ion sextuplets (five QA groups – one anion) are all observed within PMETAC chains (Figure 3.14). The observed ion pockets form with QA groups from neighbouring monomers surrounding the anion, QA groups from different sections of the chain and the other PMETAC chains within the modelled PMETAC brush.

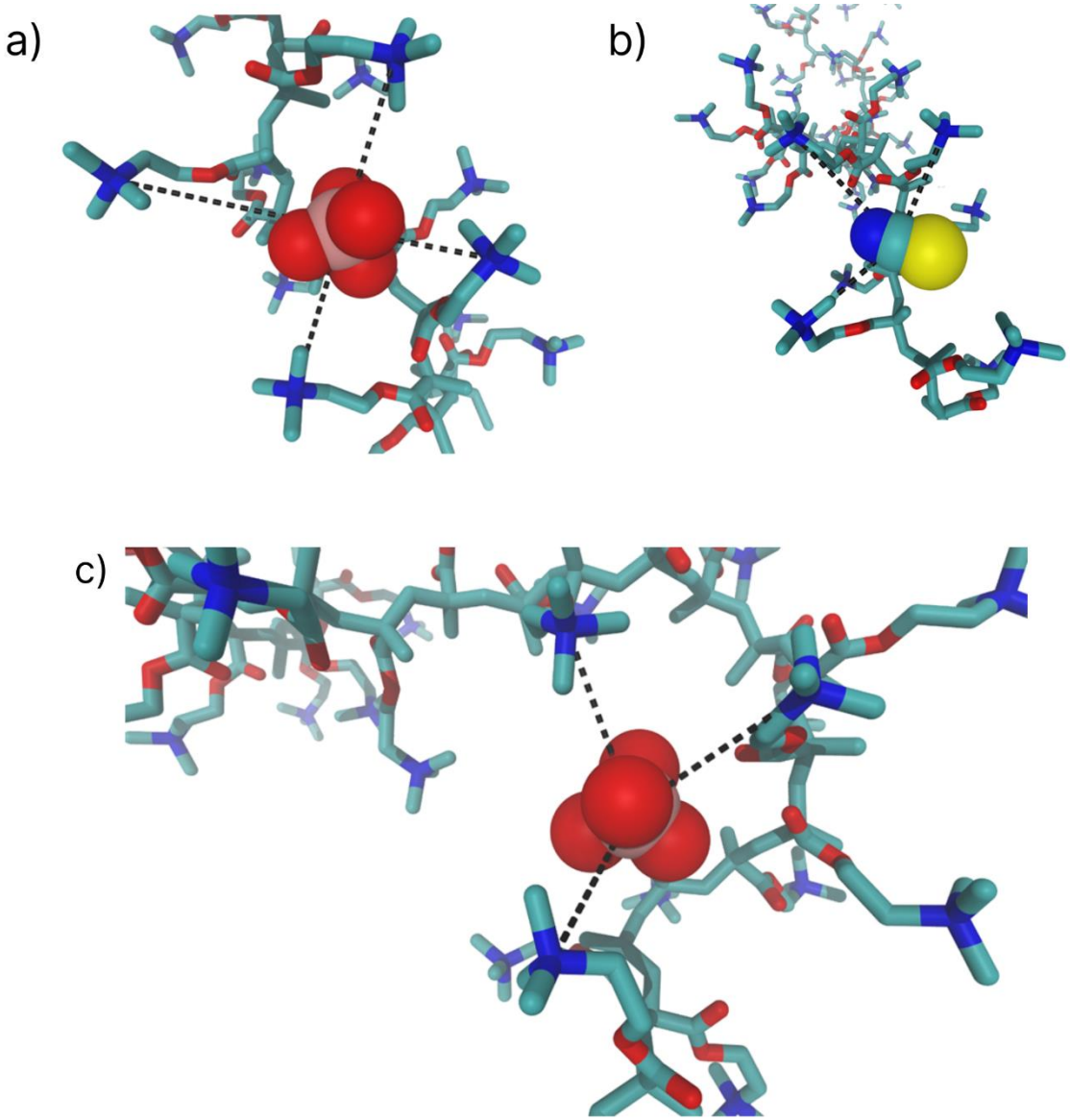


**Figure 3.13** Configurations illustrating examples of ion pockets for a) an ion quintuplet made up of one $ClO_4^-$ anion and four QA groups along the PMETAC chains, b) an ion quadruplet made up of one $SCN^-$ anion and between three QA groups along the PMETAC chains, c) an ion quadruplet made up of one $ClO_4^-$ anion and three QA groups along one of the PMETAC chain. Only relevant anions are displayed, and water molecules and hydrogen atoms are not shown for clarity. Carbon atoms are cyan, sulfur atoms are yellow, nitrogen atoms are blue, oxygen atoms are red and chlorine atoms are pink. Representations of specific-ion interactions have been added as dashed lines, to better demonstrate the ion clustering in each system

$ClO_4^-$ anions prefer to form larger ion pockets with the QA groups than the $SCN^-$ anions demonstrated by the higher frequency of quadruplets, quintuplets, and sextuplets (Figure 3.14). This may be due to the slightly larger ionic radii of $ClO_4^-$ anions (2.41 Å[137]) compared to $SCN^-$ anions (2.15 Å[138]). A consequence of these larger ion pockets is that the PMETAC chains must bend to accommodate $ClO_4^-$ anions and the monomers throughout the chains are observed to rearrange themselves to situate pendant QA groups into the optimal position for forming ion pockets (Figure 3.13). Thus, a more collapsed conformation is observed in the presence of $ClO_4^-$ anions.

a)

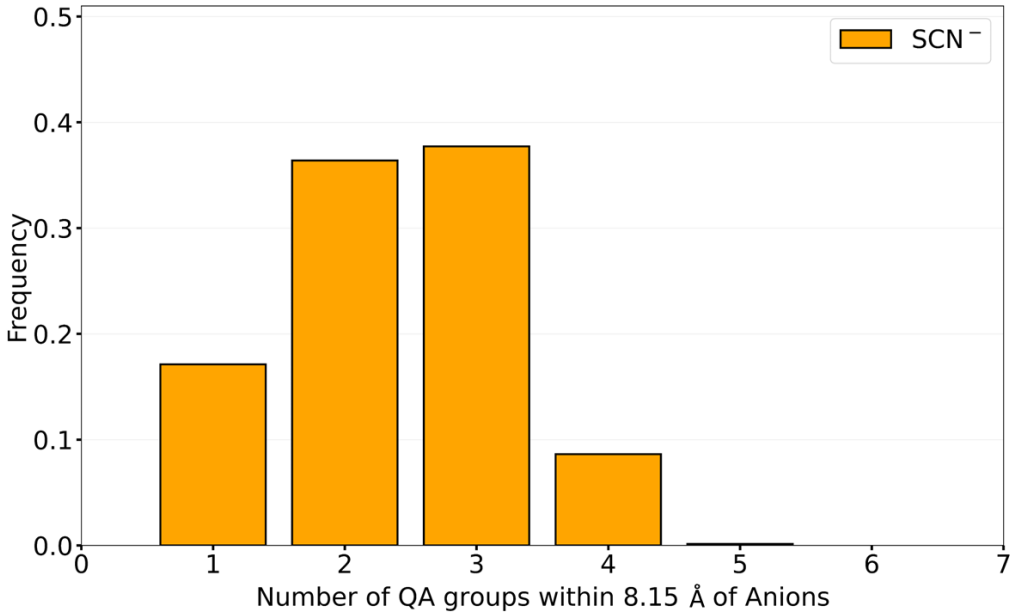


b)

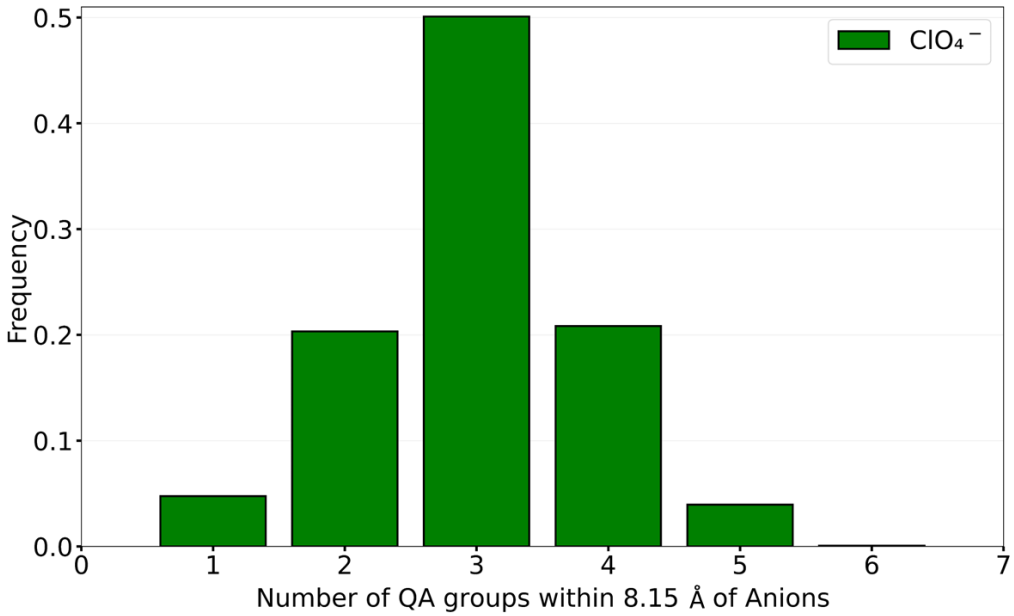


**Figure 3.14** Plots of frequency of the number of QA groups on the PMETAC groups within 8.15 Å of a) $SCN^-$ anions and b) $ClO_4^-$ anions for the last frame of the simulated trajectory.

Finally, several theories predict the strength of ion pairing with QA groups in the PMETAC brush increases from $Cl^-$ to $SCN^-$ to $ClO_4^-$. The LMWA theory[40,45] suggests that this is due to the ionic hydration of the anions increases from $ClO_4^-$ to $SCN^-$ to $Cl^-$ and the ionic dispersion interaction theory[42] agrees as the polarisability increases from $Cl^-$ to $SCN^-$ to $ClO_4^-$. Our findings seem to support these theories as demonstrated by the tendency for $ClO_4^-$ anions to reside in the first solvation shell of QA groups for a longer period compared to $SCN^-$ (Figure 3.9), combined with the preference of $ClO_4^-$ to form higher-order ion clusters (Figure 3.10) and larger ion pockets (Figure 3.16b).

## 3.5 Conclusion

In this chapter, it has been reported that the studied salt solutions, 0.5 M NaSCN and 0.5 M $NaClO_4$, induced a less swollen conformation within the simulated PMETAC brush compared to in water. A more pronounced decrease in brush height and dehydration of the PMETAC chains was observed in $NaClO_4$ compared to NaSCN solution, thus following the expected order predicted by the Hofmeister series. The observations presented here are in good agreement with previous experimental[5,8,39] investigations, thus showing that the chosen atomic parameters, from the AMBER force fields:[90] ff14SB[99] and General Amber force field (GAFF)[100] parameter sets, have captured the specific-ion behaviour of a PMETAC brush in the presence of highly concentrated chaotropic anions, $ClO_4^-$ and $SCN^-$.

Previous experimental studies[5,8,39] have suggested that changes in hydration and conformation of PMETAC brushes are linked to ion pairs forming between chaotropic anions and QA groups along the PMETAC chains. Due to the complexity of the PB system, along with the timescales involved in ion pairing, it is challenging to gather further information regarding ion pairs using

experimental methods.[46] A computational study by Santos *et al.*[5] employed atomistic MD simulations to examine ion pairing further. They presented graphs showing RDFs for the QA groups and the salt anions under investigation. Through the analysis of these graphs, Santos *et al.*[5] proposed that chaotropic anions formed strong ion pair interactions with QA groups. Although the RDFs do clearly indicate the studied chaotropic anions are associating more closely with the QA groups than the kosmotropic anions, a constraint of using RDFs is that no information about the dynamics of anions in close contact with the brush is provided. Therefore, the ion pairing inferred from the RDFs could, in fact, be indicative of the expected brief encounters between the salt anions and QA groups on the PMETAC chains due to their thermal motion within the solution.

The results presented in this chapter sought to address this limitation. The lifetimes of specific-anion interactions were deemed essential to study as the definition of ion pairs is dependent on both the distance between the ions and the amount of time the ions reside in that specified region.[46] Graphs displaying the lifetime distributions of anions in the first solvation shell of QA groups verified that ion pairs formed between QA groups and the $ClO_4^-$ and $SCN^-$ anions.

By identifying the anions and QA groups involved in ion pairing interactions, it was possible to further analyse conformations and motifs present. It became clear that the term “ion pairing” was an oversimplification of the specific-ion interactions occurring within the PMETAC brush. Multiple $ClO_4^-$ and $SCN^-$ anions were found to be paired simultaneously to QA groups, consequently forming higher-order ion clusters. Ion pockets were also observed wherein multiple QA groups were simultaneously paired to one of the studied chaotropic anions. The changes in hydration and conformation of the brush can not only be linked to the presence of

ion pairs but also the frequency and size of higher-order ion clusters and ion pockets. $ClO_4^-$ were observed to form larger pockets with QA groups on the PMETAC chains. A consequence of this is the bending of the chains to better accommodate the $ClO_4^-$ anions. The monomers along the PMETAC chains rearrange themselves to situate the pendant QA groups into the optimal position for forming ion pockets. The formation of ion pockets, therefore, influences the conformation of the PMETAC chains and encourages a less swollen conformation. Furthermore, ion pockets, along with ion pairs and higher-order ion clusters, have been shown to influence the hydrophobicity of the chains therefore influencing the hydration of the PMETAC chains.

Finally, atomistic MD simulations have been shown to be valuable in elucidating the mechanisms involved in specific-ion interactions within PMETAC brushes. Structural and dynamical properties, however, have been found to vary with the size of the simulation cell in previous MD investigations.[139–142] The next chapter will attempt to understand effects of increasing the size of the PMETAC brush systems, from modelling two polymer chains per brush system to modelling eight polymer chains.

# CHAPTER 4: ION PAIRING AND HIGHER-ORDER ION CLUSTERS IN AN EIGHT-CHAIN POLYELECTROLYTE BRUSH MODEL

## 4.1 Introduction

The findings presented in the previous chapter have shown that it is possible to employ atomistic MD simulations to detect ion pair interactions within poly (2-(methacryloyloxy) ethyl trimethylammonium chloride (PMETAC) brushes in the presence of highly chaotropic salt anions, $SCN^-$ and $ClO_4^-$. The frequency and size of higher-order ion clusters have been linked to the observed changes in structural features and hydration levels of PMETAC chains.

These results, however, have been generated from simulations performed within a finite simulation cell containing *two* PMETAC chains. Ideally, many hundreds of polymer chains would be modelled, thus, representing a realistic polymer brush (PB). Despite ongoing improvements in computer facilities and MD programmes, this is still currently computationally unfeasible. As a compromise, a small number of polymer chains are, instead, modelled while employing periodic boundary conditions (PBCs). PBCs form an infinite lattice by replicating the original simulation box through all directions in space (a 2D representation of this is illustrated in Figure 2.1). By setting PBCs in all dimensions, as used in the simulations discussed in Chapter 3, both the surface and the two modelled PMETAC chains within the simulation have been infinitely extended.

It is well-known, however, that some structural and dynamical properties may vary with the size of the simulation box.[139–142] Studies focusing on diffusion coefficients and viscosities, for example, have found that these measurements tend to change with an increase in the size of the system due to finite-size effects.[140,142,143] Hence, for calculations focusing on the determination of properties, such as diffusion coefficients, finite-size effects must be taken into

account and corrections are sometimes applied.[143] Furthermore, the nature of the two-chain PMETAC brush systems means that polymer chains are often interacting with periodic images of themselves.

In this chapter, the PMETAC brush is expanded, from modelling two polymer chains per PMETAC system (as seen in Chapter 3) to modelling eight polymer chains (Figure 4.1). The eight-chain system contains more distinct chains, therefore reducing self-interactions through PBCs, and reducing finite-size effects. However, by increasing the number of polymer chains within the PMETAC brush system, the number of atoms simulated is dramatically increased, thus substantially increasing the computational workload. The purpose of this chapter is to investigate if the two-chain PMETAC system reported in Chapter 3, is representative of the eight-chain system reported here.

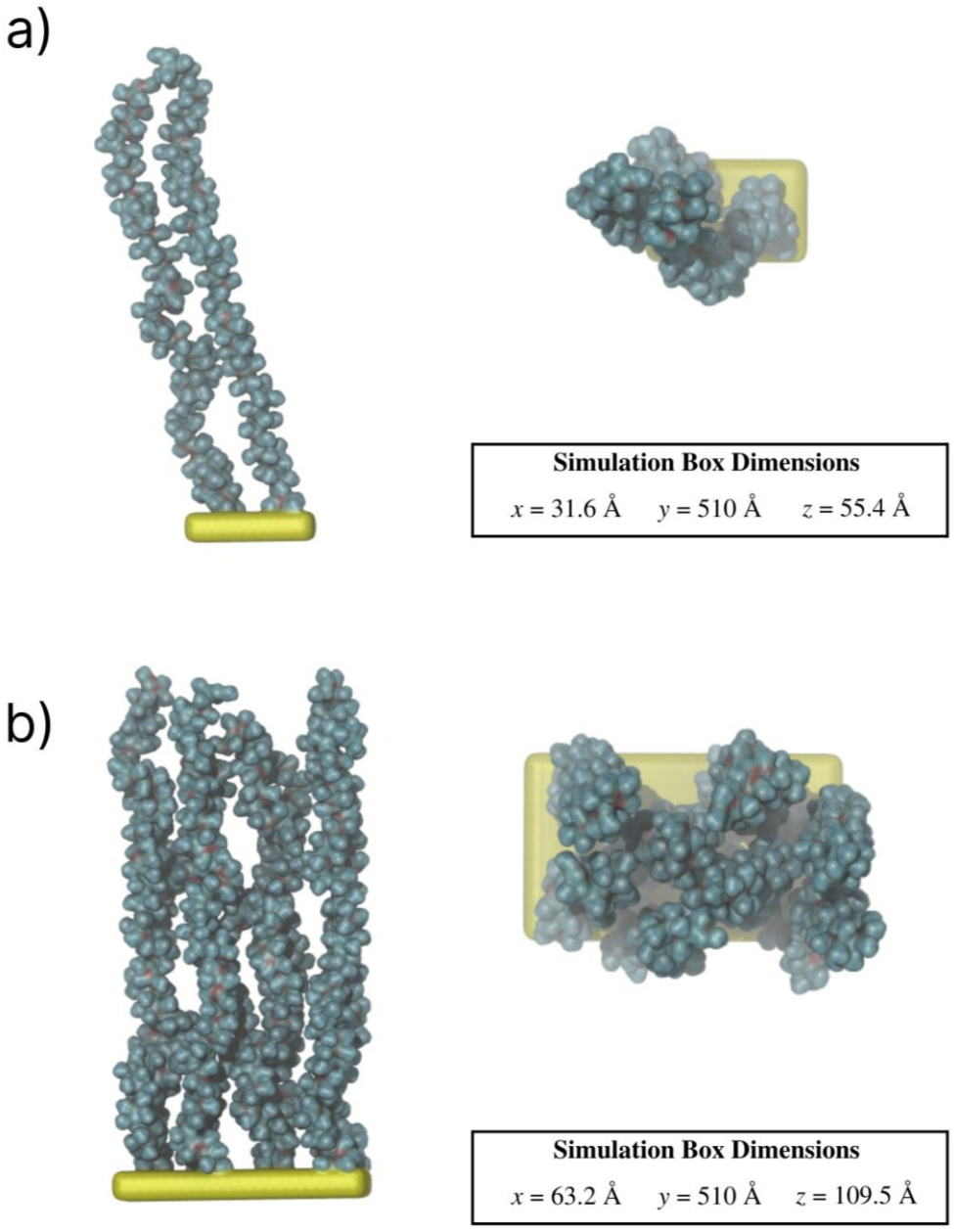


**Figure 4.1** Final configurations illustrating the a) side and top view of two-chain PMETAC brush system, b) side and top view of eight-chain PMETAC brush system. Only PMETAC chains (cyan and red) and the surface (yellow) are displayed in each picture. Water molecules, hydrogen atoms, and chloride counterions are not shown for clarity.

## 4.2 Methods

### 4.2.1 System Description

Atomic coordinates for the initial configurations of the modelled eight PMETAC chains, each consisting of 100 monomer units, were built using the TopoTools plugin for Visual Molecular Dynamics programme (VMD)[129] and in-house codes. Each chain was tethered at a distance of 3.162 nm between grafting points, leading to a grafting density of 0.1 chains $nm^{-2}$. PMETAC chains were initially constructed as fully stretched rod-like chains perpendicular to the surface (defined using LAMMPS[88] intrinsic functions) consisting of four layers of sulfur atoms that remained fixed throughout the simulation. The initial configuration of the PMETAC brush consisted of an array of chloride counterions.

A combination of two AMBER[90] force fields, ff14SB[99] and the General Amber force field (GAFF),[100] were used to model the polymer chains, thiol initiators and surface. The rigid three-site SPC/E model was used to explicitly represent water molecules.[115,116] The chloride counterions of PMETAC were modelled using Joung and Cheatham's set of parameters specific for use with the SPC/E water model.[130] The atomic charges for the polymer chains and thiol initiators were calculated with the Hartree−Fock self-consistent field theory and the 6-31G* basis as described in restrained electrostatic potential (RESP) methodology.[131]

The PMETAC chains were orientated in the simulation box in such a way that the polymer chains were parallel to the y-axis and normal to the *xz*-plane. Periodic boundary conditions (PBCs) were set in the *x*, *y* and *z* directions. Interactions between the top of the PMETAC chains and the periodic image of the surface in the *y*-direction were prevented because the simulation box was larger than the fully stretched chains of the polymer combined with the non-bonded interaction cut-off.

### 4.2.2 Simulation Details

Atomistic MD simulations were performed using LAMMPS (large-scale atomic/molecular massively parallel simulator).[88,89] The Velocity Verlet algorithm[105] was used with a time step of 2 fs to integrate Newton's equations of motion. Initial velocities were taken from a Maxwell distribution at 298 K and 1 atm. Energy minimisation, using the conjugate gradient method, was performed for all the systems until a mean force of lesser than $1.0 \times 10^{-6}$ kcal mol$^{-1}$ Å$^{-1}$ was achieved. Equilibrium runs were performed on the PMETAC brush systems, in a canonical ensemble (NVT) at 500 K for 28 ns, before the system was cooled to 298 K and simulated for approximately 10 ns.

Following equilibration, production runs were executed in the same conditions as the equilibrium run for 4 ns. The last snapshot of the equilibration process was used as the initial configuration. In both the equilibration and production steps the Noose-Hoover thermostat[107] was employed. The SHAKE algorithm[132] was used to constrain the bond lengths and bond-bending angles of water molecules. The cut off of the interatomic potential is set at 11.0 Å with long-range electrostatic interactions between charged species handled using the particle−particle particle-mesh (pppm) method[109] with a root-mean accuracy of $10^{-6}$. Analyses of the trajectories were performed by a combination of LAMMPS,[88] MDAnalysis[144,145] and in-house codes.

## 4.3 Results

### 4.3.1 Conformation and Hydration of PMETAC Brush

The end-to-end brush heights ($< z_e >$) of the PMETAC eight-chain system, in 0.5 M NaSCN and 0.5 M $NaClO_4$ solutions are shown in Figure 4.2. The presence of these studied salt solutions

induced a significant decrease in brush height. The decrease in brush height was more prominently observed in $NaClO_4$ solution.

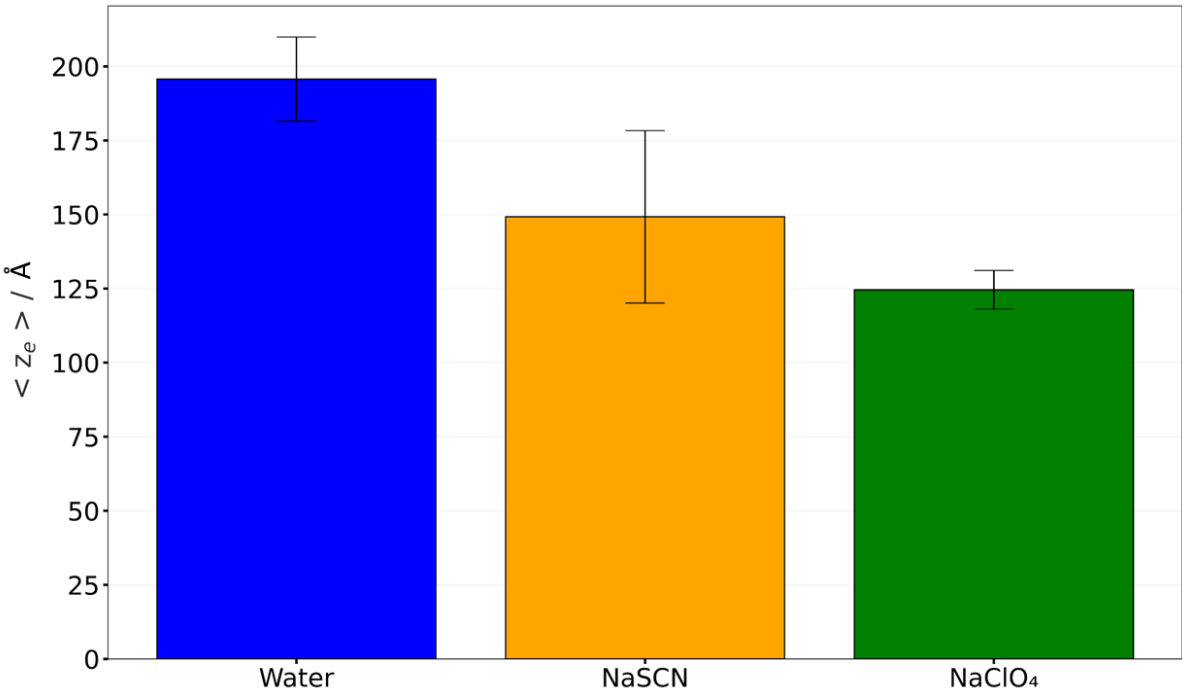


**Figure 4.2** Plot of variation in the average end-to-end brush height (< $z_e$ >) of the PMETAC chains in the presence of water (blue), 0.5 M NaSCN (orange) and 0.5 M $NaClO_4$ solution (green). Error bars are shown representing the standard deviation of the set of end-to-end brush height values per PMETAC brush system.

Furthermore, in the presence of both 0.5 M $NaClO_4$ and NaSCN solutions there was significant loss of water within the PMETAC chains (Figure 4.3). The loss of water molecules was more prominent for the brush in the presence of $NaClO_4$ solution than NaSCN.

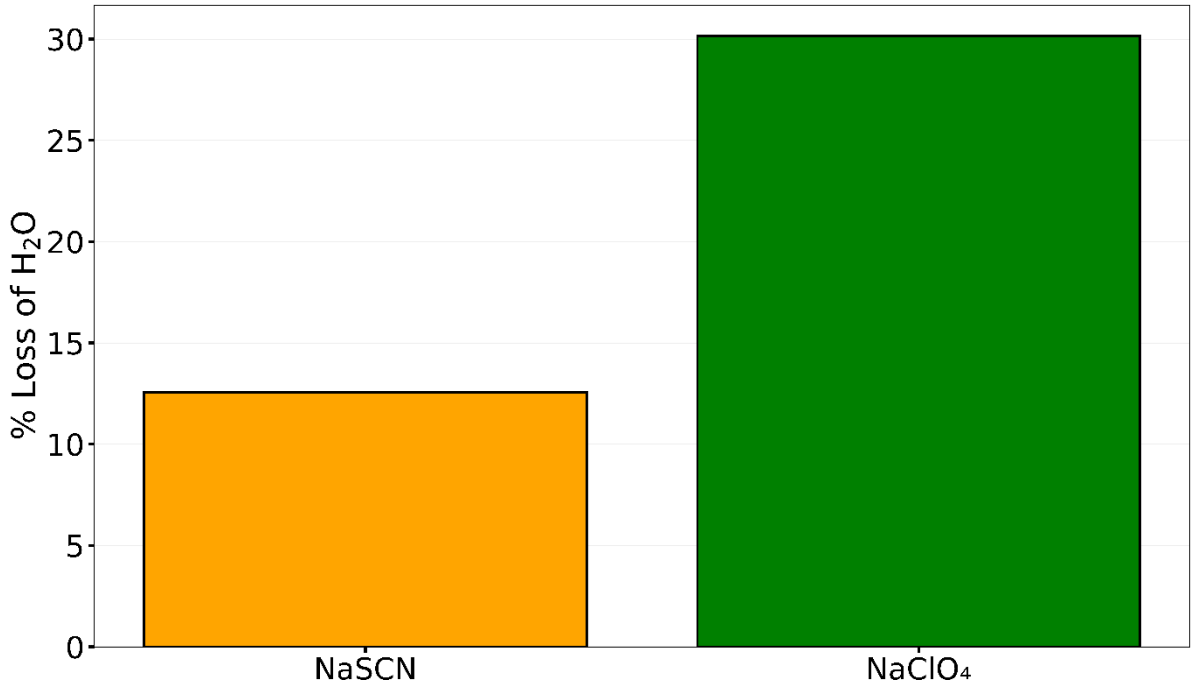


**Figure 4.3** Plot of percentage loss of water molecules within the brush in the presence of 0.5 M NaSCN solution and 0.5 M $NaClO_4$ solution. Values are recorded in Appendix 4: Table A.4.3

### 4.3.2 Specific-Ion Interactions

Throughout Chapter 3, it has been demonstrated that hydration levels and conformational behaviours of PMETAC brushes are influenced by ion pairing and by higher-order ion clustering. The definition of an ion pair, discussed in Section 3.4.2, states that an ion pair is formed when an anion resides, for longer than 600 ps, within 8.15 Å of QA groups of the PMETAC brush. Considering this definition, graphs showing distributions of lifetimes for the studied chaotropic anions within 8.15 Å of QA groups are displayed in Figure 4.4. Ion pairing was observed between QA groups and $ClO_4^-$ and $SCN^-$ anions in the eight-chain PMETAC brush systems.

a)

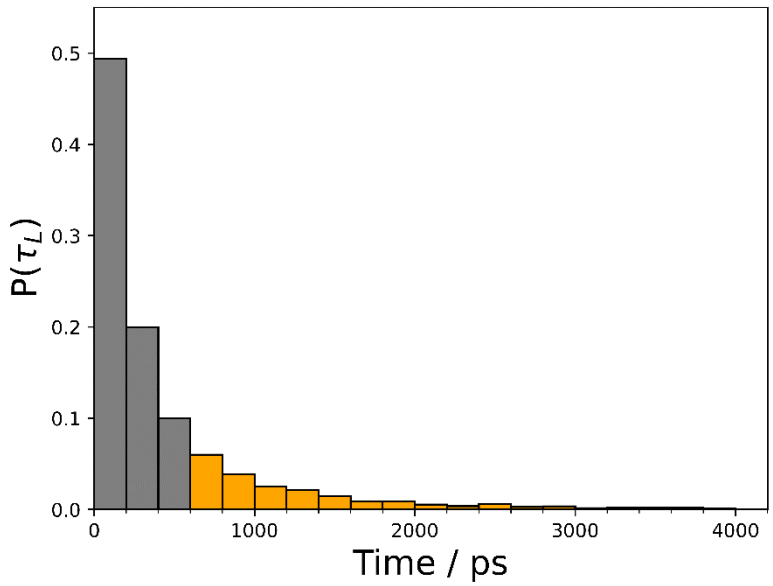


b)

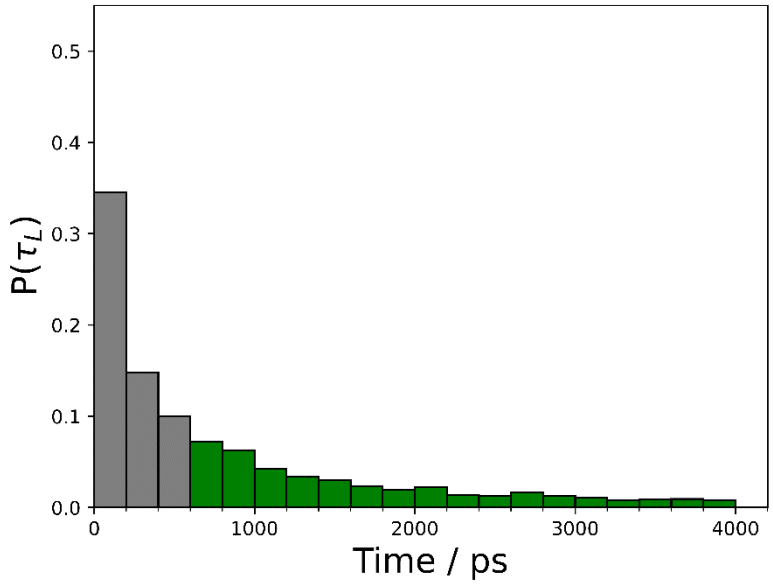


**Figure 4.4** Plots of the normalised distribution of lifetimes a) for $SCN^-$ anions within 8.15 Å of the nitrogen atoms of QA groups ($N_{QA}$) along the PMETAC chains. b) for $ClO_4^-$ anions within 8.15 Å of the nitrogen atoms of QA groups ($N_{QA}$) along the PMETAC chains. Only ion paired anions are displayed ($t \geq 600$ ps) in colour.

As shown by Figure 4.5, almost all QA groups in the eight-chain PMETAC brush system are involved in ion pairing interactions with $ClO_4^-$ and $SCN^-$ anions. Higher-order ion clusters dominate specific-anion interactions observed both in the presence of $ClO_4^-$ and $SCN^-$ anions.

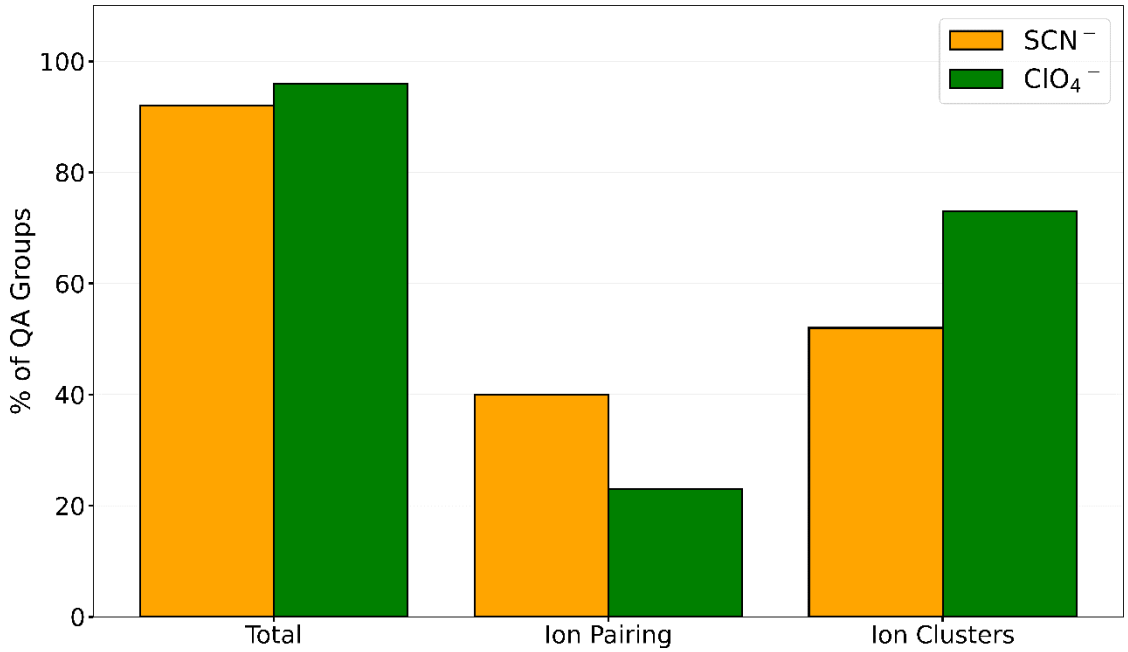


**Figure 4.5** Plot of percentage of QA groups on the PMETAC chains interacting with $SCN^-$ and $ClO_4^-$ anions within 8.15 Å of each other for a time longer than 600 ps, ion pairs and higher-order ion clustering over the trajectory. Values are recorded in Appendix 5: Table A.5.3.

## 4.4 Discussion

As the PMETAC brush system was expanded from containing two-chains to eight-chains, the number of atoms and, therefore, interactions within the simulation cell increased significantly. The eight-chain PMETAC brush simulations were over eight times slower than those run for the two-chain systems and were consequently performed for significantly less time (Appendix 2:

Figures A.2.1 and A.2.2). Despite this, similar structural behaviour was observed for the two-chain and eight-chain PMETAC systems. NaSCN and $NaClO_4$ solutions were observed to induce a decrease in the height of the PMETAC chains, more prominently observed for the brush in the presence of $ClO_4^-$ anions (Figures 3.4 and 4.2). Furthermore, the average end-to-end brush height values recorded for the eight-chain PMETAC are similar to those presented for the two-chain model (Figure 3.4). Similarities, both in terms of trends (Figures 3.5 and 4.4) and values (Appendix 4: Tables A.4.1 and A.4.3), continued upon investigating the dehydration process of the differently sized brush models which occurred in the presence of the studied salt solutions.

Both the two-chain and the eight-chain PMETAC brush systems reveal similar structures and behaviours regarding specific-anion interactions. Higher-order ion clustering dominated specific-anion interactions for $SCN^-$ and $ClO_4^-$ anions in the eight-chain PMETAC system as was observed in the two-chain PMETAC brush systems (Figures 3.10 and 4.5). Minor variations in percentage values were reported (Appendix 5: Tables A.5.1 and A.5.4) which could be due to differences in simulation times between the PMETAC brush systems.

By comparing values of average end-to-end brush height and percentage loss of water for the two-chain and eight-chain PMETAC systems, it is clear that the fundamental features of the hydration and conformational behaviour have not been significantly affected by expanding the size of the simulated PMETAC brush. As expected, the eight-chain PMETAC brush model produced very similar results to its two-chain counterpart, both qualitatively and quantitatively. The findings from the atomistic MD simulations for the two-chain PMETAC brushes were, therefore, validated and it can be suggested that the effects of interactions between the

PMETAC chains are successfully captured by the smaller, simpler two-chain PMETAC brush model.

## 4.5 Conclusions

Results from the two-chain and eight-chain PMETAC brush systems are similar in terms of their conformation, hydration, and specific-anion interactions in the presence of $ClO_4^-$ and $SCN^-$ anions. The macroscopic properties studied in this thesis, along with findings related to ion pairing and higher-order ion clustering, show no system-size dependencies.

These conclusions indicate that researchers employing MD simulations to examine specific-ion interactions in PBs may be able to justify only modelling very few polymer chains. This is vital as using atomistic MD simulations to investigate PB systems containing eight-chains was time consuming and computationally expensive. This was due to the large number of atoms being modelled combined with uncompromisable simulation requirements, for example, explicit representation of solvent molecules. Modelling water explicitly can reproduce solvation effects of real solvent-like hydrophobic effects[87] which are crucial to capture when investigating ion pairs, despite the extensive simulation time required. Reducing the computational expense and simulation time by limiting the number of polymer chains modelled, offers researchers the opportunity to investigate a wider variety of PB systems within one project. For example, specific-ion interactions have been reported for many different types of PBs: strong PE brushes, weak PE brushes, neutral PBs,[4] and more complex systems such as polymer films.[4] Modelling these systems and systematically studying specific-ion effects within each one would be beneficial in furthering our understanding of the responsiveness of PBs and optimising PBs for use in these practical applications.

These findings are taken advantage of throughout the rest of this thesis. Simulations of a polyzwitterionic brush, PSBMA, containing two modelled polymer chains are discussed in the next chapter. Specific-ion interactions between PSBMA brushes, which contain the chaotropic QA group (as is present in PMETAC brushes) and highly concentrated $ClO_4^-$ and $SCN^-$ anions will be explored. The effects of chaotropic ions on the hydration and conformation of the PZ brush will be examined and compared with results generated for PMETAC brushes (discussed in both Chapters 3 and 4).

# CHAPTER 5: ION PAIRING AND HIGHER-ORDER ION CLUSTERING IN A TWO-CHAIN ATOMISTIC POLYZWITTERIONIC BRUSH MODEL

## 5.1 Introduction

Polyzwitterionic (PZ) brushes consist of net-neutral zwitterionic polymers grafted densely to a substrate.[4] A surface modified by PZ brushes, can effectively resist protein adsorption and, therefore, PZ brushes have many potential biomedical applications.[7,15,146] The protein resistant characteristics can be modulated by specific-ion effects as they are dependent on both hydration and conformation properties of PZ brushes.[7,60,147]

Specific-ion interactions have been discussed and studied in Chapters 3 and 4 for polyelectrolyte (PE) brushes. In contrast to research carried out on PE brushes,[4–6,8,39,55,127] studies into the effects of kosmotropic and chaotropic ions on PZ brushes are relatively rare.[4,7,27] It is believed that ion pairing interactions are responsible for the specific-ion effects of PZ brushes, as has been observed for PE brushes. However, even less is known about the conformations and lifetimes of ion pairs within PZ brushes. Furthermore, the mechanism involved in how the type of ion impacts the hydration and structural behaviour of PZ brushes is still somewhat unclear.

A study by Wang *et al*.[7] examined a typical PZ brush, poly(sulfobetaine methacrylate) (PSBMA) brush (monomer illustrated in Figure 5.1), in a range of sodium salt solutions to investigate the role of increasing ionic strength as well as specific-ion interactions. A PSBMA brush comprises of pendant groups of sulfobetaine that contain a cationic quaternary ammonium (QA) group separated from an anionic sulfonate group by an alkyl spacer and belongs to a class of common PZ brushes called poly(sulfobetaine)s. According to Wang *et al.*,[7] the conformation of PSBMA brushes is influenced by two competing factors:

1. interchain/intrachain dipole−dipole cohesive interactions between sulfobetaine pendant groups.
2. interactions between water molecules and charged groups on the zwitterionic units.

Interchain/intrachain interactions favour a collapsed structure within PSBMA brushes, whereas a swollen conformation is observed upon an enhancement to the extent of hydration levels within the chains.

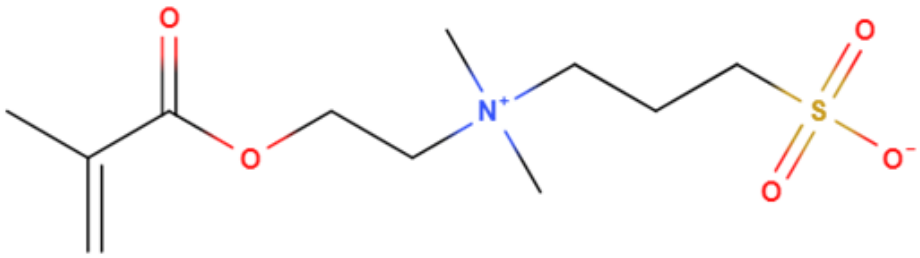


**Figure 5.1** Chemical structure of the sulfobetaine methacrylate (SBMA) monomer.

Quartz crystal microbalance with dissipation (QCM-D) was employed in order to explore the hydration and conformation of PSBMA brushes.[7] The variation in frequency measurements ($\Delta f$) relates to mass changes within the brush, or in other words, the increase or decrease in water molecules coupled to the PSBMA brush. For electrolyte solutions in the high ionic strength regime (> ~ 0.1 M), the levels of hydration within the PSBMA brush increased. Chaotropic anions were found to induce the lowest increase in hydration levels within PSBMA brushes and the anion trend for $\Delta f$ was reported as, $SCN^- < ClO_4^- < ClO_3^- < Br^-$, regarding specific-anion effects

on PSBMA brush hydration. $ClO_4^-$ anions induced greater brush hydration than was observed for $SCN^-$.

To explain the observed results, Wang *et al.*[7] suggested that in highly concentrated electrolyte solutions, there may be dissociation of ion pairs between the studied anions and QA groups along the PSBMA brush. Ion pair dissociation leaves QA groups free to bind with water molecules and, consequently, hydration levels within the brush increase. It is more difficult for a stronger ion pair to disassociate; therefore, this results in lower brush hydration levels. Within the same research, however, QCM-D measurements carried out in the low ionic strength regime, suggested that $ClO_4^-$ anions form stronger ion pairs with QA groups than $SCN^-$ anions. Therefore, this study does not fully explain why $ClO_4^-$ anions enhanced hydration levels within PSBMA brushes more than $SCN^-$.

It is clear that further research is required to improve our understanding of the interplay of interactions within PZ brushes and the role of ion pairing in influencing their conformation and hydration.[4,7,27] In this chapter, atomistic molecular dynamics (MD) simulations are used to study the influence of 0.5 M $NaClO_4$ and 0.5 M NaSCN, interacting with a PSBMA brush. According to the Hofmeister Series (Figure 1.2), both $ClO_4^-$ and $SCN^-$ anions are known to be strongly chaotropic anions, with stronger chaotropic characteristics displayed by $ClO_4^-$ anions. It is expected that both $ClO_4^-$ and $SCN^-$ anions will form ion pairs with QA groups within the PSBMA brush. The variation of brush height and hydration properties with the studied salt solutions are examined and the method for detecting ion pairs and higher-order clusters outlined in Chapter 3, is adapted for PSBMA brushes, therefore, the lifetimes and conformations of newly formed ion pairs are analysed.

## 4.2 Methods

### 4.2.1 System Description

Atomic coordinates for the initial configurations of the modelled two PSBMA chains each consisting of 100 monomers were built using the TopoTools plugin for Visual Molecular Dynamics programme (VMD)[129] and in-house codes. Each chain was tethered so that the distance between grafting points was 3.162 nm. PSBMA chains were initially constructed as fully stretched rod-like chains perpendicular to the surface (defined using LAMMPS[88] intrinsic functions) consisting of four layers of sulfur atoms, which remained fixed throughout the simulation.

A combination of two AMBER[90] force fields, ff14SB[99] and the General Amber force field (GAFF),[100] were used to model the PZ chains, thiol initiators and surface. These force fields are commonly used in combination and have been used in the simulation of polymer[101] and protein systems.[102,103] The rigid three-site SPC/E model was used to explicitly represent water molecules and was chosen because it is computationally inexpensive and widely used.[115,116] The atomic charges for the PSBMA chains and thiol initiators were calculated with the Hartree−Fock self-consistent field theory and the 6-31G* basis as described in restrained electrostatic potential (RESP) methodology.[131]

The PSBMA chains were orientated in the simulation box in such a way that the PZ chains were parallel to the *y*-axis and normal to the *xz*-plane. Periodic boundary conditions (PBCs) were set in the *x*, *y* and *z* directions. Interactions between the top of the PZ chains and the periodic image of the surface in the *y*-direction were prevented because the simulation box was larger than the fully stretched chains of the PSBMA combined with the non-bonded interaction cut-off distance.

### 4.2.2 Simulation Details

Atomistic MD simulations were performed using LAMMPS.[88] The Velocity Verlet algorithm[105] was used, with a time step of 2 fs to integrate Newton's equations of motion. Initial velocities were taken from a Maxwell distribution at 298 K and 1 atm. Energy minimisation, using the conjugate gradient method, was performed for all the systems until a mean force of less than $1.0 \times 10^{-6}$ kcal $mol^{-1}$ $Å^{-1}$ was achieved. Equilibrium runs were performed on the PSBMA brush systems in a canonical ensemble (NVT) at 500 K for 35 ns, before the system was cooled to 298 K and simulated for a further 30 ns.

Following equilibration, production runs were executed under the same conditions as the equilibrium run for 4 ns. The last snapshot of the equilibration process was used as the initial configuration. In both the equilibration and production steps, the Noose-Hoover thermostat[107] was employed. The SHAKE algorithm[132] was used to constrain the bond lengths and bond-bending angles of water molecules. The cut-off for the interatomic potential is set at 11.0 Å with long-range electrostatic interactions between charged species handled using the particle−particle particle-mesh (pppm) method[109] with a root-mean accuracy of $10^{-6}$.

Analyses of the trajectories were performed by a combination of LAMMPS[88], MDAnalysis[144,145] and in-house codes. All the analyses presented in this chapter have been performed considering the last 4 ns of each of the simulations.

## 5.3 Results

### 5.3.1 Conformation and Hydration of PSBMA Brush

Final configurations of PSBMA brush systems in water, 0.5 M $NaClO_4$ and 0.5 M NaSCN solutions are shown Figure 5.2. It is evident that the salt ions are distributed throughout the simulation box.

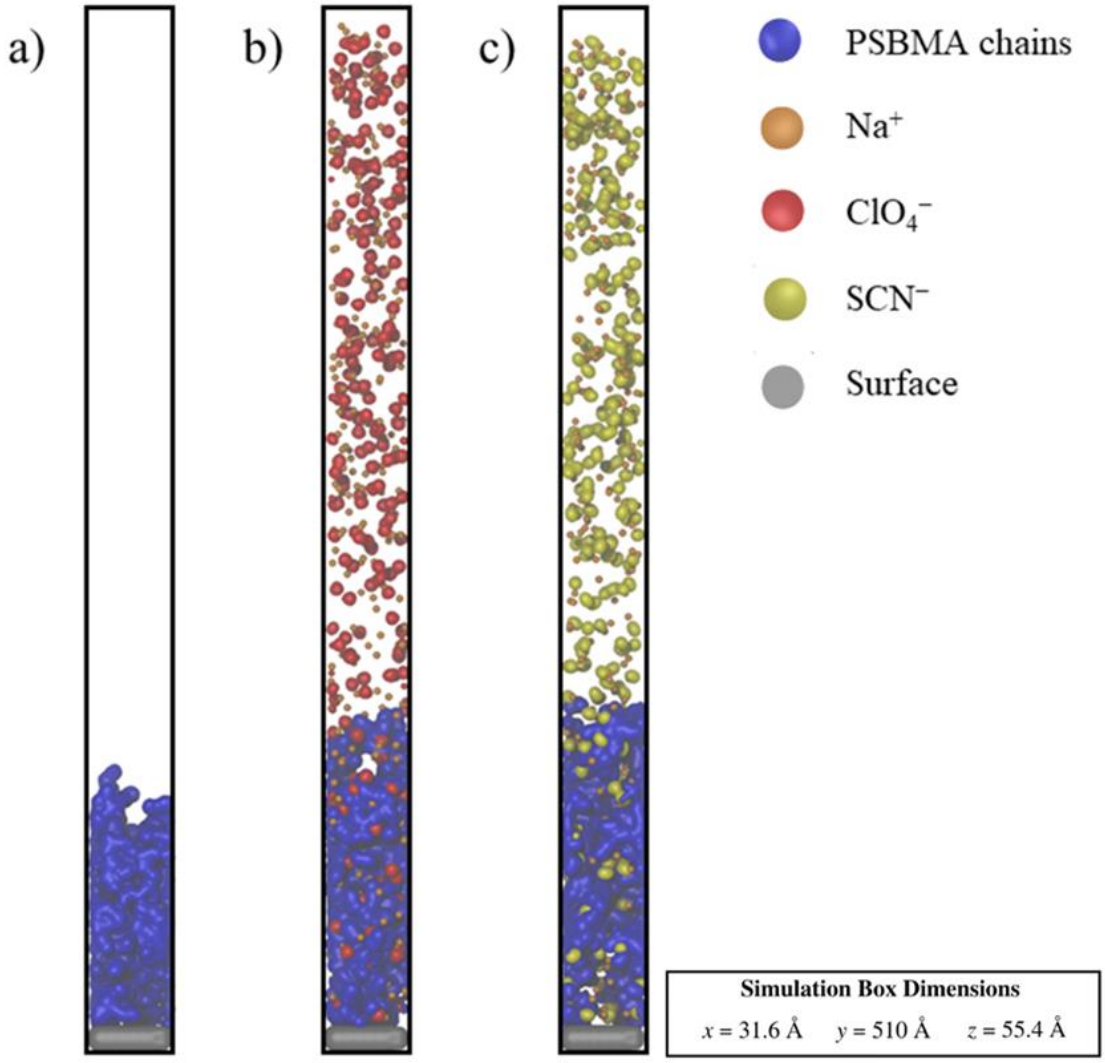


**Figure 5.2** Representation of the final configurations of the PSBMA chains in the presence of a) water, b) 0.5 M $NaClO_4$ solution and c) 0.5 M NaSCN solution. PSBMA chains are shown in blue. Sodium cations are depicted in orange, $ClO_4^-$ anions are in red, and $SCN^-$ anions are in yellow. Water molecules are not displayed for clarity.

As can be seen in Figure 5.2, the conformation of the PSBMA brush (shown in blue) was noticeably altered in the presence of 0.5 M $NaClO_4$ and 0.5 M NaSCN solutions. The end-to-end brush height (< $z_e$ >) of the PSBMA brushes in the studied solutions is presented in Figure 5.3. The height of the PSBMA brush was observed to increase in the studied salt solutions, and this effect was more prominent in the presence of $SCN^-$ compared to $ClO_4^-$ anions.

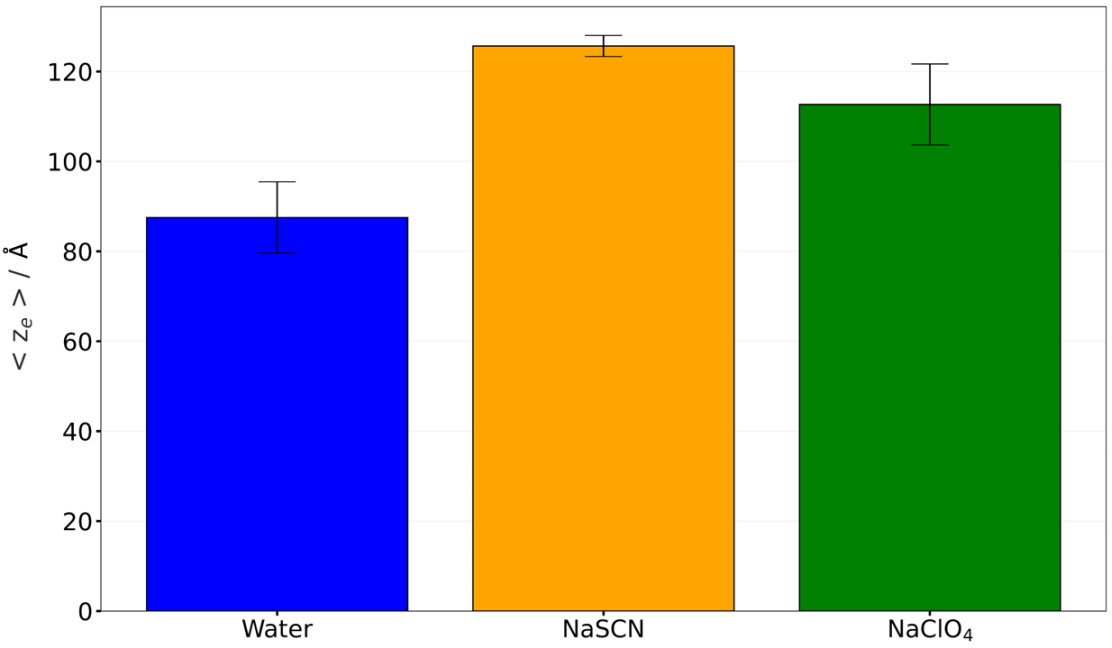


**Figure 5.3** Plot of variation in end-to-end brush height (< $z_e$ >) of the PSBMA chains in the presence of water (blue), 0.5 M NaSCN (orange) and 0.5 M $NaClO_4$ (green) solution. Error bars are shown representing the standard deviation of the set of end-to-end brush height values per PSBMA brush system.

The conformation of PZ brushes is known to be related to the interchain/intrachain dipole−dipole cohesive interactions within the PZ brush.[4,7,27] Radial distribution functions (RDFs)

of the nitrogen of QA groups ($N_{QA}$) along one PSBMA chain with the $N_{QA}$ on the other PSBMA chain are plotted in Figure 5.4. A greater proportion of QA groups are more likely to be found near each other in water than in either studied salt solutions, as indicated by the relative heights of both main peaks. The height of the first peak in the RDFs is lowest in the presence of $SCN^-$ anions compared to in water and $NaClO_4$ solution.

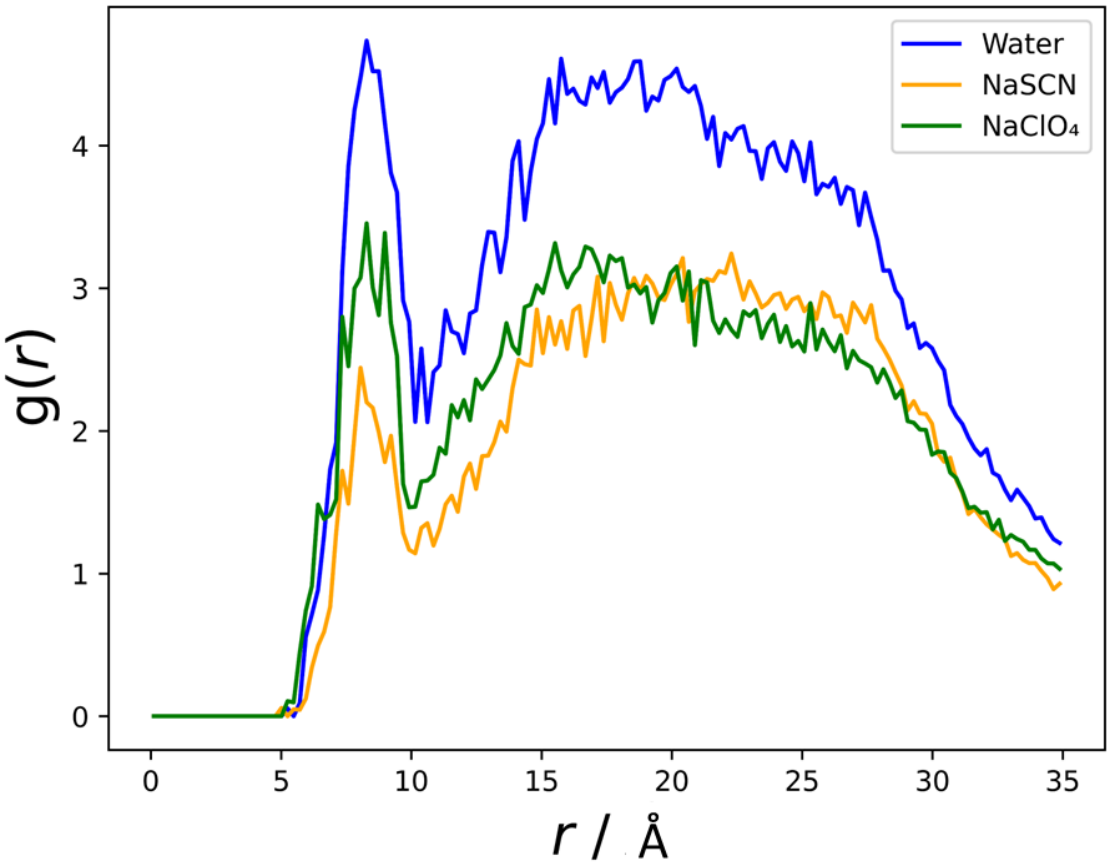


**Figure 5.4** Plot of radial distribution functions (RDFs) of the nitrogen of the QA group ($N_{QA}$) with the nitrogen of the QA groups along the PSBMA chains in the presence of water (blue), 0.5 M NaSCN (orange) and 0.5 M $NaClO_4$ (green) solution.

Upon the addition of NaSCN and $NaClO_4$ solutions, the observed change in conformation was accompanied by a significant increase in hydration levels within the PSBMA brush. As illustrated

in Figure 5.5, there was an observed increase in the number of water molecules within the PSBMA brush for both salt solutions under investigation. This was more prominently demonstrated for the brush in the presence of NaSCN than $NaClO_4$ solution.

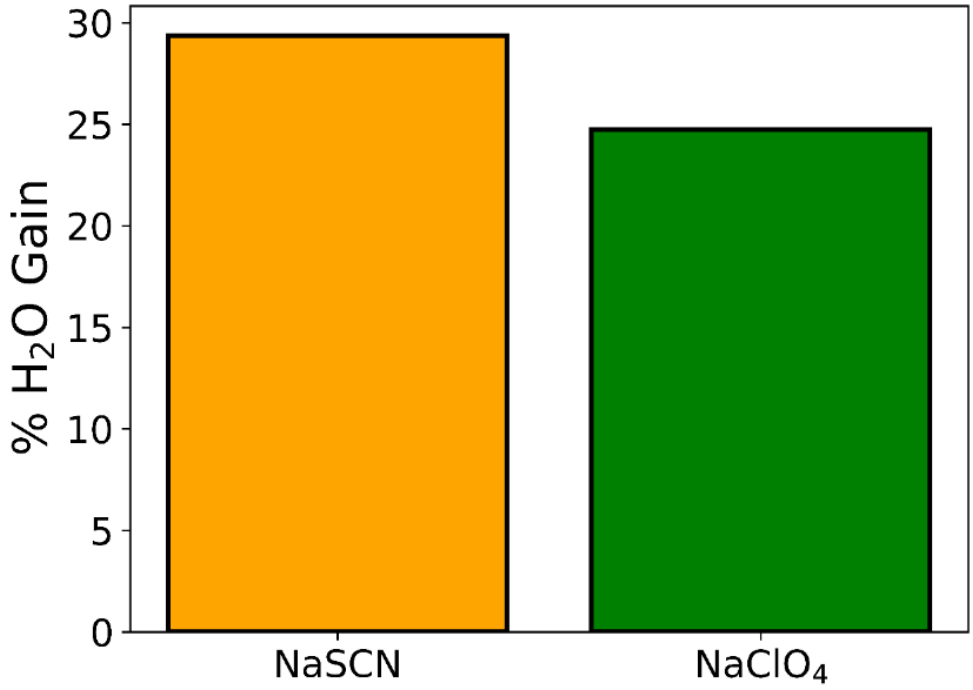


**Figure 5.5** Plot of percentage gain of water molecules within the PSBMA brush in the presence of 0.5 M NaSCN (orange) and 0.5 M $NaClO_4$ (green) solution. Values are recorded in Appendix 4: Table A.4.2

### 5.3.2 Specific-Ion Interactions

*Interactions with Anions*

Figure 5.6 shows the $N_{QA}$– $CA_{Anion}$ RDFs, where $CA_{Anion}$ represents the central atom of $ClO_4^-$ and $SCN^-$. The relative height of the first peak for the $ClO_4^-$ anions is larger compared to that for the $SCN^-$ anions thus implying a greater proportion of the $ClO_4^-$ anions were associating with the QA groups along the PSBMA chains.

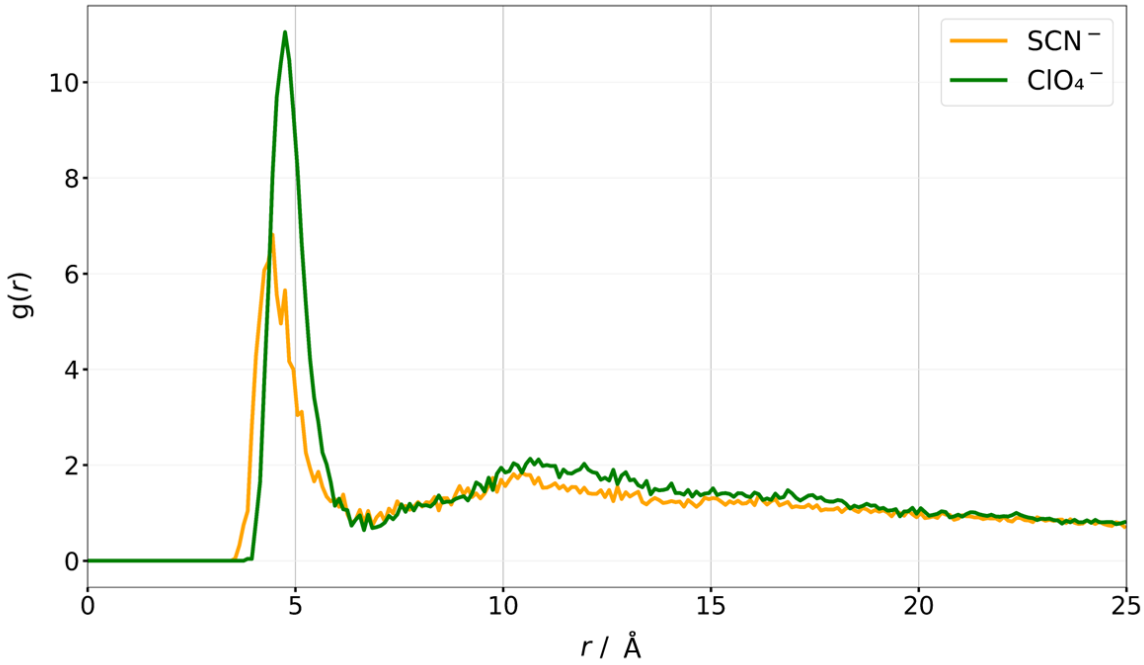


**Figure 5.6** Plot of radial distribution functions (RDFs) of the nitrogen in the QA group ($N_{QA}$) of the PSBMA chains with the $CA_{anion}$ of the $SCN^-$ anions (orange) and the $CA_{anion}$ of the $ClO_4^-$anions (green).

From the RDFs in Figure 5.6, the radius of the first coordination shell of QA groups was approximated to be 6.75 Å for the PSBMA salt solution systems under investigation. This value was used as *R* (equation 3.1) to detect ion pairs within the PSBMA brush systems, employing the same method outlined in detail in Chapter 3: Section 3.4.2. The effects of brush confinement, for the PSBMA brush systems, were estimated by calculating the diffusion coefficient (using the diffusion coefficient plug-in[133] in VMD[129]) of the $Cl^-$ counterions ($0.547 \times 10^{-9}$ $m^2$ $s^{-1}$) which were confined within the PMETAC brush but were not involved in ion pairing (Figure 3.9a). Consequently, in this chapter, it was proposed that an ion pair was formed when the studied anion resides for at least 400 ps, within 6.75 Å from QA groups in the PSBMA brush.

Graphs showing the distribution of lifetimes for the studied anions within 6.75 Å of the QA groups in the PSBMA brushes are shown in Figure 5.7. Ion pairs were observed to be present in both studied salt solutions. The ion pairs between the $SCN^-$ anions and QA groups were more labile than the ion pairs found in the $ClO_4^-$ system as indicated by the relatively shorter lifetimes of $SCN^-$ anions.

a)

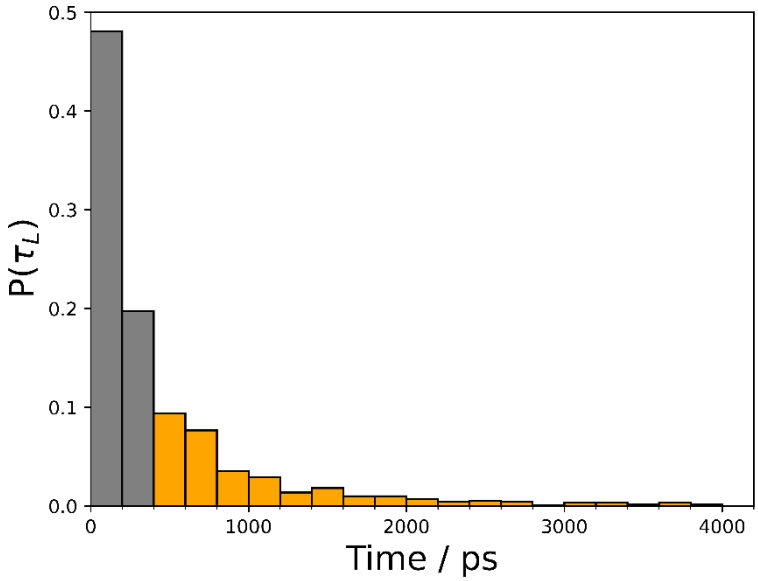


b)

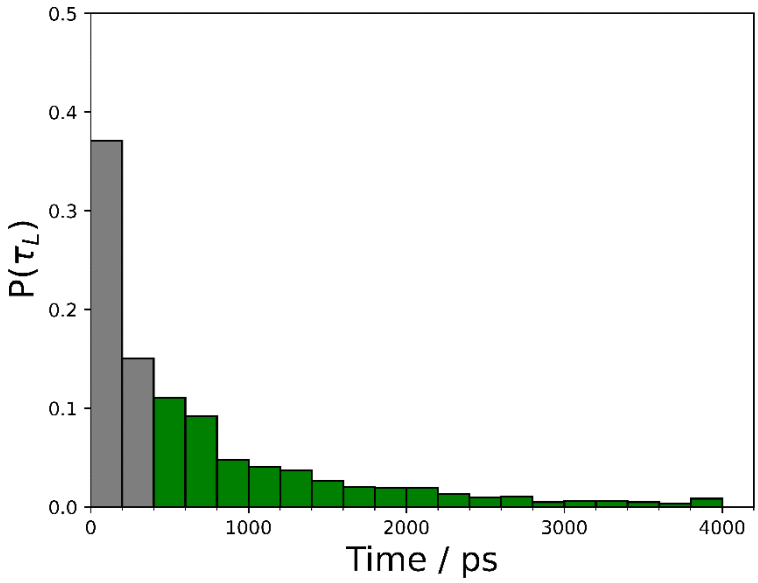


**Figure 5.7** Plots of normalised distributions of lifetimes for a) the $SCN^-$anions within 6.75 Å of the nitrogen atoms of the QA groups ($N_{QA}$) along the PSBMA chains. b) the $ClO_4^-$ anions within 6.75 Å of the nitrogen atoms of the QA groups ($N_{QA}$) along the PSBMA chains. Only ion paired anions are displayed ($t \geq 400$ ps) in colour.

Upon further analysis, both ion pairing and higher-order ion clustering, in which the QA groups interact simultaneously with two or more anions for 400 ps or longer, were observed for the PSBMA brush systems in both $NaClO_4$ and NaSCN solutions. The presence of $SCN^-$ anions was found to favour ion pairing with 55 % of QA groups (Figure 5.8) within the PSBMA brush (an example is shown in Figure 5.9a) involved in this type of ion interaction. Higher-order ion clusters were predominantly detected in the presence of $ClO_4^-$ anions, 54 % of QA groups in the PSBMA brush (Figure 5.8) were interacting with one or more $ClO_4^-$ anions (an example is shown in Figure 5.9b).

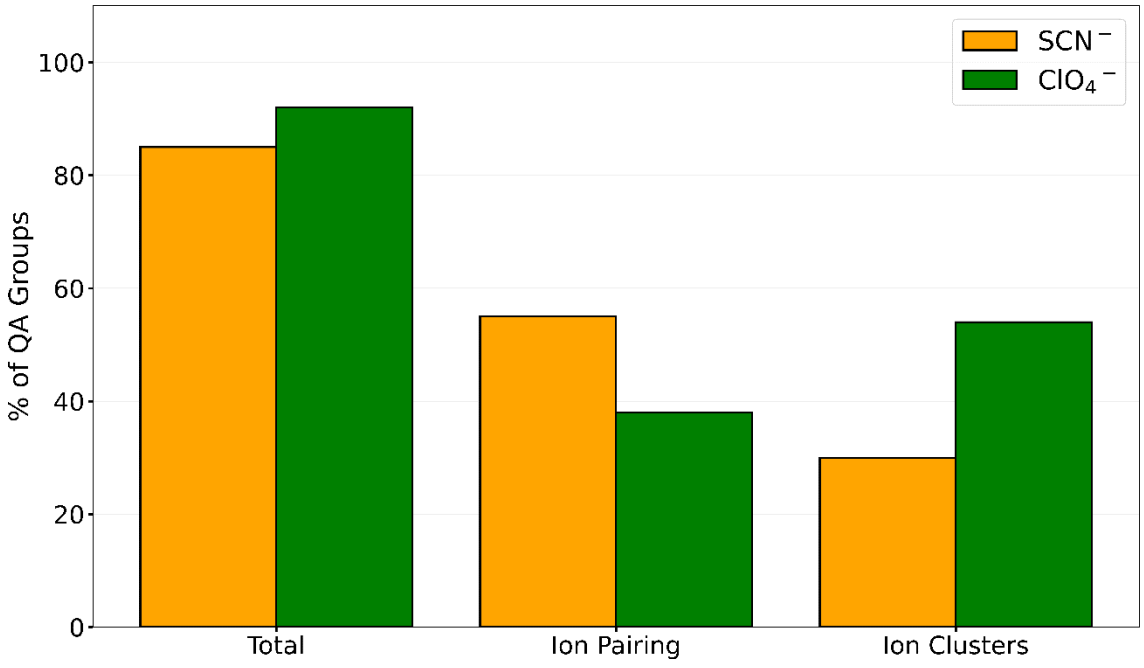


**Figure 5.8** Plot of the percentage of QA groups on the grafted PSBMA chains bound to the external salt anions, ion pairing, and higher-order ion clustering averaged over the trajectory for $SCN^-$ (orange) and $ClO_4^-$ anions (green). Values are recorded in Appendix 5: Table A.5.2.

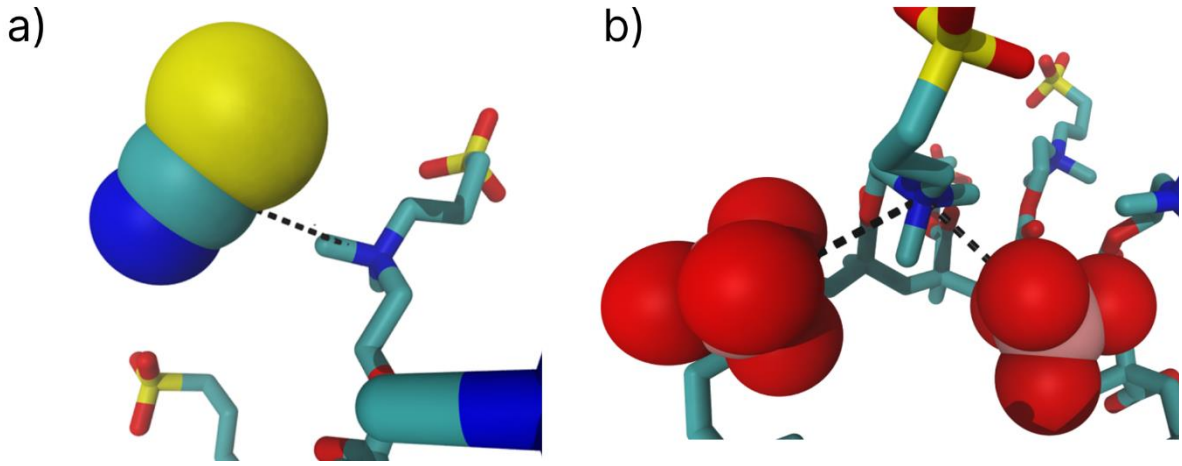


**Figure 5.9** Configurations illustrating examples of a) an ion pair forming between a QA group along the PSBMA grafted chains and one $SCN^-$ anion and b) a higher-order ion cluster forming between a QA group along the PSBMA grafted chains and two $ClO_4^-$ anions. Only relevant anions are displayed in each picture, and water molecules and hydrogen atoms are not shown for clarity. Carbon atoms are cyan, sulfur atoms are yellow, nitrogen atoms are blue, oxygen atoms are red and chlorine atoms are pink. Representations of specific-ion interactions have been added as dashed lines, to better demonstrate the ion pairing or clustering in each system.

Higher-order ion clusters in the form of ion pockets were also observed within the PSBMA brush systems in the presence of $NaClO_4$ and NaSCN solutions. An ion pocket consists of multiple QA groups interacting simultaneously with the studied anions for at least 400 ps (Figure 5.10). The observed ion pockets form with QA groups from neighbouring monomers surrounding the anion, together with QA groups from different sections of the chain, as well as different chains.

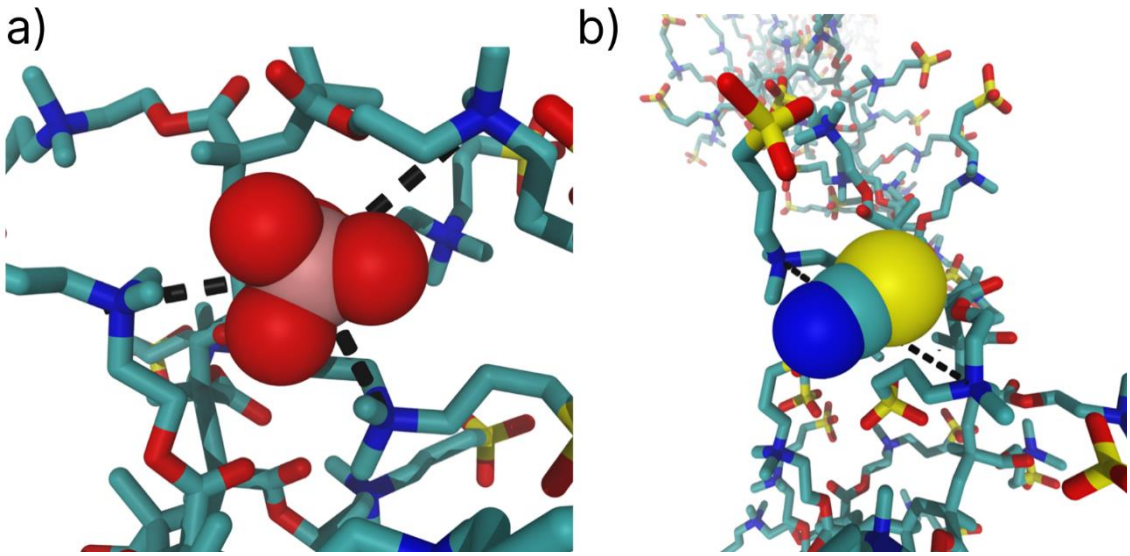


**Figure 5.10** Configurations illustrating examples of higher-order ion clusters in the form of ion pockets for a) an ion quadruplet made up of one $ClO_4^-$ anion and three QA groups along the PSBMA chains and b) an ion triplet made up of one $SCN^-$ anion and between two QA groups along the PSBMA chains. Only relevant anions are displayed in each picture, and water molecules and hydrogen atoms are not shown for clarity. Carbon atoms are cyan, sulfur atoms are yellow, nitrogen atoms are blue, oxygen atoms are red and chlorine atoms are pink. Representations of specific-ion interactions have been added as dashed lines, to better demonstrate the ion pairing or clustering in each system.

Figure 5.11 shows a frequency bar graph of the number of QA groups surrounding the anions in the last frame of the simulated trajectory. Ion pockets in the presence of $SCN^-$ anions are dominated by ion triplets ($SCN^-$ anion surrounded by two QA groups). Whereas in the presence of $ClO_4^-$ anions, ion quadruplets are often seen.

a)

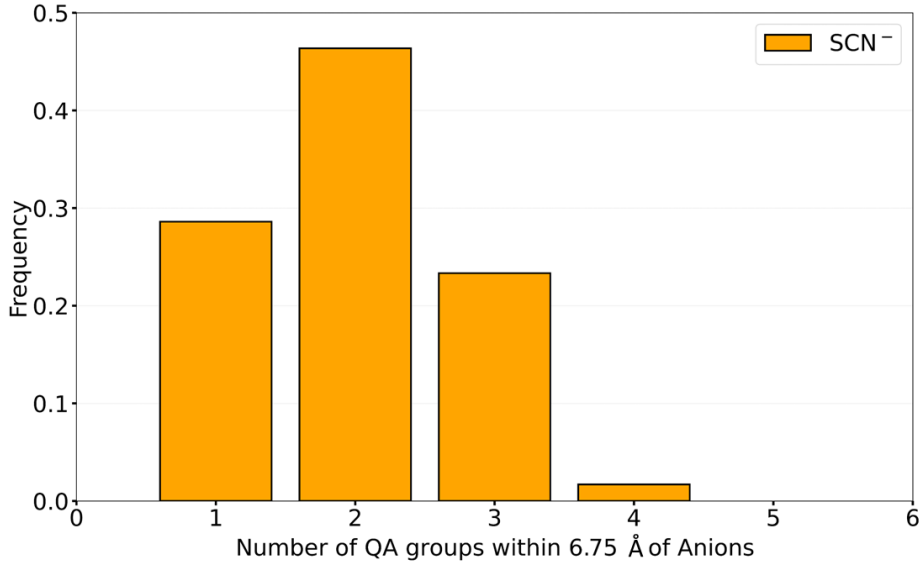


b)

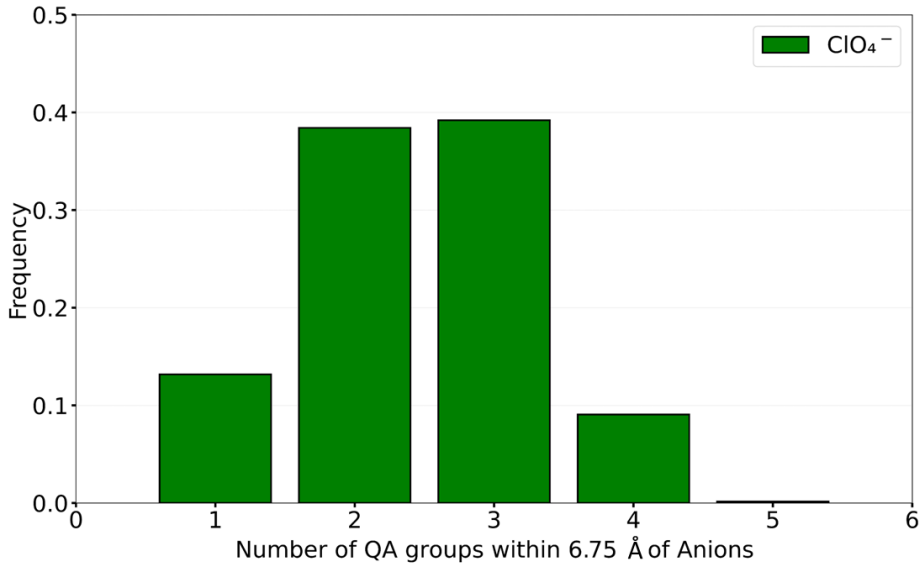


**Figure 5.11** Plots of the number of QA groups within 6.75 Å of a) $SCN^-$ anions (orange) and b) $ClO_4^-$ anions (green) taken from the last frame of trajectory.

*Interactions with Cations*

Due to the chemical structure of the PSBMA brush, $Na^+$ cations interactions with the PSBMA brush were examined. As can been seen in Figure 5.1, SBMA contains an anionic sulfonate group. Interactions between the sodium cations and the sulfonate groups were investigated using the same method to detect ion pairs discussed at length in Section 3.4.2. For the $Na^+$ cations, *R* is defined as 4.55 Å (approximated from the RDFs shown in Appendix 6: Figure A.6.1). The diffusion coefficient[133] was estimated to be, $D = 0.465 \times 10^{-9}$ $m^2$ $s^{-1}$ which is an average of the diffusion coefficients of the non-ion-paired $Na^+$ cations from the PMETAC brush system in NaSCN and $NaClO_4$ solutions (Appendix 6: Table A.6.1).

Therefore, an ion paired $Na^+$ cation is defined as residing in the first coordination shell of the sulfonate groups (*R* = 4.55 Å) along the PSBMA chains for a time longer than 600 ps. Graphs showing the distribution of lifetimes are shown in Figure 5.12. It was observed that $Na^+$ cations are involved in ion pairing with the sulfonate groups along the PSBMA brush in both NaSCN and $NaClO_4$ solutions.

a)

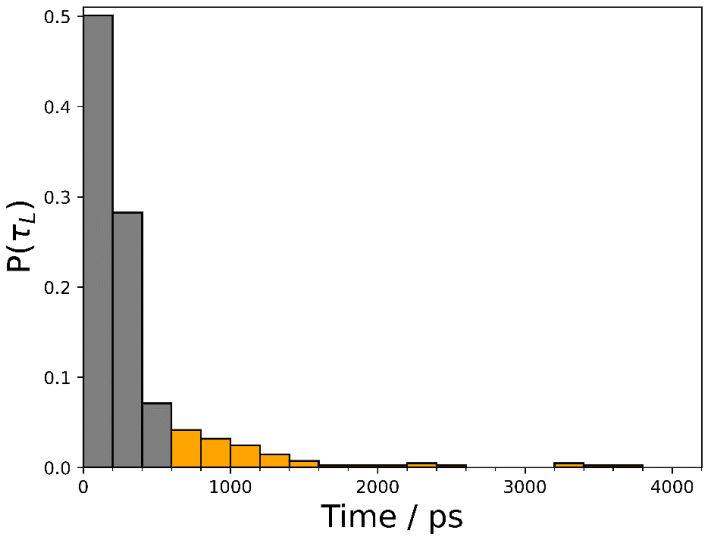


b)

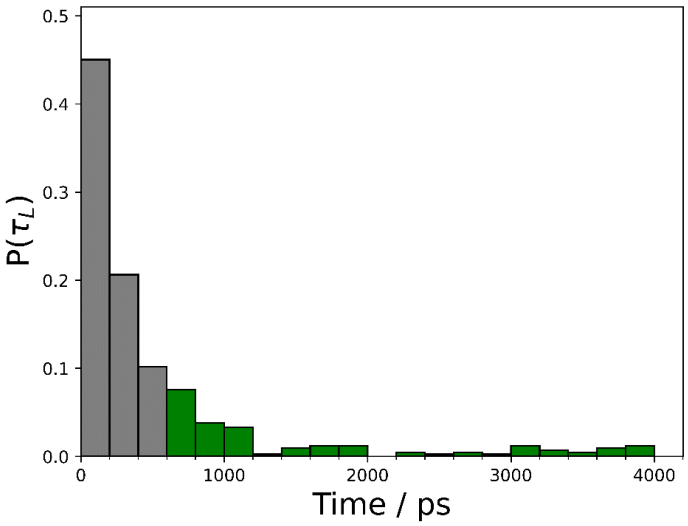


**Figure 5.12** Plot of the normalised distribution of lifetimes a) for the $Na^+$ cations within 4.55 Å of the sulfur atoms of the sulfonate groups ($S_{sulfonate}$) along the PSBMA chains in 0.5 M NaSCN. b) for the $Na^+$ cations within 4.55 Å of the sulfur atoms of the sulfonate groups ($S_{sulfonate}$) along the PSBMA chains in 0.5 M $NaClO_4$. Only ion paired $Na^+$ cations are displayed ($t \geq 600$ ps) in colour.

Although ion pairing between sulfonate groups and $Na^+$ cations can be observed in the PSBMA brush system in both $NaClO_4$ and NaSCN solutions, significantly less sulfonate groups are involved in ion pairing (Figure 5.13) compared to that seen for ion pairing interactions between QA groups and studied anions (Figure 5.8). More sulfonate groups are involved in interactions with $Na^+$ cations in the presence of $NaClO_4$ compared to NaSCN. This is true for both ion pairing and higher-order ion clustering (Figure 5.13).

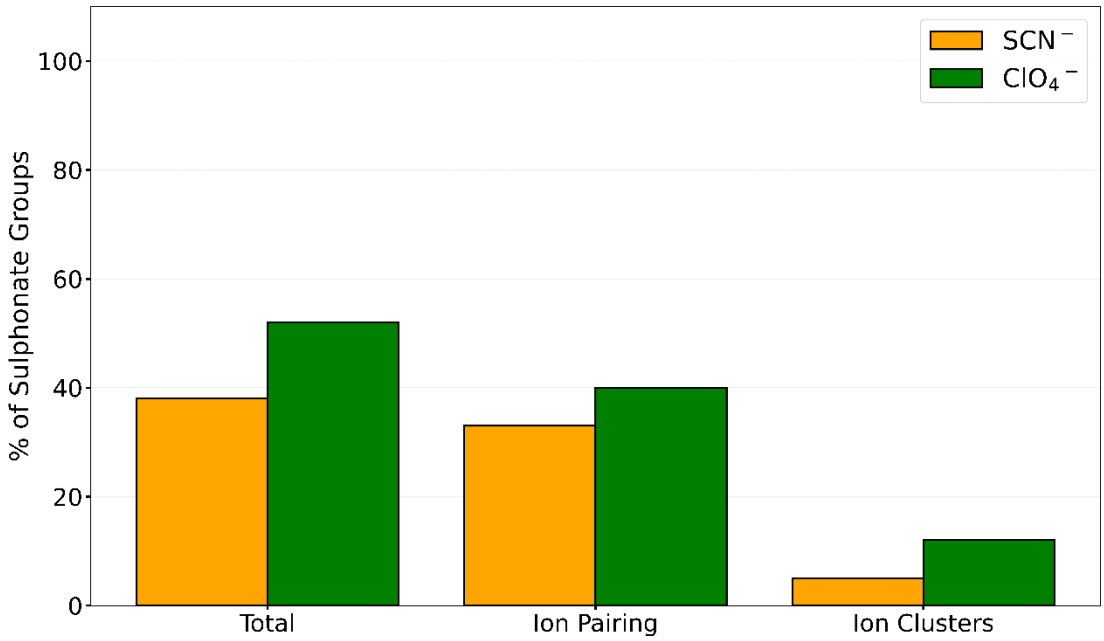


**Figure 5.13** Plot of the percentage of sulfonate groups on the PSBMA chains bound to the $Na^+$ cations, ion pairing, and higher-order ion clustering averaged over the trajectory for 0.5 M NaSCN solution (orange) and 0.5 M $NaClO_4$ solution (green).

## 5.4 Discussion

### 5.4.1 Conformation and Hydration of PSBMA Brush

Results presented in this chapter demonstrate that the presence of water, NaSCN and $NaClO_4$ solutions influences the conformation and hydration of PSBMA brushes. In water, PSBMA chains aggregate due to interchain/intrachain dipole−dipole cohesive interactions between sulfobetaine pendant groups (Figure 5.4). In 0.5 M NaSCN and 0.5 M $NaClO_4$ solutions, however, the PSBMA chains display a more swollen conformation as indicated by a larger end-to-end brush height ($< z_e >$) (Figure 5.3) and increased number of water molecules within the brush (Figure 5.5). The findings presented here demonstrate, as predicted by PZ literature,[7,29] that the studied salt ions diffuse into the PSBMA brush (Figure 5.2), disrupt interchain/intrachain interactions between the sulfobetaine pendant groups (Figure 5.4), and consequently the chains expand (Figure 5.3).[4]

The effectiveness of $ClO_4^-$ and $SCN^-$ anions at inducing a swollen conformation, within the PSBMA brush, is the reverse of that expected from the Hofmeister series (Figure 1.2). $ClO_4^-$ anions would typically be expected to have a stronger influence as $ClO_4^-$ anions are generally reportedly to be more chaotropic in nature.[7,39] It must be noted, however, that the reported position of these two anions within the Hofmeister series is reversed in some publications.[19,148] In this chapter, it was found that the presence of $SCN^-$ has a greater effect on the conformation of the PSBMA brush, disruption to interchain/intrachain associates (Figure 5.4), increase in the height of the brush (Figure 5.3) and increase in hydration levels than the presence of $ClO_4^-$ anions (Figure 5.5). To understand the difference in the behaviour of the brush in the presence of $ClO_4^-$ and $SCN^-$, ion pairing interactions were explored.

### 5.4.2 Ion Pairs and Higher-Order Ion Clusters

Graphs showing the distribution of lifetimes of $SCN^-$ and $ClO_4^-$ within the first coordination shell of QA groups (Figure 5.7), indicate that ion pairing is present within the PSBMA brushes. Higher-order ion clustering along with ion pockets were also observed for the brush in both studied salt solutions (Figures 5.8, 5.9, 5.10 and 5.11).

The findings in this chapter suggest the strength of ion pairing with the QA groups in the PSBMA brush increases from $SCN^-$ to $ClO_4^-$. As demonstrated by the tendency for $ClO_4^-$ anions to reside in the first solvation shell of the QA groups for a longer period compared to the $SCN^-$ anions (Figure 5.7), combined with the preference of $ClO_4^-$ to form higher-order ion clusters (Figure 5.8) and larger ion pockets (Figure 5.11). These results agree with several theories which predict the strength of ion pairing with the QA groups in the PSBMA brush increases from $SCN^-$ to $ClO_4^-$. The LMWA theory[40,45], for example, suggests that this is due to the ionic hydration of the anions increases from $ClO_4^-$ to $SCN^-$ and the ionic dispersion interaction theory[42] also agrees as the polarisability of the anions increases from $SCN^-$ to $ClO_4^-$.

According to the same theories, ion pairing would not be expected to be observed between the negatively charged sulfonate groups positioned along the PSBMA chains and the common $Na^+$ cations, present in 0.5 M $NaClO_4$ and NaSCN solutions. Although brief electrostatic interactions may occur, according to LMWA[45], ion pairs would not form because the $Na^+$ cations are borderline kosmotropic whereas the sulfonate groups are known to be chaotropic. Graphs shown in Figure 5.12 contradict these predictions. Evidence suggesting the presence of both ion pairing and higher-order ion clustering has been observed (Figure 5.13) within the PSBMA brush

systems between the sulfonate groups and $Na^+$ cations, albeit at a lower frequency to that seen for specific-anion interactions. While this phenomenon could arise from the overestimation of ion pairing by force fields (Section 3.4.2), it could also be related to the specific-anion interactions discussed. Upon the formation of ion pairs and higher-order ion clusters of QA groups with $SCN^-$ and $ClO_4^-$ anions, the sulfonate groups twist away from the newly formed QA-anion pairing species, thus leaving them free to engage in other interactions. The increased predominance of ion pairing species within the PSBMA chains with the $ClO_4^-$ anions may explain the increased interactions between sulfonate groups and $Na^+$ cations.

### 5.4.3 Influence of Ion Pairs and Higher-Order Ion Clusters

The presence of ion pairing interactions, both QA-anion and sulfonate- $Na^+$ interactions, within the PSBMA brush may explain differences observed in hydration for PSBMA chains in $NaClO_4$ and NaSCN solutions. To explore this, interactions between water molecules and the charged groups on the zwitterionic units of the PSBMA brush, which, as has been discussed in the introduction of this chapter, are known to influence conformational behaviour have been examined.

Firstly, the amount of water molecules in the first solvation shell of the QA groups is reduced (Figure 5.14) despite the overall increase in water throughout the PSBMA brush (Figure 5.5) in both studied salt solutions. Ion pairs and clusters are known to be hydrophobic and the higher frequency of higher-order ion clusters in the presence of $ClO_4^-$ anions may cause more significantly dehydrated QA groups. This may be, in part, why PSBMA chains are less hydrated and less swollen in the presence of $NaClO_4$ (Figures 5.3 and 5.5) compared to NaSCN solution.

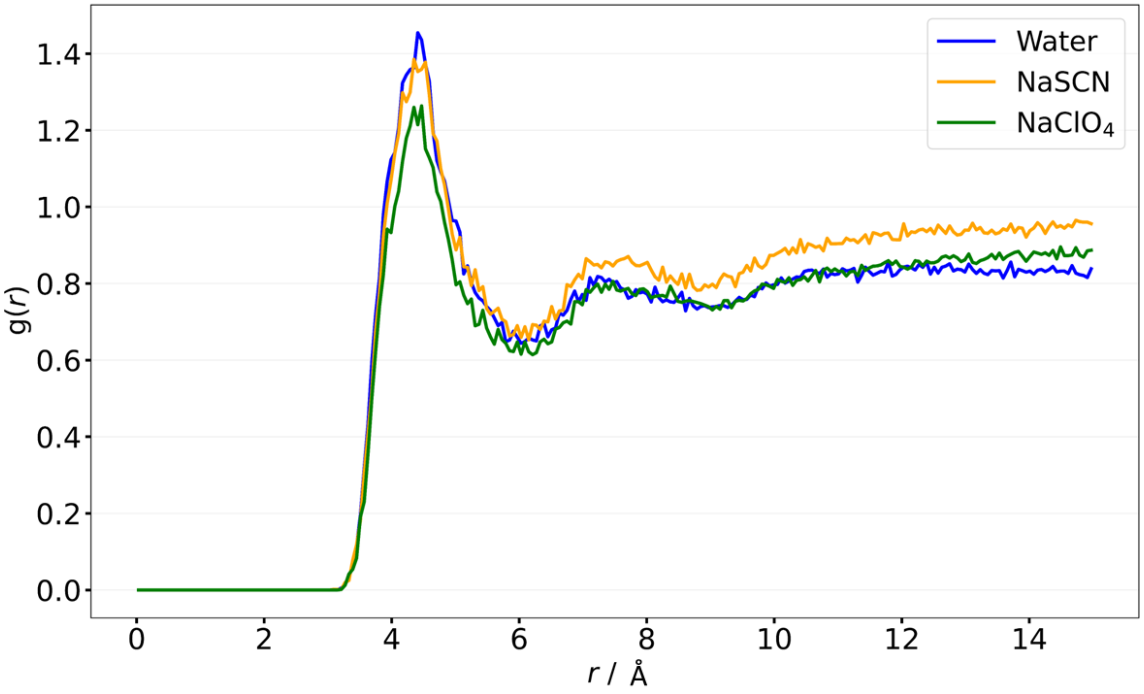


**Figure 5.14** Plot of the radial distribution functions (RDFs) of the nitrogen of QA groups ($N_{QA}$) of PSBMA chains with the oxygen of water molecules ($O_W$) in the presence of water (blue), 0.5 M NaSCN (orange) and 0.5 M $NaClO_4$ (green) solution.

Secondly, the trends for the hydration of the PSBMA brush can be further explained by examining the hydration of the sulfonate groups. Figure 5.15 shows plots of RDFs of the sulfonate group ($S_{sulfonate}$) with the oxygen of the water molecules ($O_W$). There is an increase in the amount of water molecules within the first solvation shell of each sulfonate group of PSBMA in NaSCN solution. This is somewhat counterintuitive as it would be expected that the system with the most QA groups-anion interactions, explicitly the $NaClO_4$ solution system (Figure 5.8), to be most effective at breaking interchain/intrachain interactions, therefore, leaving the sulfonate groups free to be hydrated. However, as evident by Figure 5.4, the interchain/intrachain dipole−dipole cohesive interactions within the PZ brush were more disrupted by the presence of NaSCN. Moreover, less sulfonate groups are involved in ion pairing

and clustering with the $Na^+$ cations in the presence of NaSCN compared to $NaClO_4$ (Figure 5.14). These findings may mean sulfonate groups, in NaSCN, are less sterically hindered and, therefore, better able to interact with water molecules. Hence, enhanced hydration of sulfonate groups in the presence of NaSCN solution is observed and leads to increased hydration of the PSBMA chains (Figure 5.5).

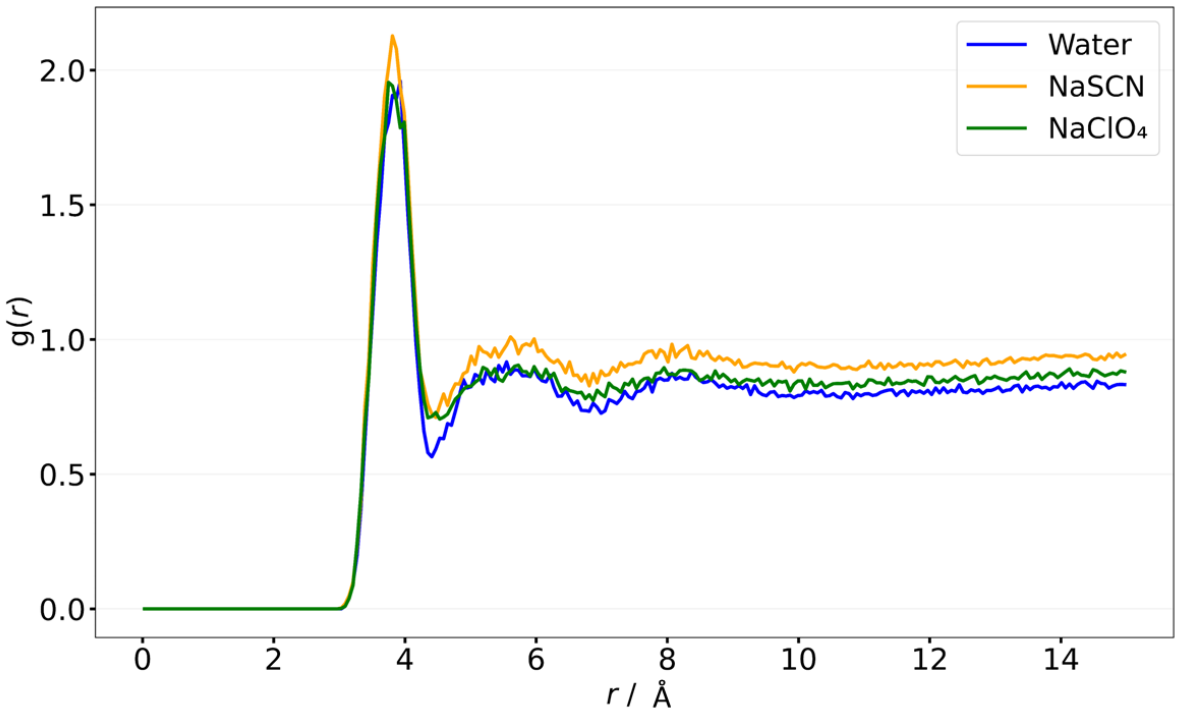


**Figure 5.15** Plot of radial distribution functions (RDFs) of the sulfur of the sulfonate group ($S_{sulfonate}$) of PSBMA chains with the oxygen of the water molecules ($O_W$) in the presence of water (blue), 0.5 M NaSCN (orange) and 0.5 M $NaClO_4$ (green) solution.

Finally, the conformation for PSBMA chains in $NaClO_4$ and NaSCN solutions is linked to the presence of ion pairing interactions. The formation of ion pockets may prevent the PSBMA chains from stretching fully as the chains bend to accommodate pockets the studied anions. The

larger ion pockets formed with $ClO_4^-$ anions (Figure 5.11) means that this effect is greater in $NaClO_4$ solution.

### 5.4.4 Comparisons

Finally, the responsiveness of PMETAC (Chapter 3) and PSBMA brushes in $NaClO_4$ and NaSCN solutions can be compared. Both brushes were observed to interact in a similar fashion with the studied chaotropic anions. This is reflected in Figures 3.5 and 5.6, where a greater proportion of $ClO_4^-$ anions associate with QA groups present in both brushes compared to $SCN^-$ anions. The interactions were observed to take the form of ion pairing (Figure 3.10 and 5.8) as had been previously predicted by the LMWA,[40,45] ion-dispersion theories[42] as well as previous research.[5,7–9] The term "ion pairing", however, does not fully describe the specific-anion interactions occurring within the PMETAC and PSBMA brushes. Higher-order ion clusters and ion pockets have been observed. Higher-order ion clustering dominates for both brushes in the presence of $ClO_4^-$ anions. Moreover, $ClO_4^-$ were observed to form larger pockets with QA groups in PMETAC and PSBMA brushes. These results suggest that $ClO_4^-$ anions may form stronger ion pairs with QA groups of both studied brushes.

Despite similarities in specific-anion interactions reported in both PBs, the observed effect of forming ion pairs, higher-order ion clusters and ion pockets is markedly different for PMETAC and PSBMA brushes. The presence of the $NaClO_4$ and NaSCN induced a collapse within the PMETAC brush (Figure 3.4), contrastingly, a swelling was reported for the PSBMA brush (Figure 5.3). This was expected and is an example of the well-known "anti-polyelectrolyte effect". It has also been observed that the presence of $NaClO_4$ solution had a more pronounced effect on

hydration and conformation of PMETAC (Figures 3.3, 3.4, 3.5, 3.8 and 3.12), whereas NaSCN had a more significant influence over the PSBMA brush (Figures 5.2, 5.3, 5.4 and 5.5).

Changes in hydration and conformation of PMETAC and PSBMA brushes are linked to the presence of ion pairs as well as the frequency and size of the higher-order ion clusters and ion pockets. These pairing species induce the opposite behaviour within the two brushes. In both PBs, for example, QA groups dehydrate (Figures 3.12 and 5.14) due to the formation of hydrophobic ion pairs and clusters. While this seems to be one of the major driving factors involved in the collapse of PMETAC, it may be less important within the PSBMA brush where the disruption of interchain/intrachain interactions, as well as the increased hydration of the sulfonate groups, seem to be more influential.

## 5.5 Conclusions

Specific-ion interactions within PZ brushes are rarely studied; despite the known influence of kosmotropic and chaotropic ions on several important properties of these types of brushes like their protein-resistance.[4,7,27] Studies that do exist have placed great importance on the formation and dissociation of ion pairs and have sought to link this to the responsiveness of PSBMA brushes.[7] To the best of our knowledge, PSBMA brushes have never before been investigated using atomistic MD simulations.

In this chapter, a fully atomistic description of PSBMA brushes has been achieved thus allowing for the exploration of the local structures and lifetimes of ions within the brushes along with macroscopic changes. It has been observed that the studied salt solutions, 0.5 M NaSCN and 0.5

M $NaClO_4$, induce a swollen conformation within the simulated PSBMA brushes. According to previous investigations,[7,29] a more pronounced swelling of the PSBMA chains, or in other words, a stronger specific-ion effect, may have been expected in the presence of NaSCN and $NaClO_4$ solutions. Longer simulations could be required to better reproduce experimental findings.

A larger increase in brush height and hydration of the PSBMA chains was observed in NaSCN compared to $NaClO_4$ solution. These findings contradict the anionic order predicted by the Hofmeister series as $ClO_4^-$ anions would typically be expected to have a stronger influence on the conformational properties of PSBMA brushes and are generally reportedly to be more chaotropic in nature.[7,39]

The strength of ion pairing interactions within the simulated PSBMA brush, however, does seem to follow the predicted order of the Hofmeister series, along with theories such as the LMWA and ionic dispersion theories. More ion pairing interactions were observed in the presence of $ClO_4^-$ anions, higher-order ion clusters were more frequent and larger ion pockets were formed between QA groups and $ClO_4^-$ anions compared to $SCN^-$ anions. These findings seem to suggest that $ClO_4^-$ form stronger ion pairing interactions with QA groups along the grafted PSBMA chains than $SCN^-$ anions. The hydration and conformational behaviour of PSBMA chains are influenced by the presence and strength of ion pairing interactions, along with the frequency and size of higher-order ion clusters and ion pockets.

Furthermore, interactions between sulfonate groups along the PSBMA chains and the studied salt solutions were examined. It was observed that there were increased interactions between

the sulfonate groups and the $Na^+$ common counterions when the PSBMA brush was in $NaClO_4$ solution. The sulfonate groups were consequently less able to interact with water in the presence of $NaClO_4$ thus perhaps causing a reduction in the hydration of PSBMA chains.

As a result of unexpected ion pairing interactions between the sulfonate groups and the $Na^+$ cations, it may be conducive to run MD simulations analysing the effects on ion pairing of changing the cation of the studied electrolyte solutions. It must be noted, however, that Wang *et al.*[7] found very little cation-dependency in his research. Cation-dependency within PZ brushes should be further investigated and may prove to be important as the results, reported in this chapter, indicate that cations present in added electrolyte solutions may play a role in determining the conformation and hydration levels of the PSBMA brush.

The nature and conformations of ion pairing, higher-order ion clustering and ion pockets elucidated thus far in this thesis, expands our understanding of specific-ion interactions between PE and PZ brushes and chaotropic anions. Numerous avenues of research could now be embarked on. For example, it could prove to be pertinent to examine the structure and dynamics of water molecules around the ion pairing species. It is well-known that due to the number of additional interactions, the structure and dynamics of water are modified in biological systems (biological water)[149] and these changes significantly affect responses in the human body.[149–151] Parallels can be drawn between biological water and water contained within PBs. Future investigations into the distribution and local arrangement of water molecules around ion pairs, higher-order ion clusters and ion pockets could potentially provide additional information about the changes within the structure of PBs in the presence of chaotropic anions.

Furthermore, thus far, only electrolyte solutions containing strongly *chaotropic* anions have been examined. However, both experimentally[4,6,8,39,127] and computationally,[5,56] it is known that *kosmotropic* anions influence conformation and hydration behaviours of these PBs by way of a different mechanism. In the next chapter, initial investigations are undertaken to examine to behaviour of $SO_4^{2-}$ anions with PMETAC brush models.

# CHAPTER 6: INTERACTIONS BETWEEN SULPHATE ANIONS AND ATOMISTIC POLYELECTROLYTE BRUSH MODELS.

## 6.1 Introduction

The Hofmeister series ranks the relative influence of ions on the physical behaviour of a wide variety of processes.[31,152] Within the series, ions are classified as either *kosmotropes* (structure-making), or *chaotropes* (structure-breaking) (Figure 1.2).[31,148,152] Chaotropic and kosmotropic ions have distinct effects on species in solution.[5,7,8,27,31,70,148,152–154] Thus far in this thesis, effects of strongly *chaotropic* ions on polyzwitterionic (PZ) and polyelectrolyte (PE) brushes, have been discussed and investigated. However, previous experimental studies have shown that the addition of *kosmotropic* anions can also influence hydration levels and conformational behaviour within PZ and PE brushes.[3,6,7,27]

Kou *et al.*[8] examined a PE brush, poly (2-(methacryloyloxy) ethyl trimethylammonium chloride) (PMETAC) brush. PMETAC brushes were systematically studied in the presence of a range of sodium salt solutions, some of which contained kosmotropic anions and others chaotropic anions, using quartz crystal microbalance with dissipation (QCM-D) and spectroscopic ellipsometry (SE). It was found that chaotropic anions induced a more pronounced collapse than kosmotropic anions, as had been observed in previous research from Azzaroni *et al.*[11] and Wei *et al.*[58]

Somewhat unexpectedly, however, an increase in ionic strength of highly kosmotropic $Na_2HPO_4$ solution and $Na_2SO_4$ solution (from 1 mM to 500 mM) has been found to only minimally affect hydration levels and conformational behaviour within the PMETAC brush.[8] Brush collapse would have been expected to occur in the presence of any highly concentrated electrolyte solution due

to the increased screening of chain charges and changes in osmotic pressure. It was later suggested by Wanless *et al.*[6] that the negligible effect on brush responsiveness, observed in the presence of $HPO_4^{2-}$ and $SO_4^{2-}$, could be due to the divalent nature of these anions. It is believed that a bridging-type interaction between neighbouring chains could occur as the divalent anions simultaneously interact with two quaternary ammonium (QA) groups. The brush would consequently become cross-linked, as has been previously proposed in research by Wang *et al.*[67] and Moya *et al.*[155] studying the behaviour of PDMA and PMETAC brushes, respectively, in the presence of $SO_4^{2-}$ anions. This cross-linking of polymer chains within the PMETAC brush is deemed to be responsible, in part, for the lack of variation in brush thickness and hydration levels in the presence of differently concentrated $Na_2HPO_4$ and $Na_2SO_4$ solutions.[6]

The unresponsive nature of PMETAC brushes in $Na_2SO_4$ solutions was also observed in molecular dynamics (MD) simulations performed by Santos *et al*..[5] No significant conformational changes in the PMETAC brush were reported in the presence of kosmotropic $SO_4^{2-}$ anions (150 mM). Swelling coefficients were used to report changes in the height of the brush, defined as the maximum height of the brush in the studied solution divided by the maximum height of the brush in its dry state (in cyclohexane solution). In water, the swelling coefficient was reported as 2.1, whereas the swelling coefficient was approximately 2.0 in 0.15 M $Na_2SO_4$ solution.[5] The change in conformation was minimal.

These results have been suggested to be caused by an absence of ion pairs formed between QA groups along the PMETAC brush and $SO_4^{2-}$ anions.[3,6] The Law of Matching Water Affinities (LMWA)[45] (Figure 1.4) states that strongly hydrated, kosmotropic anions will not form ion pairs with weakly hydrated, chaotropic QA groups of the PMETAC brush. Specific-ion interactions

between the brush and kosmotropic anions were, instead, concluded to be dominated by the ability of kosmotropic anions to engage in competition with QA groups for water molecules that are situated within the PMETAC chains.[8] Graphs showing radial distribution function plots indicated that $Na_2SO_4$ anions interacted weakly with QA groups and strongly with the aqueous solvent. These findings do not support the idea suggested by Wanless *et al.*[6] that $SO_4^{2-}$ anions enable bridging-type interactions between neighbouring PMETAC chains.

Within the same research by Santos *et al.*,[5] GROMOS-derived parameters were used to represent components, including salt ions, contained within the studied PMETAC brush systems. There have previously been reports, however, that salts containing divalent oxyanions can be challenging to simulate using non-polarisable force fields such as GROMACS.[156] Very few MD simulations of salts consisting of these anions have been performed,[156–159] but in those that do exist and specifically for $Na_2SO_4$ solutions, a range of sulfate force fields have been examined and excessive ion aggregation has been reported.[157–159] Mason *et al.*[157] observed nanometre-scale ion aggregates, in the form of dynamic wormlike chains and plates, from MD simulations of aqueous guanidinium sulfate.[157] Several tests were consequently carried out to determine whether clustering might be a simulation artifact. However, aggregates were found not be due to the periodicity of the system, the concentration of ions or an artifact of the chosen water model.[157] It became clear that the excessive aggregation of $Na_2SO_4$ was due to the non-polarisable atomistic parameters. Although Santos *et al.*[5] did not report $Na_2SO_4$ aggregation, they did not observe a significant change in the height of the brush in $Na_2SO_4$ solution and also found the GROMACS parameters failed to reproduce the experimental differences in behaviour of the PMETAC brush in $Na_2SO_4$ and NaCl, both kosmotropic salt solutions.

Interactions between $SO_4^{2-}$ anions and PMETAC brushes evidently require further examination to fully understand the molecular mechanism involved and their effects on conformational brush behaviour. In this chapter, atomistic MD simulations have been used to study the influence of highly concentrated electrolyte solution, 0.5 M $Na_2SO_4$, interacting with the two-chain and eight-chain PMETAC brush models. Sodium was used as a common counterion within the studied electrolyte solution to allow comparison with the effects of $SO_4^{2-}$ anions and the chaotropic $ClO_4^-$ and $SCN^-$ anions (Chapter 3). According to the Hofmeister Series (Figure 1.2), $SO_4^{2-}$ is one of the most kosmotropic anions. It is expected that the $SO_4^{2-}$ anions will not form ion pairs with the QA groups within the PMETAC brush. The variation of brush height and hydration properties with the studied salt solutions were examined and the appropriateness of using non-polarisable force fields to represent $Na_2SO_4$ solutions is discussed.

## 6.2 Methods

### 6.2.1 System Description

Atomic coordinates for the initial configurations of the modelled two and eight polymer chains each consisting of 100 monomers were built using the TopoTools plugin for Visual Molecular Dynamics programme (VMD)[129] and in-house codes. Each chain was tethered so that the distance between the grafting points was 3.162 nm, leading to a grafting density of 0.1 chains $nm^{-2}$. Polymer chains were initially constructed as fully stretched rod-like chains perpendicular to the surface (defined using LAMMPS[88] intrinsic functions) consisting of four layers of sulfur atoms that remained fixed throughout the simulation. The $Na^+$ and $SO_4^{2-}$ salt ions were initially placed 150 Å above the PMETAC chains within the two-chain system. In the eight-chain PMETAC brush system, however, $Na^+$ and $SO_4^{2-}$ salt ions were initially placed approximately 20 Å above the PMETAC chains.

A combination of two AMBER[90] force fields, ff14SB[99] and the General Amber force field (GAFF),[100] were used to model the polymer chains, ions, thiol initiators and surface. These force fields are often used in combination and have been used in the simulation of polymer[101] and protein systems.[102,103] The rigid three-site SPC/E model was used to explicitly represent water molecules and was chosen because it is computationally inexpensive and widely used.[115,116] The atomic charges for the polymer chains and thiol initiators were calculated with the Hartree−Fock self-consistent field theory and the 6-31G* basis as described in restrained electrostatic potential (RESP) methodology.[131]

The polymer chains were orientated in the simulation box in such a way that the chains were parallel to the *y*-axis and normal to the *xz*-plane. Periodic boundary conditions (PBCs) were set in the *x*, *y* and *z* directions. Interactions between the top of the chains and the periodic image of the surface in the *y*-direction were prevented because the simulation box was larger than the fully stretched chains combined with the non-bonded interaction cut-off distance.

### 6.2.2 Simulation Details

Atomistic MD simulations were performed using LAMMPS.[88] The Velocity Verlet algorithm[105] was used with a time step of 2 fs to integrate Newton's equations of motion. Initial velocities were taken from a Maxwell distribution at 298 K and 1 atm. Energy minimisation, using the conjugate gradient method, was performed for all the systems until a mean force of less than $1.0 \times 10^{-6}$ kcal mol$^{-1}$ Å$^{-1}$ was achieved. Equilibrium runs were performed on the two-chain PBs in a canonical ensemble (NVT) at 500 K for 35 ns, before the system was cooled to 298 K and simulated for 30 ns. The eight-chain PB systems were simulated for significantly less time, 4 ns at 500 K, followed by 2 ns at the same temperature but with force added to $Na^+$ and $SO_4^{2-}$ salt ions to encourage interactions with the PMETAC chains. The additional forces were then

removed, and the simulation ran for 25 ns at 500 K. The system was then cooled to 298 K and simulated for an additional 6 ns.

Following equilibration, production runs were executed in the same conditions for 4 ns. The last snapshot of the equilibration process was used as the initial configuration. In both the equilibration and production steps the Noose-Hoover thermostat[107] was employed. The SHAKE algorithm[132] was used to constrain the bond lengths and bond-bending angles of water molecules. The cut-off for the interatomic potential is set at 11.0 Å with long-range electrostatic interactions between charged species handled using the particle−particle particle-mesh (pppm) method[109] with a root-mean accuracy of $10^{-6}$. Analyses of the trajectories were performed by a combination of LAMMPS[88], MDAnalysis[144,145] and in-house codes.

## 6.3 Results

The addition of 0.5 M $Na_2SO_4$ solution caused no discernible change in the height of the PMETAC brush (Appendix 7: Figure A.7.1). This contrasts with the collapse in brush conformation as demonstrated by a significant decrease in brush height (Figures 3.4 and 4.2), while in the presence of 0.5 M $NaClO_4$ and 0.5 M NaSCN solutions. The lack of a significant conformational change in the PMETAC brush in the presence of $SO_4^{2-}$ anions, reported in this thesis, suggests that the chosen atomistic parameters from the AMBER force fields range[90] may not be accurately describing the behaviour of $SO_4^{2-}$ anions.

## 6.4 Discussion

### 6.4.1 Specific-Ion Interactions

It has been discussed, throughout this thesis, that understanding the interactions between salt ions and each PB system is essential to understanding the conformational behaviour and

hydration levels within PBs. Figure 6.1 shows the final configuration of the two-chain PMETAC brush system in 0.5 M $Na_2SO_4$ solution. From this, it is clear that no $Na^+$ or $SO_4^{2-}$ ions have diffused into the brush. $Na_2SO_4$ anions have, instead, aggregated together at a considerable distance ($\sim$ 100 Å) away from the average maximum height of the PMETAC chains. Therefore, no screening of QA groups is possible, and the chains remained fully hydrated.

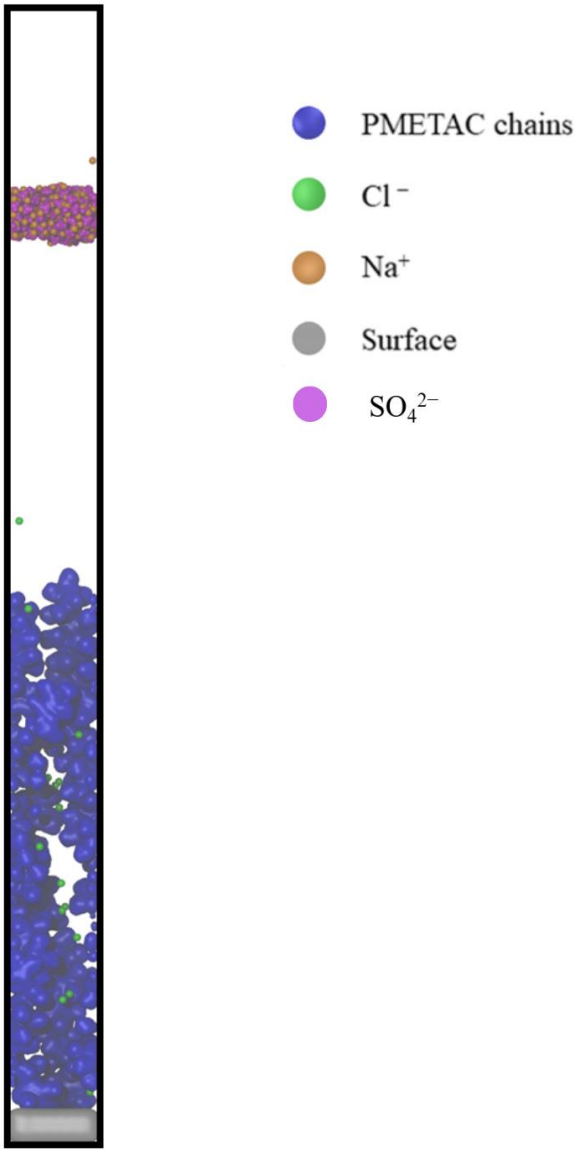


**Figure 6.1** Configuration for the two-chain PMETAC brush in the presence of 0.5 M $Na_2SO_4$ solutions. PMETAC chains are shown in blue. $Cl^-$ are green. $Na^+$ are orange and $SO_4^{2-}$ are magenta. Water molecules are not displayed for clarity.

The same phenomenon was observed for the eight-chain PMETAC brush system. This was despite modifying the starting positions of $Na_2SO_4$ salt ions by initially placing them significantly closer to the PMETAC chains and testing whether $Na_2SO_4$ ions could be forced into interacting

with the PMETAC brush. Nevertheless, only two $SO_4^{2-}$ anions diffused into the brush, the rest are, again, involved in aggregation above the fully stretched PMETAC chains (Figure 6.2).

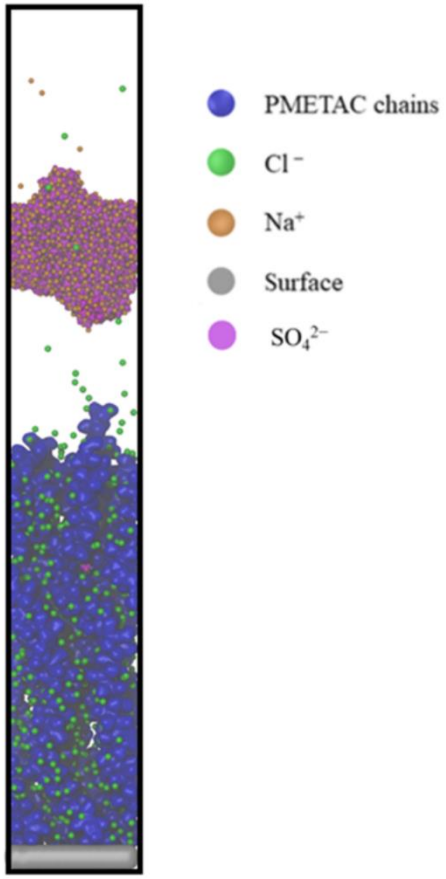


**Figure 6.2** Configuration of the eight-chain PMETAC system in the presence of 0.5 M $Na_2SO_4$. PMETAC chains are shown in blue. $Cl^-$ are green. $Na^+$ are orange and $SO_4^{2-}$ are magenta. Water molecules are not displayed for clarity.

$Na_2SO_4$ salt ions were observed to form a dynamic aggregate and, consequently, most $SO_4^{2-}$ anions (and $Na^+$ cations) are unavailable for interactions with the simulated PMETAC brushes. For both the two-chain and eight-chain PMETAC brush systems, no significant change in brush height was observed.

### 6.4.2 $Na_2SO_4$ Ion Aggregation Phenomenon

The results presented in this chapter show that excessive aggregation of $Na_2SO_4$ ions occurred within the simulated PMETAC brush systems, as discussed in Section 6.1 for previous studies employing MD techniques.

To avoid the dynamic aggregation of $Na_2SO_4$ ions observed in this chapter and in previous studies, it may be fruitful to further alter the starting configurations used throughout this chapter and initially place the ions in $Na_2SO_4$ solutions throughout the brush (rather than above the chains). Nevertheless, it is possible that aggregates may then form with QA groups along the PMETAC chains. Alternatively, a fundamental alteration in the modelling of the $Na_2SO_4$ solution is required. It has been reported that unrealistic aggregation behaviour is not observed for polarisable models of $SO_4^{2-}$ anions.[156,160] It is believed that this is due to the polarisation of the first solvation shell of $SO_4^{2-}$ anions.[156,160] The anions are consequently stabilised and the contact ion pairing leading to large aggregates tends to be supressed.[156,160] By including electronic polarisation effects, aggregation of $Na_2SO_4$ may be avoided and specific-ion interactions with the PMETAC brushes may be explored. Including an explicit polarisation effect, however, considerably increases the computational cost of the simulations. The computational cost of building and running a PB system and subsequent simulation is already substantial, therefore, the additional cost of polarisability effects may be unfeasible. A significant compromise in the size of the simulated PB would be required. This thesis has suggested that finite size effects have minimal influence on the brush systems so it may be possible to simulate one or two polymer chains. To compensate for the extra computational cost, however, it may also be necessary to reduce the length of the polymer chains which could affect the reproducibility of results experimentally.

## 6.5 Conclusions

This chapter has presented results generated from atomistic MD simulations performed on the two-chain and eight-chain PMETAC brush in 0.5 M $Na_2SO_4$ solution. The height of brush in the presence of kosmotropic $SO_4^{2-}$ anions was found to be unchanged from the height of the brush in water. It was found that the $Na_2SO_4$ ions were observed to aggregate above the polymer chains in the form of one large dynamic ion cluster. Almost all, if not all, $SO_4^{2-}$ anions and $Na^+$ cations in the two-chain and eight-chain PMETAC brush systems are so strongly involved in aggregation, they are unavailable to interact with the PMETAC chains. This lack of interactions leads to no discernible change in the hydration and conformation properties of the PMETAC chains.

It has been consequently concluded in this chapter that the parameters, from the ff14SB[99] and GAFF[100] parameter sets, while accurate for describing the properties of PMETAC brushes in the chaotropic salt solutions presented in Chapters 3 and 4, may not be accurately describing the behaviour of $SO_4^{2-}$ anions and their interactions with PMETAC brush systems. Previous simulations using non-polarisable force fields have also reported excessive aggregation of salts containing divalent oxyanions seen throughout this chapter.[156–159] The computational investigation by Santos *et al*.[5] and discussed in Section 6.1, used non-polarisable force fields from GROMOS parameter sets.[161] Although they did not report the salt aggregation discussed in this chapter, they did not observe a significant change in the height of the brush in $Na_2SO_4$ solution. Furthermore, they found that the parameters failed to reproduce the experimental differences in the behaviour of the PMETAC brush in $Na_2SO_4$ and NaCl, both kosmotropic salt solutions. To explore this, they examined effects on the conformation of the brush of assigning different atom types within the GROMOS parameter set 54A7 to the sulfur and oxygen atoms in

sulfate anions. No significant improvements were observed regarding reproducing experimental results.[5] The behaviour of $SO_4^{2-}$ anions, therefore, would more than likely not be altered by changing the atom types within the AMBER parameter sets within our study.

Results presented in this chapter indicate that more sophisticated models are required to accurately describe the behaviour of $SO_4^{2-}$ anions and their interactions with the studied PBs. It has been previously reported that polarisable models do not tend to reproduce the unrealistic aggregation behaviour for $SO_4^{2-}$ anions that has been observed throughout this chapter.[156,160] However, balancing the computational expense related to the explicit inclusion of polarisability effects with an adequate amount of time for equilibration of brush dynamics is a necessary consideration when performing atomistic simulations on PBs.

For future computational studies exploring the effects of kosmotropic anions on PBs, it may be effective to first attempt simulating a different type of kosmotropic anion, such as the monovalent acetate anion. Although significantly less kosmotropic than $SO_4^{2-}$ anions, acetate anions have been found to influence the behaviour of PMETAC brushes. In research undertaken by Kou *et al.,* [8] acetate anions were found to induce a collapse within the PMETAC brush to a significantly lesser extent than monovalent chaotropic anions. Specific-ion interactions between acetate anions and the studied PBs should be investigated first before further investigating complex polarisable models for $SO_4^{2-}$ anions.

In future computational studies, including those using polarisable models to study sulfate anions or those examining different kosmotropic ions within the PB models, it will be important to

explore the structure and dynamics of water. Experimental research has suggested that specific-ion interactions involving kosmotropic anions with PBs are due to competition with QA groups for water molecules that are situated within the brushes. A robust method will be needed to explore the hydrogen-bond network observed in the water contained in PBs. The importance of the role of water in multiply charged ionic system has been highlighted in a standalone study discussed in the next chapter. Conformational transitions have been reported for flexible molecules with two charge centres at a distinct number of water molecules and investigated systematically.

# CHAPTER 7: EFFECTS OF HYDRATION ON THE CONFORMATIONAL BEHAVIOUR OF FLEXIBLE MOLECULES WITH TWO CHARGE CENTRES

## 7.1 Introduction

This chapter is based on the paper, "Effects of Hydration on the Conformational Behaviour of Flexible Molecules with Two Charge Centres" published in the Journal of Physical Chemistry A in 2020.[91] We examined alkyl-dicarboxylate di-anions, [$^{-}O_2C(CH_2)_mCO_2^{-}$] ($DC_m$) and alkyl-diammonium di-cations [$^{+}H_3N(CH_2)_mNH_3^{+}$] ($DA_m$), in which the two distinct charge centres are separated by a hydrophobic, flexible alkyl $(CH_2)_m$ chain, over a range of alkyl chain lengths (*m*). Using global optimisation techniques, the conformational behaviour of these di-ions was investigated in unhydrated, implicitly solvated, and explicitly solvated conditions (where the number of water molecules modelled is defined as *n*).

The presence of ionic functional groups are critical for the hydration of large biomolecules.[150,162] In proteins and peptides containing the 20 naturally occurring amino acids, there are only three types of ionic group present: ammonium, guanidinium and carboxylate.[163] Investigations into the extent of interactions between these ionic groups and water can give insight into the behaviour of peptides and proteins.[162,164,165] $DC_m$ and $DA_m$ can act as a simple model for peptides.[166] it is thought that some solvent-mediated folding processes could perhaps be better understood by studying the stepwise hydration of these types of di-ions in the gas phase.[163,166–172]

Before our paper was published in 2020, several theoretical[169,173] and experimental studies[171,172,174–177] had been undertaken to understand the interactions of both the $DA_m$ and $DC_m$ with finite water clusters $(H_2O)_n$. Hydrated $DA_m$ were methodically studied by Jahangiri *et al.,*[173]

for $m$ = 5 - 10 and $n$ = 10 - 40, using molecular dynamics (MD) simulations. For small numbers of water molecules, the two charged ends of the $DA_m$ were found to be hydrated by two separate, small water clusters.[173] This is in agreement with the experimental results of Kebarle and co-workers,[178] who measured the stepwise binding energies of $DA_m$ for $n$ = 1 - 6. Jahangiri *et al.*[173] found that, as $n$ is increased, a conformational transition occurs wherein the $DA_m$ folds and both charged ends of the molecule are hydrated by a single, larger water cluster. Demireva *et al.*[174] also observed this conformational transition using infrared photodissociation experiments with $DA_7(H_2O)_{<12}$. The number of water molecules at which the "unfolded-to-folded" conformational transition occurs is the critical hydration number ($n$*). As the alkyl chain length of $DA_m$ increases, $n$* was found to increase, with more water molecules required to form a water bridge between the terminal ionic groups.[173]

This phenomenon has also been observed experimentally and computationally for micro-solvated $DC_m(H_2O)_n$ molecules, where $m$ = 6 and $n$ = 1 - 20, by Yang *et al.*.[166] They found, using a combination of photoelectron spectroscopy and MD simulations, that each water molecule adds to alternate ends of the linear $DC_6$ di-anion. At $n$ = 16, the conformational transition from unfolded-to-folded occurs. The two negatively charged ends are screened and brought closer together via a water bridge, while the increased number of hydrogen bonds overcomes the Coulombic repulsion present between the two charge centres.[166] This leads to the flexible backbone adopting a bent configuration with both carboxylate groups embedded within a single water cluster.

This chapter reports and discusses the systematic study that was undertaken to investigate the evolution of the conformational and energetic behaviour of $DA_m$ and $DC_m$, with flexible backbones consisting of 3 - 11 methylene units, as they undergo stepwise hydration. We

examined $DA_m$ and $DC_m$ over a larger range of alkyl chain lengths ($m$) than has been previously reported and determined, for the first time in many cases, their respective critical hydration numbers ($n^*$). $n^*$ is defined, in this study, as the number of water molecules present when the folded conformation is first observed as the putative global minimum (GM). Furthermore, this study demonstrated the suitability of the basin-hopping (BH) Monte Carlo algorithm[122,179] for examining the hydration of flexible, multi-charged systems.

## 7.2 Methodology

### 7.2.1 Methods

$DA_m$ and $DC_m$ molecules, with alkyl chain lengths $m$ = 3 - 11, were modelled using the standard parameters found in the ff99SB atomistic force field,[99,100] within the AMBER simulation package.[90] ff99SB is a computationally inexpensive force field which has a proven track record.[99,100] However, to verify the suitability of the AMBER force field, we confirmed that the minima determined using ff99SB corresponded to minima on the density functional theory (DFT) landscape by performing local minimisations using the B3LYP xc functional with the aug-cc-pVDZ basis set,[180] as implemented with the Gaussian09 package.[181]

Water clusters, $(H_2O)_n$, for $n$ = 1 - 25, were modelled using the TIP4P rigid body potential,[182] which was chosen because of its computational efficiency. Furthermore, TIP4P water clusters have been studied extensively,[110,182–186] with good putative GM determined up for up to 36 water molecules.[185] [180] The H-O-H bond angle was fixed at 104.52° and the H-O bond lengths were fixed at 0.9572 Å. The lone pair on the oxygen atom, was fixed at 0.15 Å from the O atom, along the H-O-H bond angle bisector, acted as a pseudoatom and the site of the oxygen's charge.[110,112] Potential parameters are shown in Table 7.1. Implicitly solvated di-ions were modelled using the continuum electrostatic Born hydration model[187] (external dielectric constant = 80.4 f $m^{-1}$),

which uses a pairwise de-screening approximation, as implemented in the SANDER simulation package.[90,97]

**Table 7.1** TIP4P water parameters

| **Molecule** | **Site** | **ε / kcal mol$^{-1}$** | ***σ* /Å** | ***q* /e** |
|---|---|---|---|---|
| **TIP4P $H_2O$** | O | 0.648 | 3.2 | 0 |
| | Lone pair | 0 | 0 | –1.04 |
| | H | 0 | 0 | 0.52 |

For each $D_m(H_2O)_n$ (where $D_m$ stands for $DC_m$ or $DA_m$) system, low energy structures were generated from a short BH run (10,000 steps). The 10 lowest energy, unique structures were used as the starting point for ten longer BH runs (100,000 steps), to find the putative GM. In this investigation, the Monte Carlo geometry perturbations were carried out in blocks of 100 moves of the same type. Three move classes were used: rotations, translations, and short, high temperature MD runs. During the rotation moves, all molecular fragments within the cluster are rotated by a random angle between ± π radians. For the translation moves, a random molecule has a random displacement applied to it relative to the rest of the cluster. 1000 steps were used in the MD simulations and were run at 1000 K with a time step interval of 0.001 ps.

### 7.2.2 Methods for Data Analysis

Analyses of the systems were performed with cpptraj[188] and in-house codes. The total conformational energy, including intra-molecular and inter-molecular interactions, of the hydrated di-ion $D_m(H_2O)_n$ with an alkyl chain length of *m* and *n* water molecules, is defined as $E(m, n)$. The hydration energy ($E_{hyd}(m, n)$) for $D_m(H_2O)_n$ is calculated using equation 7.1:

$$E_{hyd}(m, n) = E(m, n) - \left(E(\text{frozen } D_m) + E\left(\text{frozen } H_2O_n\right)\right) \quad (7.1)$$

where $E$(frozen $D_m$) is the energy of the isolated di-ion, with its conformation fixed (frozen) to that in the $D_m(H_2O)_n$ complex, and $E$(frozen $(H_2O)_n$) is the total energy of the water cluster(s), with the same conformation as in the $D_m(H_2O)_n$ complex.

The second difference in energy ($\Delta_2(m, n)$) for $D_m(H_2O)_n$, is calculated using equation 7.2:

$$\Delta_2(m, n) = 2E(m, n) - \left(E(m - 1, n) + E(m + 1, n)\right) \quad (7.2)$$

where a more positive value of $\Delta_2(m, n)$ indicates a less stable conformation. Boltzmann weightings are applied to various properties according to the formula:

$$\overline{\chi} = \frac{\sum e^{\Delta U_i \beta} \chi_i}{\sum e^{\Delta U_i \beta}} \quad (7.3)$$

where $\beta = 1/k_B T$ and the difference between the putative GM and the energy of the minimum, *i*, is denoted by $\Delta U_i$. The weighted mean is taken over all structural isomers of unique energy found in all basin-hopping runs for each size of system. A theoretical temperature of $T$ = 300 K

was used to maintain consistency with our previous computational studies and provide an insight into behaviour at approximate ambient temperature.

The $DC_m$ series, where $m$ = 3 - 11, were investigated in unhydrated conditions using DFT calculations to clarify certain results generated in unhydrated conditions using the basin-hopping technique. The conformational energy of each di-anion was calculated using the B3LYP xc functional with the aug-cc-pVDZ basis set,[189] implemented within the Gaussian09 package.[181]

## 7.3 Results

### 7.3.1 Unhydrated Di-ions

*Alkyl-diammonium Di-cations*

A plot of the conformational energies, as a function of carbon chain length, for unhydrated $DA_m$, for $m$ = 3 – 11 is shown in Appendix 8: Figure A.8.1. The unhydrated $DA_m$ series were found to all have positive conformational energies due to Coulombic repulsive forces between the two charged ends. The smallest di-cation ($m$ = 3) has the highest positive energy value; the two ammonium charge centres are closer together and, therefore, experience the strongest, destabilising Coulombic repulsions. As the alkyl chain length increases, the conformational energy decreases and becomes less positive. The Coulombic repulsive forces become less dominant, as there is greater separation between the charged ends. The putative GM conformations of $DA_m$ were observed to be linear, with all C-C-C-C dihedral angles in the *trans* configuration. The two ionic groups are, therefore, the maximum distance apart, thus fully reducing the Coulombic repulsive forces.

*Alkyl-dicarboxylate Di-anions*

All putative GM structures were found to be linear with positive conformational energies which decrease as the alkyl chain length increases (Figure 7.1a). For the $DC_m$ series, an even number of carbons in the alkyl chain results in a more stable conformation as shown in Figure 7.1b. This effect has been previously reported in the literature for $DC_m$ and was attributed to a twist in the conformations of $DC_m$ when *m* was odd.[190,191] However, in our study no twist in the alkyl chains was observed in the putative GMs. The odd-even effect can be attributed to the energy contribution from electrostatic forces (Appendix 9: Figure A.9.1) and is also observed in results generated from DFT calculations (Appendix 10: Figure A.10.1).

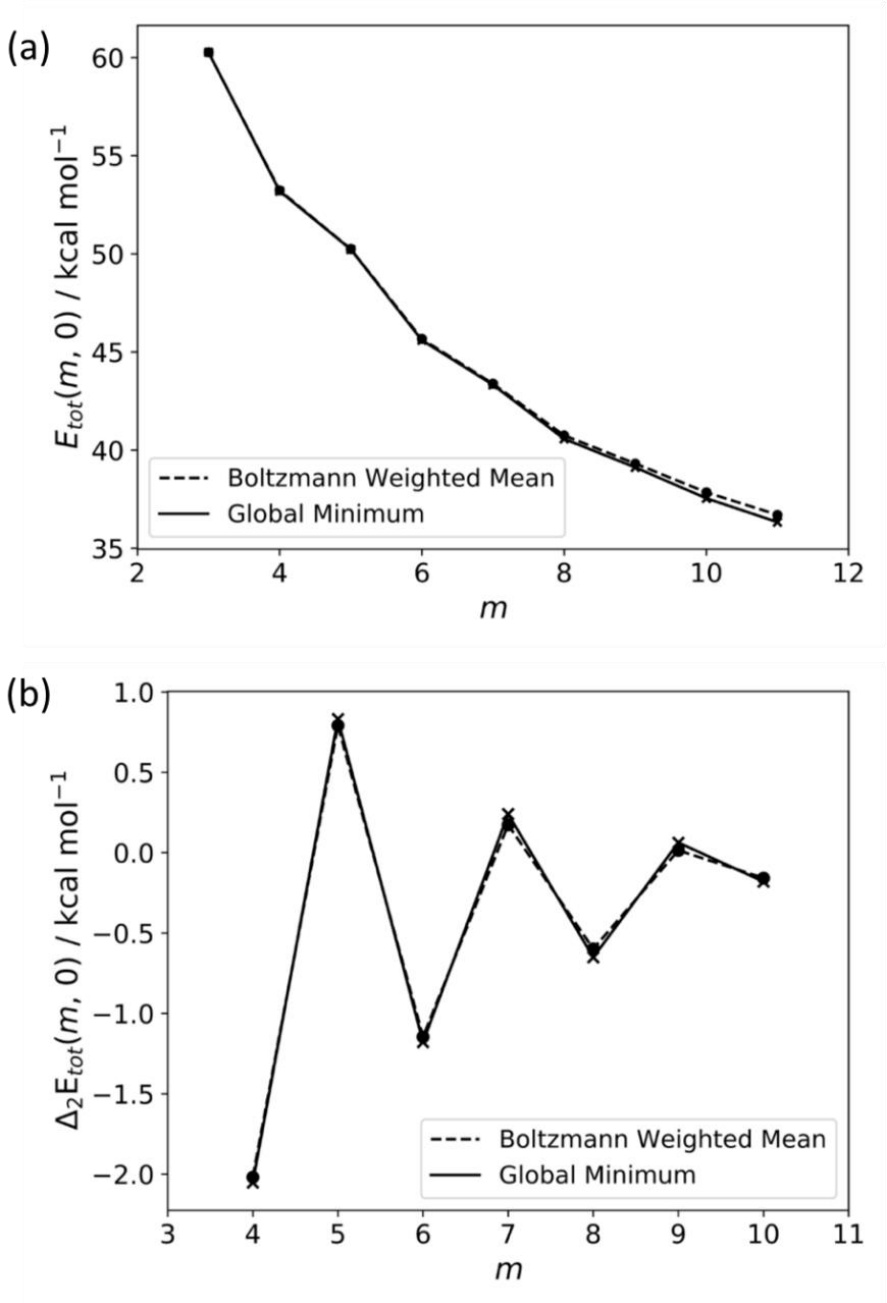


**Figure 7.1** a) A plot of the conformational energies, as a function of carbon chain length, for unhydrated $DC_m$, for $m$ = 3 - 11. b) A plot of second difference for the conformational energies of unhydrated $DC_m$, for $m$ = 4 - 10.

### 7.3.2 Explicitly Hydrated Di-ions

*Alkyl-diammonium di-cations*

A series of $DA_m$, for $m$ = 3 – 11, in water clusters of $n$ = 1 - 25, were investigated and their $n^*$ values are listed in Table 2. As $m$ increases, $n^*$ also increases. For all the di-cations studied, a single value for $n^*$ was determined, with the exception of $m$ = 3. The values for $m$ = 5 - 10 have been compared with those found experimentally[12] and computationally, [13] which are listed in Table 7.2, and are found to be lower. The differences in $n^*$ values between this study and previous investigation are addressed in the Discussion section of this Chapter.

**Table 7.2** Values of the critical hydration number as a function of alkyl chain length for $DA_m$.

| ***m*** | ***n**** **(this work)** | ***n**** **(literature)** |
|---|---|---|
| **3** | 9-11 | |
| **4** | 11 | |
| **5** | 11 | 17 (ref 173) |
| **6** | 13 | 19 (ref 173) |
| **7** | 14 | 20 (ref 173), 21 - 23 (ref 172) |
| **8** | 16 | 27 - 29 (ref 173), 24 - 26 (ref 172) |
| **9** | 18 | 27 - 29 (ref 173) |
| **10** | 22 | 27 - 29 (ref 173), 27 - 29 (ref 172) |
| **11** | 22 | |

A detailed hydration study of $DA_5$ was undertaken to fully explain the conformational behaviour illustrated in Figure 7.2. The conformational energies of $DA_5(H_2O)_{1\,-\,12}$ decrease linearly with increasing *n*, as the added water molecules stabilise the charged ammonium terminal groups (Figure 7.3a). In the range *n* = 1 - 10, sequential hydration occurs as seen in previous investigations.[173,174] Two small water clusters hydrate each ammonium end, with hydrogen bonds forming between the oxygen atom of water and the hydrogen atom of the ammonium group. When *n* < 10, for even values of *n* the system is symmetrical because the water molecules add to alternate charged ends: and a relatively more stable conformation is observed as seen in Figure 3b. The conformation of $DA_5(H_2O)_{1\,-\,10}$ is linear with an average distance between the terminal ammonium groups, $R_{NN}$, of ~ 7.66 Å (Appendix 11: Table A.11.1). The hydrophobic alkyl chain is left unhydrated.

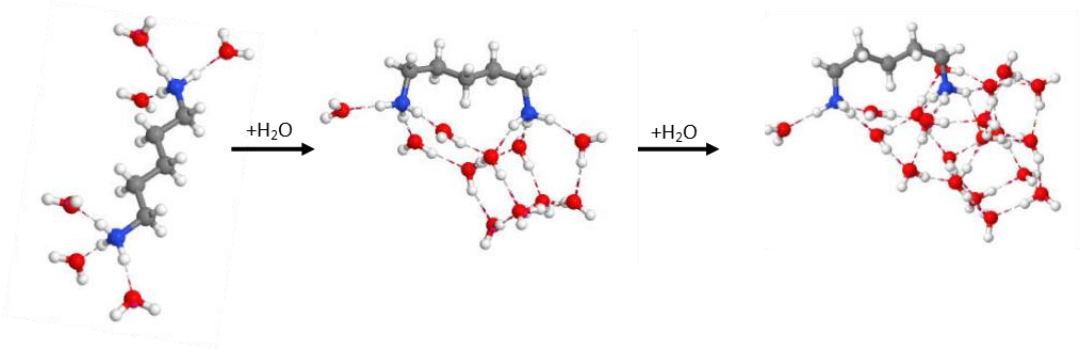


**Figure 7.2** Putative GM structures of $DA_5(H_2O)_n$ for *n* = 6, 11 and 20 (from left to right) in which the positions of the oxygen (red), nitrogen (blue), carbon (grey) and hydrogen (white) atoms are indicated. Representations of the hydrogen bonds have been added as dashed lines, to better demonstrate the water network present in each system.

As the water cluster size is increased to $n$ = 11, the two smaller water clusters merge together and $DA_5$ folds slightly ($R_{NN}$ = 5.73 Å). The hydrophobic alkyl chain bends out of the cluster to avoid hydration, while the two charged ends are both hydrated in the larger single cluster. For $n \geq 11$, the single water cluster is positioned around one of the ammonium ends with no bridging water molecules. Instead, the molecules tend to form water bridges (a water molecule is hydrogen bonded to one ammonium group and to another water molecule which is, in turn, hydrogen bonded to the other ammonium group). The di-cation becomes fully folded by 20 water molecules in the cluster (Figure 7.2) with an $R_{NN}$ value of 5.36 Å (Appendix 11: Table A.11.1).

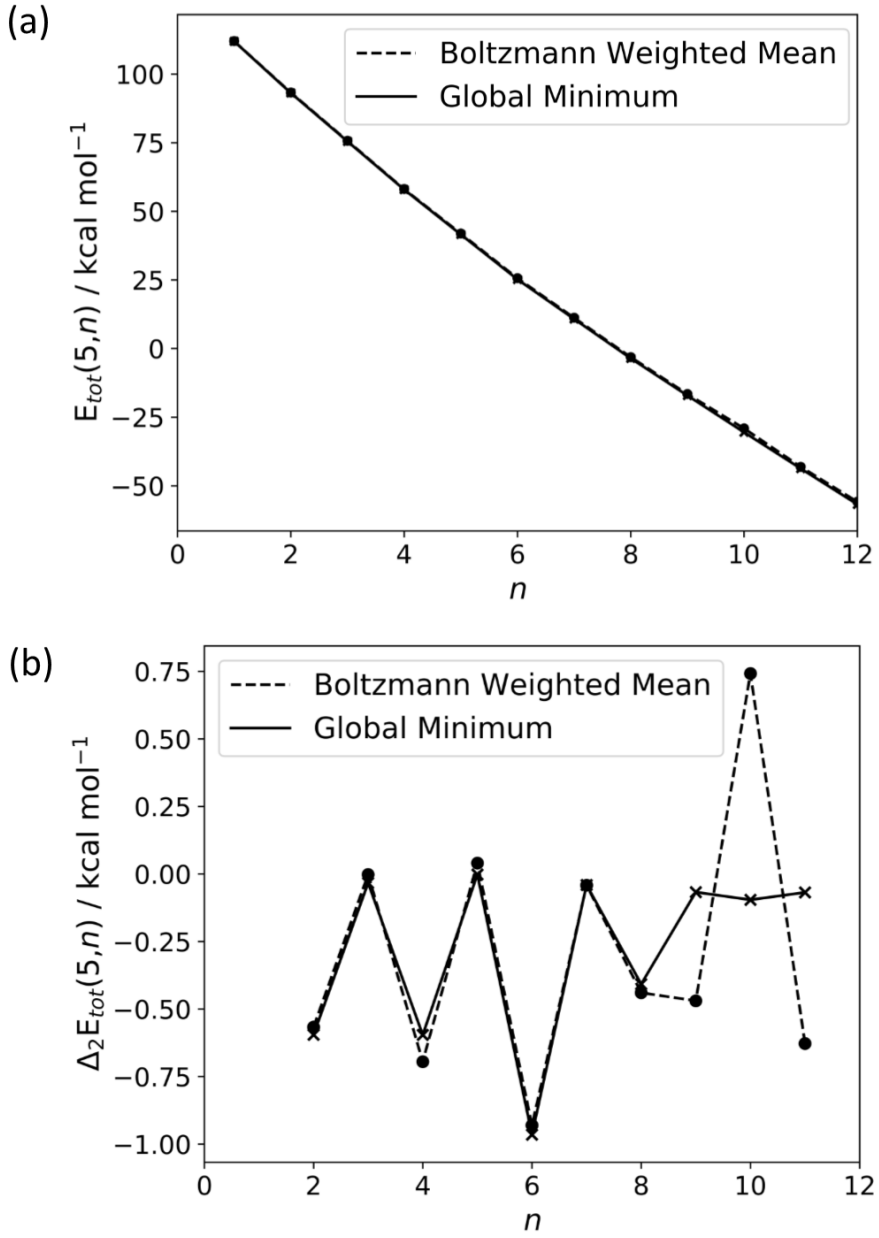


**Figure 7.3** a) A plot of the conformational energies as a function of the number of water molecules for $DA_m(H_2O)_n$ with $m$ = 5 and $n$ = 1 - 12. b) A plot of second difference for the conformational energies of $DA_m(H_2O)_n$ with $m$ = 5 and $n$ = 2 - 11.

*Alkyl-dicarboxylate Di-anions*

The variation of conformational energies with increasing alkyl chain length follows the same general trend for the $DC_m$ series in water clusters ($n$ = 1 - 12) (plots supporting this statement can be found in the paper's[91] Supporting Information, Figures S24-S35) as previously seen for unhydrated conditions (Figure 7.1). The conformational energies decrease as the alkyl chain length increases and an even number of carbon atoms in the hydrophobic chain results in a more stable conformation for $m$ < 9. As water molecules were added to each $DC_m$, there was a decrease in the conformational energies due to the extra stabilisation afforded by the interaction between the added water molecules with the carboxyl groups (plots supporting this statement can be found in the paper's[91] Supporting Information, Figures S24-S35).

**Table 7.3** Values of the critical hydration number corresponding with respective alkyl chain length for $DC_m$.

| ***m*** | ***n**** **(this work)** | ***n**** **(literature)** |
|---|---|---|
| 3 | 6 | |
| 4 | 9 | 13 (ref 176) |
| 5 | 11 | |
| 6 | 12 | 16 (ref 166), 18 - 19 (ref 176) |
| 7 | 12 | |
| 8 | 14 | 18 - 19 (ref 176) |
| 9 | 15 | |
| 10 | 15 | |
| 11 | 19 | |

As shown in Table 7.3, the *n** values for hydrated $DC_m$ increase with increasing chain length (*m*). The values at *m* = 4, 6 and 8 can be compared to those found experimentally,[166,176] and are all found to be lower.

For $m$ = 5 and $n$ = 1 - 12, the conformational energy decreases with increasing water cluster size (Figure 7.4a). As the first ten water molecules ($n$ = 1 - 10) are added, the conformation remains linear and the average distance between the carbon of the carboxylate groups, $R_{CC}$, is the maximum distance apart ($R_{CC}$ ~ 7.65 Å), to minimise Coulombic repulsive forces. The terminal carboxylate groups are distinctly solvated by two small water clusters. It is observed that for even numbers of water molecules, the two small water clusters were of equal size due to alternating addition to each charged end and the added stability of the symmetrical hydrogen bond network in the two terminal water clusters (Figure 4b). This alternating addition of water molecules to each charge centre for a $DC_m(H_2O)_n$ system was also observed by Yang *et al.*[166]

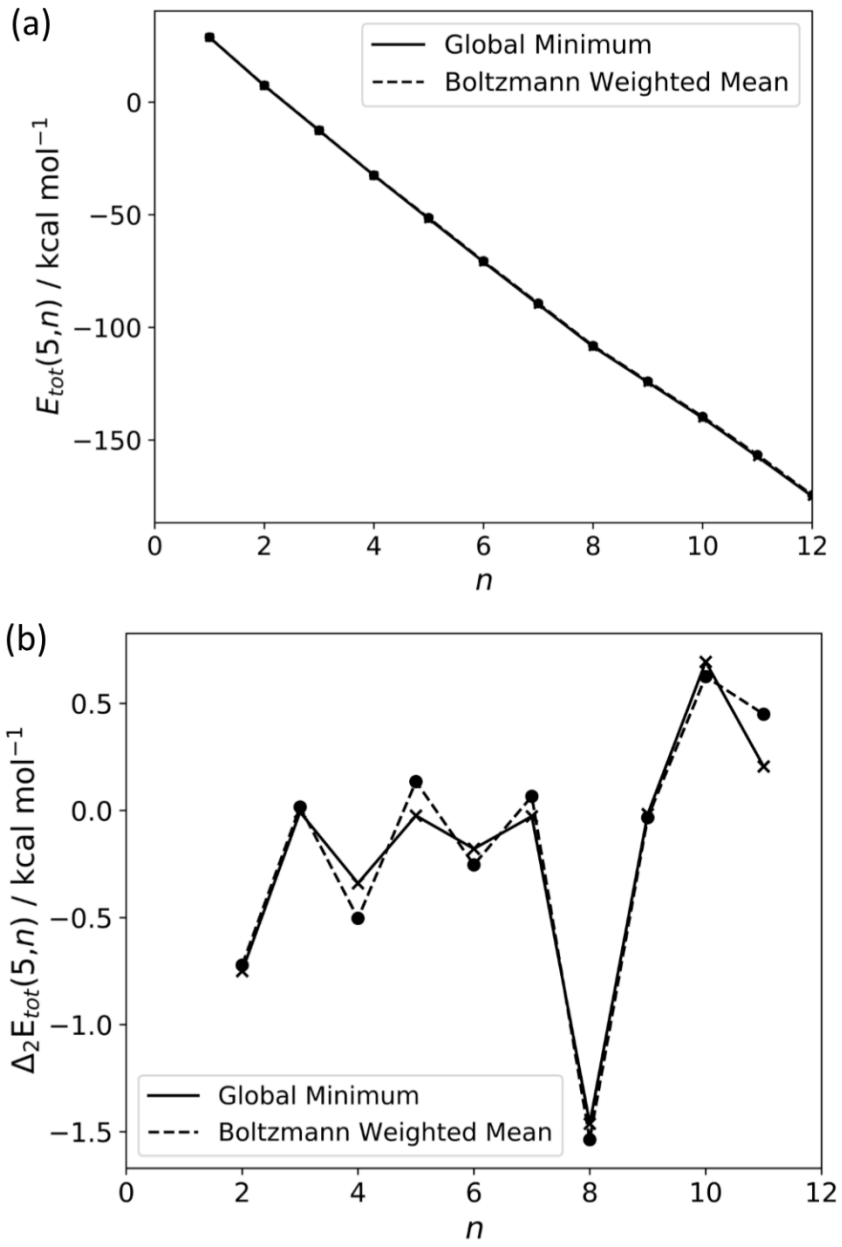


**Figure 7.4** a) A plot of the conformational energies as a function of the number of water molecules for $DC_m(H_2O)_n$ with $m$ = 5 and $n$ = 1 - 12. b) A plot of the second difference graph for the conformational energies of hydrated $DC_m(H_2O)_n$ with $m$ = 5 and $n$ = 2 - 11.

A conformational transition occurs when $n$ = 11 (Figure 7.5). The two previously separate water clusters merge and $DC_5$ folds in such a way that the two charged ends are hydrated by the resulting water cluster. The increased Coulombic repulsion between the two charged ends ($R_{CC}$

value of ~ 4.86 Å) that occurs in the folded conformation is compensated for by the additional hydrogen bonds formed in the larger water cluster.[163,166] The $DC_5$ is fully folded when $n$ = 20 (Figure 7.5) with $R_{CC}$ ~ 4.63 Å (Appendix 11: Table A.11.2). The water molecules form a strongly bound and extensive cage around the charged ends with the hydrophobic alkyl chain folded outside of the water cluster.

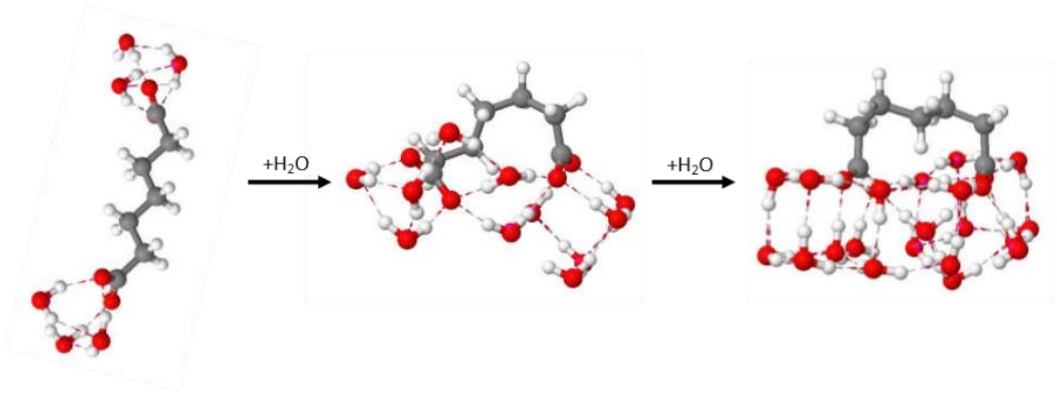


**Figure 7.5** Putative GM structures of $DC_5(H_2O)_n$ for $n$ = 6, 11 and 20 (left to right) in which the positions of the oxygen (red), carbon (grey) and hydrogen (white) atoms are indicated. Representations of the hydrogen bonds have been added as dashed lines, to better demonstrate the water network present in each system.

The hydration energies were calculated for $DC_5(H_2O)_{1-12}$ and are shown in Figure 7.6. The hydration energies steadily decrease as each water molecule is added. There is a discontinuous drop in the hydration energy when the critical hydration number ($n$* = 11) is reached, which is suggestive of a conformational transition taking place. This additional stability is also found for $DC_m$ where $m$ = 3, 4, 6 and 7 at their respective $n$* value (plots supporting this statement can be found in the paper's[91] Supporting Information, Figures S16 - S23).

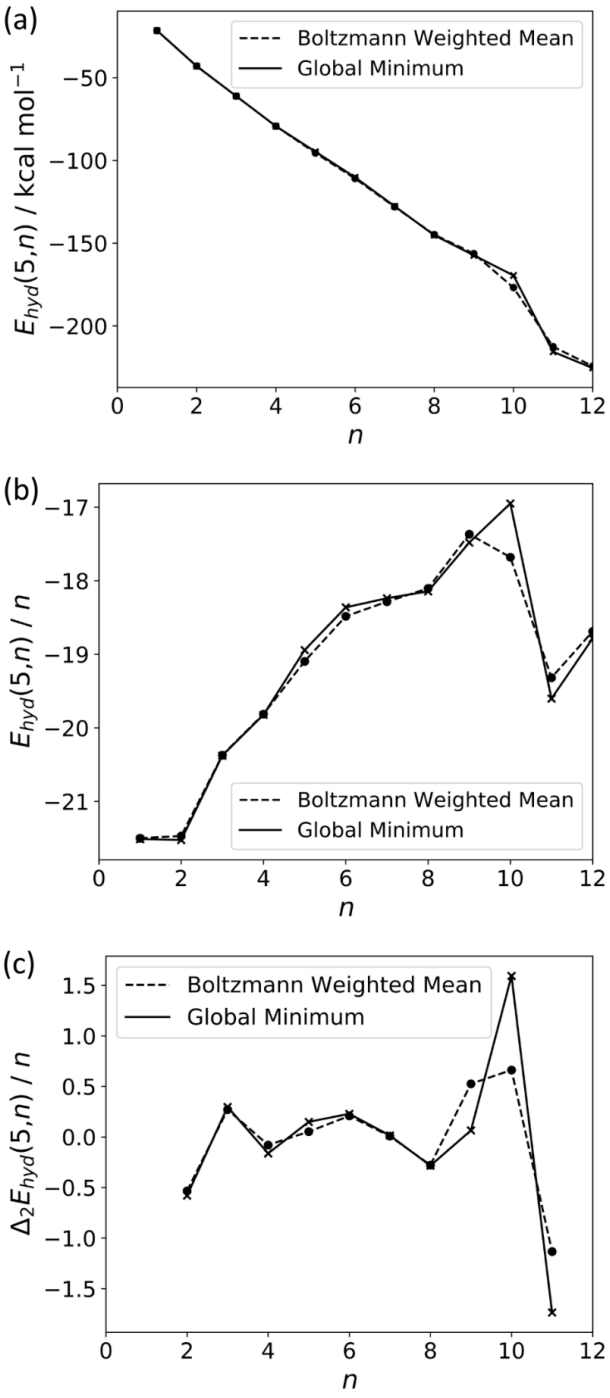


**Figure 7.6** a) A plot of the hydration energies as a function of the number of water molecules present for $DC_m(H_2O)_n$ with $m$ = 5 and $n$ = 1 - 12. b) A plot of the hydration energies per water molecule for $DC_m(H_2O)_n$ with $m$ = 5 and $n$ = 1 - 12. c) A plot of second difference of the hydration energies of $DC_m(H_2O)_n$ with $m$ = 5 and $n$ = 2 - 11.

### 7.3.3 Implicitly Solvated Di-ions

*Alkyl-diammonium Di-cations*

In implicitly solvated conditions, the conformational energies were all found to be negative due to the stabilisation of the $DA_m$ by the simulated solvated conditions (Appendix 12: Figure A.12.1). As the alkyl chain length increases, the conformational energies become less negative. As each successive methylene group is added to the alkyl chain, the hydrophobic interactions with the solvent increases which causes a destabilisation of the $DA_m$. The putative GM structures are all linear to minimise Coulombic repulsive forces between the two ammonium ends.

*Alkyl-dicarboxylate Di-anions*

The conformational energy becomes less negative as the alkyl chain length increases (Appendix 12: Figure A.12.2a). This is, again, due to the increase of hydrophobic interactions with the simulated solvent as methylene groups are added to the backbone. An even number of carbons in the alkyl chain results in a more stable conformation (Appendix 12: Figure A.12.2b). The effect is larger than that seen in unhydrated conditions and is dominated by the contribution from electrostatic interactions Appendix 12: Figure A.12.3).

## 7.4 Discussion

The $n^*$ values reported here for $DA_m$ and $DC_m$, for $m$ = 3 - 11 (Tables 7.2 and 7.3) were all found to be lower than those reported by previous investigations.[166,172,173,176] The difference in $n^*$ values, between this work and these previous studies, is most likely due to the difference in temperature at which they were determined; this was 0 K in this study but 70 K, or higher, for the others. As a consequence, the effects of entropy are not taken into account in the calculations in this study, which is expected to lead to an increase in $n^*$.[166] The entropy of the

unfolded configurations would therefore, be expected to be greater than that of the folded di-ions due increased transitional and rotational entropy contributions.

The average distances between terminal groups, $R_{NN}$ for $DA_m$ and $R_{CC}$ for $DC_m$, on either side of $n^*$, are plotted in Figure 7.7. The conformational transition can be observed by the respective colour changes, as $n$ increases. A single transition, and hence value for $n^*$, is observed for all di-ions studied (Tables 7.2 and 7.3), except $DA_3$, where there is more than one transition between linear and folded conformations. This uncertainty in $n^*$, which led to us reporting a range of $n^*$ values in Table 7.2, could be the result of the small differences in energy between linear and folded conformations at low values of $m$.

Figure 7.7 clearly illustrates that, as the alkyl chain length increases ($m$), $n^*$ increases for both $DA_m$ and $DC_m$. This is a result of the need for larger water clusters to bridge the charged ends of the larger di-ions and has been observed previously.[173] It can also be seen that $DC_m$ generally exhibit lower $n^*$ values, than $DA_m$, and adopt a much more folded conformation, indicated by smaller $R_{CC}$ values, compared to the corresponding $R_{NN}$ values (Appendix 11: Tables A.11.1 and A.10.2).

Consequently, the alkyl backbone in the folded conformation of the di-anions is, therefore, more strained than the comparable $DA_m$ (Figures 7.2 and 7.5). It is believed that these differences in structure are due to the additional stability of the $DC_m$.

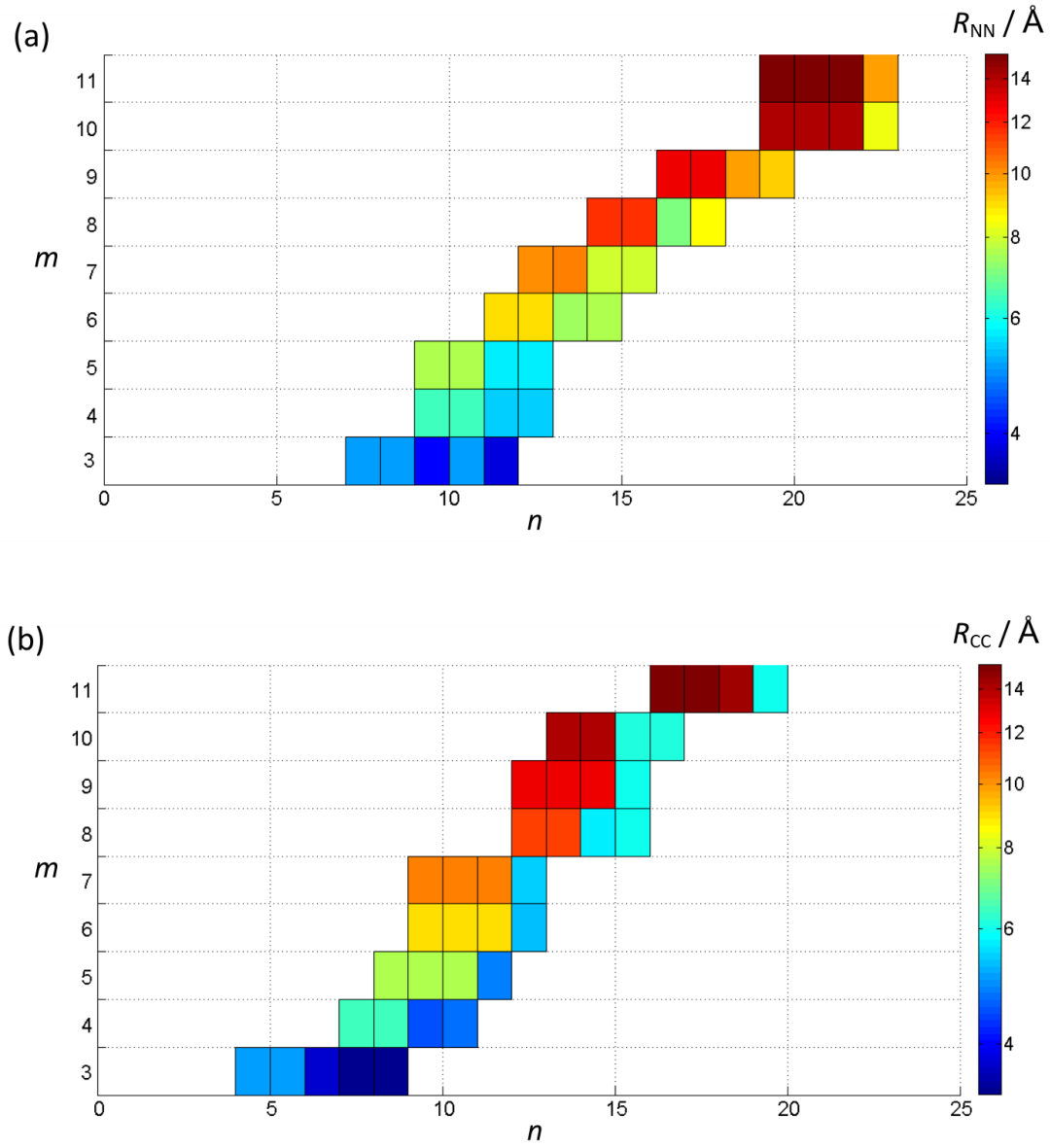


**Figure 7.7** a) A plot of the average distance between the nitrogen atoms ($R_{NN}$) of the terminal ammonium groups for selected $DA_m(H_2O)_n$ as a function of alkyl chain length ($m$) and the number of water molecules added ($n$). b) A plot of the average distance between the carbon atoms ($R_{CC}$) of the terminal carboxylate groups for selected $DC_m(H_2O)_n$ as a function of alkyl chain length ($m$) and the number of water molecules added ($n$). The values of average distance between the terminal groups for the conformations can be found in Appendix 11: Table A.11.1 and Table A.11.2.

This additional stability of the $DC_m$, indicated by the more negative conformational energies in all conditions considered, is due to the negative charge being more delocalised over the carboxylate units. Furthermore, a higher number of hydrogen bonds is observed for $DC_5$ compared with $DA_5$ (Figure 7.8). This is, in part, because of the increased number of solute-solvent interactions in the $DC_5$ systems, where each oxygen atom, in the carboxylate groups, can form hydrogen bonds to more than one water molecule (Figure 7.5). Comparatively, each hydrogen atom of the ammonium group, in the $DA_5$ systems, can only form a single hydrogen bond (Figure 7.2). These factors are thought to aid the stabilisation of $DC_5$, and therefore other $DC_m$ systems.

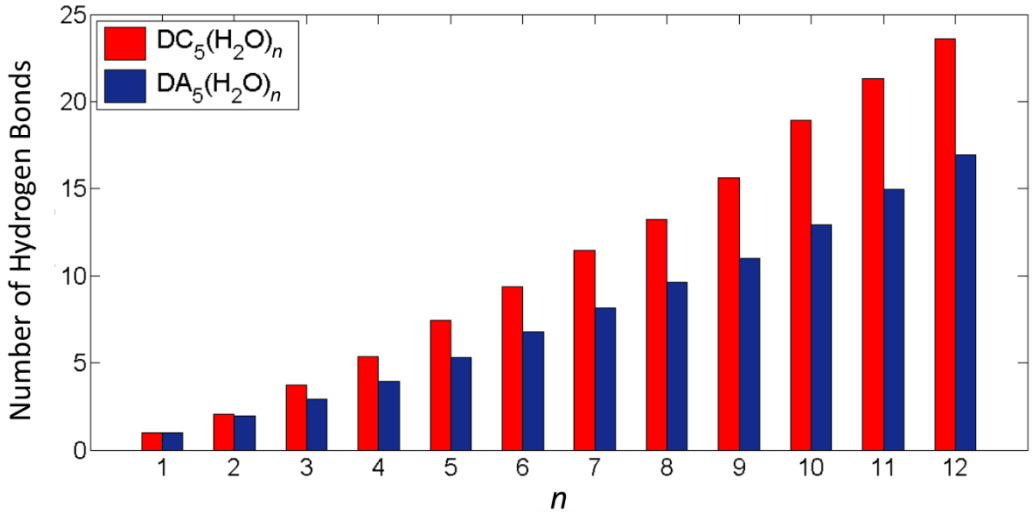


**Figure 7.8** a) A plot of the average number of hydrogen bonds detected in the $DC_5(H_2O)_n$ and $DA_5(H_2O)_n$ systems as a function of the number of water molecules, $n$ = 1 - 12.

Lastly, differences are observed in the structure of the water clusters surrounding $DA_m$ and $DC_m$ (Figure 7.2 and 7.5). It was observed that the water clusters formed pentagons in hydrated $DA_m$,

but cubes were observed for $DC_m(H_2O)_n$, albeit in somewhat distorted forms. Although the shape of the water networks generated in this study have similar structural motifs to those previously observed in small, pure water clusters (pentagons and cubes),[30,33] it appears that, in this study, the selection of the structure of the water network, is influenced by the shape of the charged terminal group and solute-solvent interactions.

## 7.5 Conclusions

Basin-hopping was used, for the first time, to systematically investigate the behaviour of $DA_m$ and $DC_m$ for a series of alkyl chain lengths in differently solvated conditions. Each series is found to follow similar conformational and energetic trends, which can be explained by considering inter- and intra-molecular interactions. For the $DC_m$ series in unhydrated, implicitly solvated and explicitly solvated conditions, an even number of carbons in the alkyl chain is found to exhibit a more stable conformation. The origin of this effect was identified to be primarily due to electrostatic contributions. DFT calculations support the existence of the odd-even effect.

For every di-ion investigated, a linear to folded conformational transition is observed at a critical hydration number, $n^*$, resulting from a change in the hydration of the two charge centres. It is found that the $n^*$ value is specific to each di-ion and is identified, for the first time, in the case of $m$ = 3, 4 and 11 for $DA_m$ and $m$ = 3, 5, 7, 9, 10 and 11 for $DC_m$. The differences between $n^*$ values discovered in this study compared to those found previously, demonstrates the universal importance of entropy in deciding the critical hydration number for all the systems considered. Finally, this study demonstrates the suitability of the BH Monte Carlo algorithm[122,179] for studying the hydration of flexible, multi-charged systems.

# CHAPTER 8: CONCLUSIONS

## 8.1 Conclusions and Future Work

The goal of this project was to investigate the hydration and conformational behaviour of polymer brushes (PBs) in different types of electrolyte solutions. Specific-ion effects of PBs are of particular interest to many industries,[11–14,16–18] such as biomedical industries,[15,27] that employ these types of polymer materials. Changes in the properties of PBs, in the presence of ions, have major implications for current and potential applications. Previous experimental studies[5,8,39] have suggested that changes in hydration and conformation of PBs are linked to ion pairs forming between ions and functional groups along the polymer chains. Due to the complexity of PBs, it is challenging to gather further information regarding ion pairs using experimental methods.[46] In this thesis, atomistic MD simulations were employed to investigate the dynamics and local structure of ion pairing interactions within a strong polyelectrolyte (PE) brush (PMETAC brush) and a polyzwitterionic (PZ) brush (PSBMA brush) in the presence of 0.5 M NaSCN, 0.5 M $NaClO_4$ and 0.5 M $Na_2SO_4$ solutions.

Properties, such as grafting density,[3,5,120] were taken into consideration during the construction of atomistic PB models. The need to explicitly represent water molecules and numerous long chain polymers was balanced with limitations on computational simulation time. Two differently sized PMETAC brush models were studied. Results from the two-chain and eight-chain PMETAC brush systems were similar in terms of their conformation and hydration. It has been shown that the properties reported on, specifically the hydration and conformation of the PMETAC brush, as well as specific-ion interactions, were not affected by the expansion of the brush model from two-chain to eight-chains. Thus, no system-size dependencies were observed and consequently, finite size effects could be concluded to have minimal importance on the properties investigated in this thesis. It must be noted that by increasing the number of atoms in the PMETAC system,

the computational workload was increased substantially. These eight-chain simulations required significantly more processing time than the two-chain PMETAC system. For researchers using MD simulations to examine PBs, the importance of having access to GPUs should not be underestimated. As the findings for the eight-chain PMETAC system (Chapter 4) were in good agreement with those for the two-chain system (Chapter 3), as well as previous investigations, it was decided that further simulations and analysis would be carried out on PB models containing only two polymer chains.

For the simulated two-chain PMETAC brush model, it was observed that NaSCN and $NaClO_4$ solutions induced a less swollen conformation compared to when the brush was in water. A more pronounced decrease in brush height and dehydration of the PMETAC chains was observed in $NaClO_4$ compared to NaSCN solution, thus following the expected order predicted by the Hofmeister series. These observations were in good agreement with previous experimental[5,8,39] investigations thus showing that the chosen atomic parameters (AMBER force fields:[90] ff14SB[99] and General Amber force field (GAFF)[100] parameter sets) captured the specific-ion behaviour of PMETAC brushes in the presence of highly concentrated chaotropic anions, $ClO_4^-$ and $SCN^-$.

It had been predicted by Collins's law of matching water affinities (LMWA),[40,45] ion dispersion theory[42] and previous studies[4,6,8,39,127] that ion pairs would form between chaotropic quaternary ammonium (QA) groups along the PMETAC chains and the chaotropic $ClO_4^-$ and $SCN^-$ anions. By examining the lifetime distributions of $ClO_4^-$ and $SCN^-$ anions residing in the first solvation shell of QA groups, we have verified, that ion pairs form between QA groups and $ClO_4^-$ and $SCN^-$ anions. Conformations involved in ion pairing interactions were further analysed. It became clear that the term, "ion pairing" discussed in previous research,[4,6,8,39,127] was an

oversimplification of specific-ion interactions occurring within the PMETAC brush. Multiple $ClO_4^-$ and $SCN^-$ anions were found to be "paired" simultaneously to QA groups, consequently forming higher-order clusters. Ion pockets were also observed wherein multiple QA groups were simultaneously paired to one of the studied chaotropic anions.

The PSBMA brush was observed to interact in a similar fashion to the PMETAC brush with the $ClO_4^-$ and $SCN^-$ anions. Ion pairs, higher-order ion clusters and ion pockets were observed to form between QA groups of the PSBMA chains and the $ClO_4^-$ and $SCN^-$ anions. Despite similarities in specific-anion interactions reported in both PMETAC and PSBMA, the observed effect of forming ion pairs, clusters, and pockets, on hydration and conformational properties is markedly different for the two types of studied PBs. While the presence of $NaClO_4$ and NaSCN solutions induced a collapse within the PMETAC chains, a swelling was observed for the PSBMA brush, in an example of the well-known "anti-polyelectrolyte effect". Furthermore, $NaClO_4$ had a more pronounced effect on hydration and conformation of the PMETAC chains, but NaSCN had a more significant influence over the PSBMA brush.

For PMETAC and PSBMA, it was found that changes in hydration and conformation of the brushes can be linked to the presence of ion pairs as well as the frequency and size of higher-order ion clusters and ion pockets. $ClO_4^-$ were observed to form larger pockets with QA groups on the PMETAC and PSBMA chains. A consequence of this is the bending of the chains to better accommodate the $ClO_4^-$ anions. The monomers along the polymer chains rearrange themselves to situate the pendant QA groups into the optimal position for forming ion pockets. The formation of ion pockets therefore influences the conformation of the chains. Furthermore, ion pockets, along with ion pairs and higher-order ion clusters, have been shown to influence the

hydrophobicity of the chains therefore influencing the hydration of the PMETAC and PSBMA chains. These observations seem to be the main driving factors involved in the collapse of the PMETAC brush. The disruption of interchain/intrachain interactions, as well as the increased hydration of the sulfonate group are, however, more influential for the PSBMA brush.

To explore the proposed ion pairing interactions, future studies could attempt to experimentally elucidate the conformation of ion pairing, clustering, and ion pockets. It would perhaps be possible to take inspiration from studies investigating ion pockets within peptides.[192–196] Further computational research could be undertaken; the suitability of using machine learning potentials for the PB systems could be assessed[135] or the possibility of using MD simulations employing polarisable force fields could be explored for PMETAC and PSBMA chains.[134]

Polarisable force fields may be necessary when simulating the strongly kosmotropic anion, $SO_4^{2-}$. It was shown in Chapter 6 that the chosen atomistic parameters,[99,100] while accurate for the studied PBs with the chaotropic anions, do not seem to appropriately describe specific-interactions involving $SO_4^{2-}$ anions. Almost all, if not all, of $SO_4^{2-}$ anions and $Na^+$ cations in the two-chain and eight-chain PMETAC brush systems aggregated above the polymer chains. The ions are so strongly involved in dynamic aggregation, they are unavailable to interact with the PBs. This lack of interactions led to no discernible change in the hydration and conformation properties of PMETAC. Previous simulations using non-polarisable force fields have also reported the excessive aggregation of salts containing divalent oxyanions.[156–159] Polarisable models do not tend to reproduce the unrealistic aggregation behaviour for $SO_4^{2-}$ anions.[156,160] Nevertheless, balancing the computational expense related to the explicit inclusion of

polarisability effects with the adequate sampling of temporal−spatial scales for brush dynamics is a necessary consideration when performing atomistic simulations on PBs.

Future computational research could examine the local structure of water surrounding the ion pairs and clusters, thus providing additional information on the conformational transition of PBs and furthering our understanding of the specific-ion effect. It is known that the properties of water are significantly altered in biological systems thanks to a significant number of additional interactions.[149] This is vital as the structure and dynamics of "biological water" are known to be important for responses in the human body.[197] Parallels can be drawn between biological water and the water within the studied PBs. Atomistic MD simulations would be appropriate to employ to explore the extended hydrogen-bond network normally observed in bulk water, but which would be lost for the water contained in PBs.

The importance of the role of water in charged systems was demonstrated in a separate study discussed in Chapter 7. Basin-hopping was used, for the first time, to systematically investigate the behaviour of $DA_m$ and $DC_m$ for a series of alkyl chain lengths in differently hydrated conditions. For every di-ion investigated, a linear to folded conformational transition is observed at a distinct number of water molecules, termed as the critical hydration number, $n^*$. This work provides valuable information on how the hydration of ammonium and carboxylate ions influence larger biomolecules' conformations.

To conclude, although MD techniques have been previously used to examine the behaviour of PBs, these studies have tended to employ approximations, such as coarse-grained models and implicit solvent representations, as well as only exploring macroscopic variations within

simulated PBs. Contrastingly, a fully atomistic description of PBs has been achieved within this thesis and the analysis has focused on investigating the local structure and lifetimes of ions within the brushes. This approach has allowed us to better understand how the presence of ion pairs influence macroscopic behaviours observed for PBs along with concluding that it may be necessary to take a closer look at “ion pairing” between ions and different types of PBs. The presence of higher-order ion clusters and ion pockets have been shown to be intrinsically linked to the conformation and hydration of PMETAC and PSBMA brushes. Future investigations, both theoretical and experimental, perhaps should focus on validating and providing further insight into the conformation of higher-order ion clusters presented in Chapters 3, 4 and 5.

# REFERENCES


1. Wang, T. *et al.* Cation-specific conformational behavior of polyelectrolyte brushes: From aqueous to nonaqueous solvent. *Langmuir* **30**, 12850–12859 (2014).

2. Zhao, B. & Brittain, W. J. Polymer brushes: Surface-immobilized macromolecules. *Prog. Polym. Sci.* **25**, 677–710 (2000).

3. Das, S., Banik, M., Chen, G., Sinha, S. & Mukherjee, R. Polyelectrolyte brushes: Theory, modelling, synthesis and applications. *Soft Matter* **11**, 8550–8583 (2015).

4. Liu, G. Tuning the Properties of Charged Polymers at the Solid/Liquid Interface with Ions. *Langmuir* **35**, 3232–3247 (2019).

5. Santos, D. E. S., Li, D., Ramstedt, M., Gautrot, J. E. & Soares, T. A. Conformational Dynamics and Responsiveness of Weak and Strong Polyelectrolyte Brushes: Atomistic Simulations of Poly(dimethyl aminoethyl methacrylate) and Poly(2-(methacryloyloxy)ethyl trimethylammonium chloride). *Langmuir* **35**, 5037–5049 (2019).

6. Willott, J. D., Murdoch, T. J., Webber, G. B. & Wanless, E. J. Physicochemical behaviour of cationic polyelectrolyte brushes. *Prog. Polym. Sci.* **64**, 52–75 (2017).

7. Wang, T., Wang, X., Long, Y., Liu, G. & Zhang, G. Ion-specific conformational behavior of polyzwitterionic brushes: Exploiting it for protein adsorption/desorption control. *Langmuir* **29**, 6588–6596 (2013).

8. Kou, R., Zhang, J., Wang, T. & Liu, G. Interactions between Polyelectrolyte Brushes and Hofmeister Ions: Chaotropes versus Kosmotropes. *Langmuir* **31**, 10461–10468 (2015).

9. Azzaroni, O., Moya, S., Farhan, T., Brown, A. A. & Huck, W. T. S. Switching the properties of polyelectrolyte brushes via 'hydrophobic collapse'. *Macromolecules* **38**, 10192–10199 (2005).

10. Willott, J. D., Murdoch, T. J., Webber, G. B. & Wanless, E. J. Nature of the Specific Anion Response of a Hydrophobic Weak Polyelectrolyte Brush Revealed by AFM Force Measurements. *Macromolecules* **17**, 56 (2016).

11. Azzaroni, O., Brown, A. A. & Huck, W. T. S. Tunable wettability by clicking counterions into polyelectrolyte brushes. *Adv. Mater.* **19**, 151–154 (2007).

12. X, G. & Ballauff, M. Spatial dimensions of colloidal polyelectrolyte brushes as determined by dynamic light scattering. *Langmuir* **16**, 8719–8726 (2000).

13. Mei, Y., Lu, Y., Polzer, F., Ballauff, M. & Drechsler, M. Catalytic activity of palladium nanoparticles encapsulated in spherical poly electrolyte brushes and core-shell microgels. *Chem. Mater.* **19**, 1062–1069 (2007).

14. He, Z. *et al.* Tuning ice nucleation with counterions on polyelectrolyte brush surfaces. *Sci. Adv.* **2**, 1600345 (2016).

15. Iwasaki, Y. & Ishihara, K. Phosphorylcholine-containing polymers for biomedical applications. *Anal. Bioanal. Chem.* **381**, 534–546 (2005).

16. Kobayashi, M., Terada, M. & Takahara, A. Polyelectrolyte brushes: A novel stable lubrication system in aqueous conditions. *Faraday Discuss.* **156**, 403–412 (2012).

17. Raviv, U. *et al.* Lubrication by charged polymers. *Nature* **425**, 163–165 (2003).

18. Leermakers, F. A. M., Zhulina, E. B. & Borisov, O. V. Interaction forces and lubrication of dendronized surfaces. *Curr. Opin. Colloid Interface Sci.* **27**, 50–56 (2017).

19. Okur, H. I. *et al.* Beyond the Hofmeister Series: Ion-Specific Effects on Proteins and Their Biological Functions. *J. Phys. Chem. B* **121**, 1997–2014 (2017).

20. Milner, S. T. Polymer Brushes. in *Science* vol. 251 905–913 (Wiley, 1991).

21. Advincula, R. C. Surface initiated polymerization from nanoparticle surfaces. *J. Dispers. Sci. Technol.* **24**, 343–361 (2003).

22. Jennings, G. K. & Brantley, E. L. Physicochemical Properties of Surface-Initiated Polymer Films in the Modification and Processing of Materials. *Adv. Mater.* **16**, 1983–1994 (2004).

23. Radhakrishnan, B., Ranjan, R. & Brittain, W. J. Surface initiated polymerizations from silica nanoparticles. *Soft Matter* **2**, 386–396 (2006).

24. Luzinov, I., Minko, S. & Tsukruk, V. V. Adaptive and responsive surfaces through controlled reorganization of interfacial polymer layers. *Prog. Polym. Sci.* **29**, 635–698 (2004).

25. Minko, S. Responsive polymer brushes. *Polym. Rev.* **46**, 397–420 (2006).

26. Willott, J. D. *et al.* Anion-specific effects on the behavior of pH-sensitive polybasic brushes. *Langmuir* **31**, 3707–3717 (2015).

27. Wang, T. *et al.* Anion Specificity of Polyzwitterionic Brushes with Different Carbon Spacer Lengths and Its Application for Controlling Protein Adsorption. *Langmuir* **32**, 2698–2707 (2016).

28. Cheng, N., Brown, A. A., Azzaroni, O. & Huck, W. T. S. Thickness-dependent properties of polyzwitterionic brushes. *Macromolecules* **41**, 6317–6321 (2008).

29. Lowe, A. B. & McCormick, C. L. Synthesis and solution properties of zwitterionic polymers. *Chem. Rev.* **102**, 4177–4189 (2002).

30. Hofmeister, F. Zur Lehre von der Wirkung der Salze. *Arch. für Exp. Pathol. und Pharmakologie* **24**, 247–260 (1888).

31. Kunz, W., Henle, J. & Ninham, B. W. 'Zur Lehre von der Wirkung der Salze' (about the science of the effect of salts): Franz Hofmeister's historical papers. *Curr. Opin. Colloid Interface Sci.* **9**, 19–37 (2004).

32. Marcus, Y. Effect of ions on the structure of water: Structure making and breaking. *Chem. Rev.* **109**, 1346–1370 (2009).

33. Omta, A. W.; Kropman, M. F.; Woutersen, S.; Bakker, H. J. Negligible Effect of Ions on the Hydrogen-Bond Structure in Liquid Water. *J. Sci.* **301**, 347–349 (2003).

34. Funkner, S. *et al.* Watching the low-frequency motions in aqueous salt solutions: The terahertz vibrational signatures of hydrated ions. *J. Am. Chem. Soc.* **134**, 1030–1035 (2012).

35. Marcus, Y. Effect of ions on the structure of water: Structure making and breaking.

*Chem. Rev.* **109**, 1346–1370 (2009).

36. Bakker, H. J., Kropman, M. F. & Omta, A. W. Effect of ions on the structure and dynamics of liquid water. *J. Phys. Condens. Matter* **17**, S3215–S3224 (2005).

37. Kropman, M. F. & Bakker, H. J. Vibrational relaxation of liquid water in ionic solvation shells. *Chem. Phys. Lett.* **370**, 741–746 (2003).

38. Gaiduk, A. P. & Galli, G. Local and Global Effects of Dissolved Sodium Chloride on the Structure of Water. *J. Phys. Chem. Lett.* **8**, 1496–1502 (2017).

39. Kou, R., Zhang, J., Chen, Z. & Liu, G. Counterion Specificity of Polyelectrolyte Brushes: Role of Specific Ion-Pairing Interactions. *ChemPhysChem* **19**, 1404–1413 (2018).

40. Collins, K. D. Ions from the Hofmeister series and osmolytes: Effects on proteins in solution and in the crystallization process. *Methods* **34**, 300–311 (2004).

41. Collins, K. D. Ion hydration: Implications for cellular function, polyelectrolytes, and protein crystallization. *Biophys. Chem.* **119**, 271–281 (2006).

42. Ninham, B. W. & Lo Nostro, P. *Molecular Forces and Self Assembly in Colloid Nano Sciences and Biology*. *Cambridge University Press* (University Press, Cambridge, 2010).

43. Kunz, W. *Specific Ion Effects*. (World Scientific Publishing Company, 2009).

44. Mazzini, V. & Craig, V. S. J. Volcano Plots Emerge from a Sea of Nonaqueous Solvents: The Law of Matching Water Affinities Extends to All Solvents. *ACS Cent. Sci.* **4**, 1056–1064 (2018).

45. Collins, K. D. & Washabaugh, M. W. The Hofmeister effect and the behaviour of water at interfaces. *Q. Rev. Biophys.* **18**, 323–422 (1985).

46. Marcus, Y. & Hefter, G. Ion pairing. *Chem. Rev.* **106**, 4585–4621 (2006).

47. Park, K. H., Choi, S. R., Choi, J. H., Park, S. & Cho, M. Real-time probing of ion pairing dynamics with 2DIR spectroscopy. *ChemPhysChem* **11**, 3632–3637 (2010).

48. Rudolph, W. W., Irmer, G. & Hefter, G. T. Raman spectroscopic investigation of speciation in MgSO4(aq). *Phys. Chem. Chem. Phys.* **5**, 5253–5261 (2003).

49. Grandgirard, J., Poinsot, D., Krespi, L., Nénon, J. P. & Cortesero, A. M. Costs of secondary parasitism in the facultative hyperparasitoid Pachycrepoideus dubius: Does host size matter? *Entomol. Exp. Appl.* **103**, 239–248 (2002).

50. Buchner, R., Samani, F., May, P. M., Sturm, P. & Hefter, G. Hydration and ion pairing in aqueous sodium oxalate solutions. *ChemPhysChem* **4**, 373–378 (2003).

51. Kaatze, U., Hushcha, T. O. & Eggers, F. Ultrasonic broadband spectrometry of liquids: A research tool in pure and applied chemistry and chemical physics. *J. Solution Chem.* **29**, 299–368 (2000).

52. Schrödle, S., Rudolph, W. W., Hefter, G. & Buchner, R. Ion association and hydration in 3:2 electrolyte solutions by dielectric spectroscopy: Aluminum sulfate. *Geochim. Cosmochim. Acta* **71**, 5287–5300 (2007).

53. Fuoss, R. M. & Hsia, K.-L. Association of 1-1 Salts in Water. *Proc. Natl. Acad. Sci.* **57**, 1550–1557 (1967).

54. Petrucci, S., Masiker, M. C. & Eyring, E. M. The possible presence of triple ions in electrolyte solutions of low dielectric permittivity. *J. Solution Chem.* **37**, 1031–1035 (2008).

55. Zhang, J., Kou, R. & Liu, G. Effect of Salt Concentration on the pH Responses of Strong and Weak Polyelectrolyte Brushes. *Langmuir* **33**, 6838–6845 (2017).

56. Rodríguez-Ropero, F. & Van Der Vegt, N. F. A. Ionic specific effects on the structure, mechanics and interfacial softness of a polyelectrolyte brush. *Faraday Discuss.* **160**, 297–309 (2013).

57. Benková, Z., Szefczyk, B. & Cordeiro, M. N. D. S. Molecular dynamics study of hydrated poly(ethylene oxide) chains grafted on siloxane surface. *Macromolecules* **44**, 3639–3648 (2011).

58. Wei, Q., Cai, M., Zhou, F. & Liu, W. Dramatically tuning friction using responsive polyelectrolyte brushes. *Macromolecules* **46**, 9368–9379 (2013).

59. Moro, T. *et al.* Surface grafting of artificial joints with a biocompatible polymer for preventing periprosthetic osteolysis. *Nat. Mater.* **3**, 829–836 (2004).

60. Sakamaki, T. *et al.* Ion-Specific Hydration States of Zwitterionic Poly(sulfobetaine methacrylate) Brushes in Aqueous Solutions. *Langmuir* **35**, 1583–1589 (2019).

61. Chen, S., Zheng, J., Li, L. & Jiang, S. Strong resistance of phosphorylcholine self-assembled monolayers to protein adsorption: Insights into nonfouling properties of zwitterionic materials. *J. Am. Chem. Soc.* **127**, 14473–14478 (2005).

62. He, Y. *et al.* Molecular simulation studies of protein interactions with zwitterionic phosphorylcholine self-assembled monolayers in the presence of water. *Langmuir* **24**, 10358–10364 (2008).

63. Shao, Q. & Jiang, S. Molecular understanding and design of zwitterionic materials. *Adv. Mater.* **27**, 15–26 (2015).

64. Chen, S., Li, L., Zhao, C. & Zheng, J. Surface hydration: Principles and applications toward low-fouling/nonfouling biomaterials. *Polymer (Guildf).* **51**, 5283–5293 (2010).

65. Kitano, H. *et al.* Structure of water incorporated in sulfobetaine polymer films as studied by ATR-FTIR. *Macromol. Biosci.* **5**, 314–321 (2005).

66. Farhan, T., Azzaroni, O. & Huck, W. T. S. AFM study of cationically charged polymer brushes: Switching between soft and hard matter. *Soft Matter* **1**, 66–68 (2005).

67. Wang, X., Liu, G. & Zhang, G. Conformational behavior of grafted weak polyelectrolyte chains: Effects of counterion condensation and nonelectrostatic anion adsorption. *Langmuir* **27**, 9895–9901 (2011).

68. Higaki, Y. *et al.* Counteranion-Specific Hydration States of Cationic Polyelectrolyte Brushes. *Ind. Eng. Chem. Res.* **57**, 5268–5275 (2018).

69. Ramos, J. J. I. & Moya, S. E. Water content of hydrated polymer brushes measured by an in situ combination of a quartz crystal microbalance with dissipation monitoring and spectroscopic ellipsometry. *Macromol. Rapid Commun.* **32**, 1972–1978 (2011).

70. Azzaroni, O., Moya, S., Farhan, T., Brown, A. A. & Huck, W. T. S. Switching the properties

of polyelectrolyte brushes via 'hydrophobic collapse'. *Macromolecules* **38**, 10192–10199 (2005).

71. de Gennes, P. G. Conformations of Polymers Attached to an Interface. *Macromolecules* **13**, 1069–1075 (1980).

72. Milner, S. T., Witten, T. A. & Cates, M. E. Effects of Polydispersity in the End-Grafted Polymer Brush. *Macromolecules* **22**, 853–861 (1989).

73. Zhulina, E. B., Borisov, O. V. & Brombacher, L. Theory of a Planar Grafted Chain Layer Immersed in a Solution of Mobile Polymer. *Macromolecules* **24**, 4679–4690 (1991).

74. Zhulina, E. B. & Borisov, O. V. Structure and interaction of weakly charged polyelectrolyte brushes: Self-consistent field theory. *J. Chem. Phys.* **107**, 5952–5967 (1997).

75. Zhulina, E. B., Borisov, O. V., Pryamitsyn, V. A. & Birshtein, T. M. Coil-Globule Type Transitions in Polymers. 1. Collapse of Layers of Grafted Polymer Chains. *Macromolecules* **24**, 140–149 (1991).

76. Dimitrov, D. I., Milchev, A. & Binder, K. Polymer brushes in solvents of variable quality: Molecular dynamics simulations using explicit solvent. *J. Chem. Phys.* **127**, 84905 (2007).

77. Rossi, G., Elliott, I. G., Ala-Nissila, T. & Faller, R. Molecular dynamics study of a MARTINI coarse-grained polystyrene brush in good solvent: Structure and dynamics. *Macromolecules* **45**, 563–571 (2012).

78. Manav, M., Ponga, M. & Srikantha Phani, A. Stress in a polymer brush. *J. Mech. Phys. Solids* **127**, 125–150 (2019).

79. Lazutin, A. A., Kosmachev, A. N. & Vasilevskaya, V. V. Lamellae and parking garage structures in amphiphilic homopolymer brushes with different grafting densities. *J. Chem. Phys.* **151**, (2019).

80. Larin, D. E., Lazutin, A. A., Govorun, E. N. & Vasilevskaya, V. V. Self-Assembly into Strands in Amphiphilic Polymer Brushes. *Langmuir* **32**, 7000–7008 (2016).

81. Merlitz, H., Li, C. W., Wu, C. X. & Sommer, J. U. Theoretical approaches to starlike polymer brushes in Θ-solvent. *Polymer (Guildf).* **103**, 57–63 (2016).

82. Bedrov, D., Smith, G. D. & Li, L. Molecular dynamics simulation study of the role of evenly spaced poly(ethylene oxide) tethers on the aggregation of C60 fullerenes in water. *Langmuir* **21**, 5251–5255 (2005).

83. Binder, K. Scaling concepts for polymer brushes and their test with computer simulation. *Eur. Phys. J. E* **9**, 293–298 (2002).

84. Farah, K., Leroy, F., Müller-Plathe, F. & Böhm, M. C. Interphase formation during curing: Reactive coarse grained molecular dynamics simulations. *J. Phys. Chem. C* **115**, 16451–16460 (2011).

85. Cordeiro, R. M., Zschunke, F. & Müller-Plathe, F. Mesoscale molecular dynamics simulations of the force between surfaces with grafted poly(ethylene oxide) chains derived from atomistic simulations. *Macromolecules* **43**, 1583–1591 (2010).

86. Dahal, U. R., Wang, Z. & Dormidontova, E. E. Hydration and Mobility of Poly(ethylene oxide) Brushes. *Macromolecules* **50**, 6722–6732 (2017).

87. Filipe, H. A. L. & Loura, L. M. S. Molecular Dynamics Simulations: Advances and Applications. *Molecules* **27**, 2105 (2022).

88. Steve Plimton. Fast Parallel Algorithms for Short-Range Molecular Dynamics. *J. Comput. Phys.* **117**, 1–19 (1995).

89. Thompson, A. P. *et al.* LAMMPS - a flexible simulation tool for particle-based materials modeling at the atomic, meso, and continuum scales. *Comput. Phys. Commun.* **271**, 108171 (2022).

90. Case, D. A. *et al.* Amber 2017 Reference Manual. *Amber 2017* (2017).

91. Abbott, H. E., Hey, J. C., Britton, M. M. & Johnston, R. L. Effects of Hydration on the Conformational Behavior of Flexible Molecules with Two Charge Centers. *J. Phys. Chem. A* **124**, 5323–5330 (2020).

92. Rapaport, D. C. *The Art of Molecular Dynamics Simulations*. (Cambridge Univ. Press, 1995).

93. Allen, M. P. & Tildesley, D. J. *Computer Simulation of Liquids*. (Oxford University Press, 1987).

94. González, M. A. Force Fields and Molecular Dynamiccs Simulations. in *JDN 18 - Neutrons et Simulations* vol. 12 169–200 (2011).

95. Hess, B., Kutzner, C., Van Der Spoel, D. & Lindahl, E. GROMACS 4: Algorithms for highly efficient, load-balanced, and scalable molecular simulation. *J. Chem. Theory Comput.* **4**, 435–447 (2008).

96. Pearlman, D. A. *et al.* AMBER, a package of computer programs for applying molecular mechanics, normal mode analysis, molecular dynamics and free energy calculations to simulate the structural and energetic properties of molecules. *Comput. Phys. Commun.* **91**, 1–41 (1995).

97. D.A. Case, I.Y. Ben-Shalom, S.R. Brozell, D.S. Cerutti, T.E. Cheatham, III, V.W.D. Cruzeiro, T.A. Darden, R.E. Duke, D. Ghoreishi, M.K. Gilson, H. Gohlke, A.W. Goetz, D. Greene, R Harris, N. Homeyer, S. Izadi, A. Kovalenko, T. Kurtzman, T.S. Lee, S. L. AMBER 2018. (2018).

98. Bayly, C. I. *et al.* A Second Generation Force Field for the Simulation of Proteins, Nucleic Acids, and Organic Molecules. *J. Am. Chem. Soc.* **117**, 5179–5197 (1995).

99. Maier, J. A. *et al.* ff14SB: Improving the Accuracy of Protein Side Chain and Backbone Parameters from ff99SB. *J. Chem. Theory Comput.* **11**, 3696–3713 (2015).

100. Lindorff-Larsen, K. *et al.* Improved side-chain torsion potentials for the Amber ff99SB protein force field. *Proteins: Struct., Funct., Bioinf* **78**, 1950–1958 (2010).

101. Wang, J. & Hou, T. Application of molecular dynamics simulations in molecular property prediction. 1. Density and heat of vaporization. *J. Chem. Theory Comput.* **7**, 2151–2165 (2011).

102. Wang, J. & Hou, T. Application of molecular dynamics simulations in molecular property

prediction II: Diffusion coefficient. *J. Comput. Chem.* **32**, 3505–3519 (2011).

103. Caleman, C. *et al.* Force field benchmark of organic liquids: Density, enthalpy of vaporization, heat capacities, surface tension, isothermal compressibility, volumetric expansion coefficient, and dielectric constant. *J. Chem. Theory Comput.* **8**, 61–74 (2012).

104. Loup Verlet. Computer 'Experiments' on Classical Fluids. I. Thermodynamical Properties of Lennard-Jones Molecules. *Phys. Rev.* 98–103 (1967) doi:10.1088/0022-3727/9/2/008.

105. Swope, W. C., Andersen, H. C., Berens, P. H. & Wilson, K. R. A computer simulation method for the calculation of equilibrium constants for the formation of physical clusters of molecules: Application to small water clusters. *J. Chem. Phys.* **76**, 637–649 (1982).

106. Beeman, D. Some multistep methods for use in molecular dynamics calculations. *J. Comput. Phys.* **20**, 130–139 (1976).

107. NosÉ, S. A molecular dynamics method for simulations in the canonical ensemble. *Mol. Phys.* **100**, 191–198 (2002).

108. Allen, M. P. & Tildesley, D. J. Computer Simulation of Liquids. (1987).

109. Hockney, R. W. & Eastwoord, J. W. *Computer Simulation Using Particles*. (Adam Hilger, 1988).

110. Jorgensen, W. L., Chandrasekhar, J., Madura, J. D., Impey, R. W. & Klein, M. L. Comparison of simple potential functions for simulating liquid water. *J. Chem. Phys.* **79**, 926–935 (1983).

111. Guillot, B. A reappraisal of what we have learnt during three decades of computer simulations on water. *J. Mol. Liq.* **101**, 219–260 (2002).

112. Kazachenko, S. & Thakkar, A. J. Water nanodroplets: Predictions of five model potentials. *J. Chem. Phys.* **138**, 194302 (2013).

113. Mahoney, M. W. & Jorgensen, W. L. A five-site model for liquid water and the reproduction of the density anomaly by rigid, nonpolarizable potential functions. *J. Chem. Phys.* **112**, 8910–8922 (2000).

114. Schlier, C. Intermolecular Forces. *Annu. Rev. Phys. Chem.* **20**, 191–218 (1969).

115. Berendsen, H. J. C., Grigera, J. R. & Straatsma, T. P. The missing term in effective pair potentials. *J. Phys. Chem.* **91**, 6269–6271 (1987).

116. Mark, P. & Nilsson, L. Structure and dynamics of the TIP3P, SPC, and SPC/E water models at 298 K. *J. Phys. Chem. A* **105**, 9954–9960 (2001).

117. Elliott, I. G., Kuhl, T. L. & Faller, R. Compression of high grafting density opposing polymer brushes using molecular dynamics simulations in explicit solvent. *J. Phys. Chem. B* **117**, 4134–4141 (2013).

118. Ell, J. R., Mulder, D. E., Faller, R., Patten, T. E. & Kuhl, T. L. Structural determination of high density, ATRP grown polystyrene brushes by neutron reflectivity. *Macromolecules* **42**, 9523–9527 (2009).

119. Liao, W. P., Elliott, I. G., Faller, R. & Kuhl, T. L. Normal and shear interactions between high grafting density polymer brushes grown by atom transfer radical polymerization. *Soft Matter* **9**, 5753–5761 (2013).

120. Kreer, T., Metzger, S., Müller, M., Binder, K. & Baschnagel, J. Static properties of end-tethered polymers in good solution: A comparison between different models. *J. Chem. Phys.* **120**, 4012–4023 (2004).

121. Wales, D. J. *Energy Landscapes: Applications to Clusters, Biomolecules and Glasses*. (Cambridge Univ. Press, 2004).

122. Wales, D. J. & Doye, J. P. K. Global Optimization by Basin-Hopping and the Lowest Energy Structures of Lennard-Jones Clusters Containing up to 110 Atoms. *J. Phys. Chem. A* **101**, 5111–5116 (1997).

123. Stuart, M. A. C. *et al.* Emerging applications of stimuli-responsive polymer materials. *Nat. Mater.* **9**, 101–113 (2010).

124. Yameen, B. & Farrukh, A. Polymer brushes: Promises and challenges. *Chem. - An Asian J.* **8**, 1736–1753 (2013).

125. Azzaroni, O. Polymer brushes here, there, and everywhere: Recent advances in their practical applications and emerging opportunities in multiple research fields. *J. Polym. Sci. Part A Polym. Chem.* **50**, 3225–3258 (2012).

126. Mendes, P. M. Stimuli-responsive surfaces for bio-applications. *Chem. Soc. Rev.* **37**, 2512–2529 (2008).

127. Mazzini, V., Liu, G. & Craig, V. S. J. Probing the Hofmeister series beyond water: Specific-ion effects in non-aqueous solvents. *J. Chem. Phys.* **148**, 2228050 (2018).

128. Sachar, H. S. *et al.* Densely Grafted Polyelectrolyte Brushes Trigger “Water-in-Salt”-like Scenarios and Ultraconfinement Effect. *Matter* **2**, 1509–1521 (2020).

129. Humphrey, W., Dalke, A. & Schulten, K. VMD: Visual Molecular Dynamics. *J. Mol. Graph.* **14**, 33–38 (1996).

130. Joung, S. & Cheatham, T. E. Molecular dynamics simulations of the dynamic and energetic properties of alkali and halide ions using water-model-specific ion parameters. *J. Phys. Chem. B* **113**, 13279–13290 (2009).

131. Bayly, C. I., Cieplak, P., Cornell, W. D. & Kollman, P. A. A well-behaved electrostatic potential based method using charge restraints for deriving atomic charges: The RESP model. *J. Phys. Chem.* **97**, 10269–10280 (1993).

132. Ryckaert, J. P., Ciccotti, G. & Berendsen, H. J. C. Numerical integration of the cartesian equations of motion of a system with constraints: molecular dynamics of n-alkanes. *J. Comput. Phys.* **23**, 327–341 (1977).

133. Giorgino, T. Computing diffusion coefficients in macromolecular simulations: the Diffusion Coefficient Tool for VMD. *J. Open Source Softw.* **4**, 1698 (2019).

134. Jungwirth, P. Ion Pairing: From Water Clusters to the Aqueous Bulk. *J. Phys. Chem. B* **118**, 10333–10334 (2014).

135. Schran, C. *et al.* Machine learning potentials for complex aqueous systems made

simple. *Proc. Natl. Acad. Sci. U. S. A.* **118**, 1–8 (2021).

136. Dill, K. A. Dominant Forces in Protein Folding. *Biochemistry* **29**, 7133–7155 (1990).

137. Iwadate, Y., Kawamura, K., Igarashi, K. & Mochinaga, J. Effective ionic radii of NO2- and SCN- estimated in terms of the Böttcher equation and the Lorentz-Lorenz equation. *J. Phys. Chem.* **86**, 5205–5208 (1982).

138. Marcus, Y. Ionic Radii in Aqueous Solutions. *Chem. Rev.* **88**, 1475–1498 (1988).

139. Dünweg, B. & Kremer, K. Molecular dynamics simulation of a polymer chain in solution. *J. Chem. Phys.* **99**, 6983–6997 (1993).

140. Heyes, D. M., Cass, M. J., Powles, J. G. & Evans, W. A. B. Self-diffusion coefficient of the hard-sphere fluid: System size dependence and empirical correlations. *J. Phys. Chem. B* **111**, 1455–1464 (2007).

141. Zhang, Y., Guo, G., Refson, K. & Zhao, Y. Finite-size effect at both high and low temperatures in molecular dynamics calculations of the self-diffusion coefficient and viscosity of liquid silica. *J. Phys. Condens. Matter* **16**, 9127–9135 (2004).

142. Yeh, I. C. & Hummer, G. System-size dependence of diffusion coefficients and viscosities from molecular dynamics simulations with periodic boundary conditions. *J. Phys. Chem. B* **108**, 15873–15879 (2004).

143. Jamali, S. H. *et al.* Finite-Size Effects of Binary Mutual Diffusion Coefficients from Molecular Dynamics. *J. Chem. Theory Comput.* **14**, 2667–2677 (2018).

144. Gowers, R. *et al.* MDAnalysis: A Python Package for the Rapid Analysis of Molecular Dynamics Simulations. *Proc. 15th Python Sci. Conf.* 98–105 (2016) doi:10.25080/Majora-629e541a-00e.

145. Michaud-Agrawal, N., Denning, E., Woolf, T. & Beckstein, O. Software News and Updates MDAnalysis — A Toolkit for the Analysis of Molecular Dynamics Simulations. *J. Comput. Chem.* **32**, 2319–2327 (2011).

146. Chang, Y., Chen, S., Zhang, Z. & Jiang, S. Highly protein-resistant coatings from well-defined diblock copolymers containing sulfobetaines. *Langmuir* **22**, 2222–2226 (2006).

147. Xiao, S. *et al.* Structural Dependence of Salt-Responsive Polyzwitterionic Brushes with an Anti-Polyelectrolyte Effect. *Langmuir* **34**, 97–105 (2018).

148. Jungwirth, P. & Cremer, P. S. Beyond Hofmeister. *Nat. Chem.* **6**, 261–263 (2014).

149. Bagchi, B. Biological water. in *Water in Biological and Chemical Processes* 81–96 (Cambridge University Press, 2013).

150. Wyttenbach, T. & Bowers, M. T. Hydration of biomolecules. *Chem. Phys. Lett.* **480**, 1–16 (2009).

151. Pal, S. K., Peon, J. & Zewail, A. H. Biological water at the protein surface: Dynamical solvation probed directly with femtosecond resolution. *Proc. Natl. Acad. Sci. U. S. A.* **99**, 1763–1768 (2002).

152. Xie, W. J. & Gao, Y. Q. A simple theory for the hofmeister series. *J. Phys. Chem. Lett.* **4**, 4247–4252 (2013).

153. Rembert, K. B. *et al.* Molecular mechanisms of ion-specific effects on proteins. *J. Am. Chem. Soc.* **134**, 10039–10046 (2012).

154. Alonso-García, T. *et al.* Temperature-dependent transport properties of poly[2-(methacryloyloxy) ethyl]trimethylammonium chloride brushes resulting from ion specific effects. *J. Phys. Chem. C* **117**, 26680–26688 (2013).

155. Moya, S., Azzaroni, O., Farhan, T., Osborne, V. L. & Huck, W. T. S. Locking and unlocking of polyelectrolyte brushes: Toward the fabrication of chemically controlled nanoactuators. *Angew. Chemie - Int. Ed.* **44**, 4578–4581 (2005).

156. Pegado, L., Marsalek, O., Jungwirth, P. & Wernersson, E. Solvation and ion-pairing properties of the aqueous sulfate anion: Explicit versus effective electronic polarization. *Phys. Chem. Chem. Phys.* **14**, 10248–10257 (2012).

157. Mason, P. E., Neilson, G. W., Kline, S. R., Dempsey, C. E. & Brady, J. W. Nanometer-scale ion aggregates in aqueous electrolyte solutions: Guanidinium carbonate. *J. Phys. Chem. B* **110**, 13477–13483 (2006).

158. Cerutti, D. S., Le Trong, I., Stenkamp, R. E. & Lybrand, T. P. Simulations of a protein crystal: Explicit treatment of crystallization conditions links theory and experiment in the streptavidin-biotin complex. *Biochemistry* **47**, 12065–12077 (2008).

159. Chialvo, A. A. & Simonson, J. M. Solvation and ion pair association in aqueous metal sulfates: Interpretation of NDIS raw data by isobaric-isothermal molecular dynamics simulation. *Collect. Czechoslov. Chem. Commun.* **75**, 405–424 (2010).

160. Wernersson, E. & Jungwirth, P. Effect of water polarizability on the properties of solutions of polyvalent ions: Simulations of aqueous sodium sulfate with different force fields. *J. Chem. Theory Comput.* **6**, 3233–3240 (2010).

161. Pol-Fachin, L., Verli, H. & Lins, R. D. Extension and validation of the GROMOS 53A6(GLYC) parameter set for glycoproteins. *J. Comput. Chem.* **35**, 2087–2095 (2014).

162. Wyttenbach, T., Liu, D. & Bowers, M. T. Hydration of small peptides. *Int. J. Mass Spectrom.* **240**, 221–232 (2005).

163. Wende, T. *et al.* Spectroscopic characterization of solvent-mediated folding in dicarboxylate dianions. *Angew. Chemie - Int. Ed.* **50**, 3807–3810 (2011).

164. Asmis, K. R. & Neumark, D. M. Vibrational spectroscopy of microhydrated conjugate base anions. *Acc. Chem. Res.* **45**, 43–52 (2012).

165. Tobias, D. J. & Hemminger, J. C. Chemistry: Getting specific about specific ion effects. *Science (80-. ).* **319**, 1197–1198 (2008).

166. Yang, X. *et al.* Solvent-Mediated Folding of a Doubly Charged Anion. *J. Am. Chem. Soc.* **126**, 876–883 (2004).

167. Wang, X.-B. & Wang, L.-S. Photoelectron Spectroscopy of Multiply Charged Anions. *Annu. Rev. Phys. Chem.* **60**, 105–126 (2009).

168. Wang, L. S. & Wang, X. Bin. Probing Free Multiply Charged Anions Using Photodetachment Photoelectron Spectroscopy. *J. Phys. Chem. A* **104**, 1978–1990 (2000).

169. Minofar, B. *et al.* Bulk versus Interfacial Aqueous Solvation of Dicarboxylate Dianions. *J. Am. Chem. Soc.* **126**, 11691–11698 (2004).

170. Gilligan, J. J., Lampe, F. W., Nguyen, V. Q., Vieira, N. E. & Yergey, A. L. Hydration of Alkylammonium Ions in the Gas Phase. *J. Phys. Chem. A* **107**, 3687–3691 (2003).

171. Servage, K. A., Silveira, J. A., Fort, K. L. & Russell, D. H. Cryogenic Ion Mobility-Mass Spectrometry: Tracking Ion Structure from Solution to the Gas Phase. *Acc. Chem. Res.* **49**, 1421–1428 (2016).

172. Servage, K. A. *et al.* Unfolding of Hydrated Alkyl Diammonium Cations Revealed by Cryogenic Ion Mobility-Mass Spectrometry. *J. Am. Chem. Soc.* **137**, 8916–8919 (2015).

173. Jahangiri, S., Legris-Falardeau, V. & Peslherbe, G. H. Computational investigation of the hydration of alkyl diammonium cations in water clusters. *Chem. Phys. Lett.* **621**, 85–90 (2015).

174. Demireva, M., O'Brien, J. T. & Williams, E. R. Water-induced folding of 1,7-diammoniumheptane. *J. Am. Chem. Soc.* **134**, 11216–11224 (2012).

175. Xing, X. P., Wang, X. Bin & Wang, L. S. Photoelectron imaging of doubly charged anions,-O 2C(CH2)nCO2- (n = 2-8): Observation of near 0 eV electrons due to secondary dissociative autodetachment. *J. Phys. Chem. A* **114**, 4524–4530 (2010).

176. Wanko, M. *et al.* Solvent-mediated folding of dicarboxylate dianions: aliphatic chain length dependence and origin of the IR intensity quenching. *Phys. Chem. Chem. Phys.* **15**, 20463–72 (2013).

177. Kravets, M., Misztalewska-Turkowicz, I. & Sashuk, V. Plasmonic nanoprobes gauging the length and flexibility of α,ω-Alkanedicarboxylic acids with an optical readout. *Sensors Actuators, B Chem.* **343**, 130083 (2021).

178. Klassen, J. S., Blades, A. T. & Kebarle, P. Gas Phase Ion-Molecule Equilibria Involving Ions Produced by Electrospray. Hydration of Doubly Protonated Diamines. *J. Am. Chem. Soc.* **116**, 12075–12076 (1994).

179. Li, Z. & Scheraga, H. A. Monte Carlo-minimization approach to the multiple-minima problem in protein folding. *Proc. Natl. Acad. Sci. U. S. A.* **84**, 6611–6615 (1987).

180. Kabrede, H. & Hentschke, R. Global Minima of Water Clusters (H 2 O) N , N ≤ 25, Described by Three Empirical Potentials. *J. Phys. Chem. B* **107**, 3914–3920 (2003).

181. M. J. Frisch, G. W. Trucks, H. B. Schlegel, G. E. Scuseria, M. A. Robb, J. R. Cheeseman, G. Scalmani, V. Barone, G. A. Petersson, H. Nakatsuji, X. Li, M. Caricato, A. Marenich, J. Bloino, B. G. Janesko, R. Gomperts, B. Mennucci, H. P. Hratchian, J. V. Ort, D. J. F. Gaussian09, Revision A.02. (2016).

182. Sanz, E., Vega, C., Abascal, J. L. F. & Macdowell, L. G. Tracing the phase diagram of the four-site water potential (TIP4). *J. Chem. Phys.* **121**, 1165–1166 (2004).

183. Hey, J. C., Smeeton, L. C., Oakley, M. T. & Johnston, R. L. Isomers and Energy Landscapes of Perchlorate-Water Clusters and a Comparison to Pure Water and Sulfate-Water Clusters. *J. Phys. Chem. A* **120**, 4008–4015 (2016).

184. Smeeton, L. C., Farrell, J. D., Oakley, M. T., Wales, D. J. & Johnston, R. L. Structures and energy landscapes of hydrated sulfate clusters. *J. Chem. Theory Comput.* **11**, 2377–2384

(2015).

185. Kazachenko, S. & Thakkar, A. J. Improved minima-hopping. TIP4P water clusters, (H2O)n with n ≤ 37. *Chem. Phys. Lett.* **476**, 120–124 (2009).

186. Sanz, E., Vega, C., Abascal, J. L. F. & MacDowell, L. G. Phase diagram of water from computer simulation. *Phys. Rev. Lett.* **92**, (2004).

187. Case, D. A. & Tsui, V. Theory and Applications of the Generalized Born Solvation Model in Macromolecular Simulations. *Biopolym. (Nucleic Acid Sci.* **56**, 275–291 (2001).

188. Roe, D. R. & Cheatham, T. E. PTRAJ and CPPTRAJ: Software for processing and analysis of molecular dynamics trajectory data. *J. Chem. Theory Comput.* **9**, 3084–3095 (2013).

189. Dunning, T. H. Gaussian basis sets for use in correlated molecular calculations. I. The atoms boron through neon and hydrogen. *J. Chem. Phys.* **90**, 2657 (1989).

190. Thalladi, V. R., Nu, M. & Boese, R. The Melting Point Alternation in R,ω-Alkanedicarboxylic Acids Introduction: An Odyssey through 120 Years of Research. *J. Am. Chem. Soc.* **122**, 9227–9236 (2000).

191. Thompson, L. J., Voguri, R. S., Male, L. & Tremayne, M. The crystal structures and melting point properties of isonicotinamide cocrystals with alkanediacids HO2C(CH2)n−2CO2H n = 7–9. *CrystEngComm* **13**, 4188–4195 (2011).

192. Ganguly, P., Schravendijk, P., Hess, B. & Van Der Vegt, N. F. A. Ion pairing in aqueous electrolyte solutions with biologically relevant anions. *J. Phys. Chem. B* **115**, 3734–3739 (2011).

193. Van Der Vegt, N. F. A. *et al.* Water-Mediated Ion Pairing: Occurrence and Relevance. *Chem. Rev.* **116**, 7626–7641 (2016).

194. Allen, S. J., Giles, K., Gilbert, T. & Bush, M. F. Ion mobility mass spectrometry of peptide, protein, and protein complex ions using a radio-frequency confining drift cell. *Analyst* **141**, 884–891 (2016).

195. Lamb, D., Schüttelkopf, A. W., van Aalten, D. M. F. & Brighty, D. W. Charge-surrounded pockets and electrostatic interactions with small ions modulate the activity of retroviral fusion proteins. *PLoS Pathog.* **7**, 1–12 (2011).

196. Crevenna, A. H., Naredi-Rainer, N., Lamb, D. C., Wedlich-Söldner, R. & Dzubiella, J. Effects of hofmeister ions on the α-helical structure of proteins. *Biophys. J.* **102**, 907–915 (2012).

197. Bagchi, B. Water dynamics in the hydration layer around proteins and micelles. *Chem. Rev.* **105**, 3197–3219 (2005).

# APPENDICES

## Appendix 1: Molecular Dynamics Simulation Performance Discussion

The PB models simulated in Chapters 3, 4, 5 and 6 consist of between approximately 50,000 and 300,000 atoms. Consequently, particularly for the systems on the larger end of that scale, performing runs with simulation times close to experimentally relevant ones was somewhat of a challenge. This led to the need to optimise simulation performance as much as possible. For example, minimising the number of solvent molecules within each system, and increasing the temperature, from 298 K to 500 K, for the equilibrium runs.

A breakthrough for improving the performance of MD simulations of PB systems in this thesis, was gaining access to the graphical processing units (GPUs) provided by The University of Birmingham's BlueBEAR High-Performance Computing service (see http:// www.birmingham.ac.uk/bear for more details). GPUs represent a major technical improvement for atomistic MD simulations. Originally, GPUs were designed to handle computer graphics. Whereas recently, they have developed into fully programmable, high-performance processors. LAMMPS is compatible for use with GPUs. The time taken for the simulations to run was dramatically reduced as can be seen in Figure A.1.1 for the eight-chain PMETAC system.

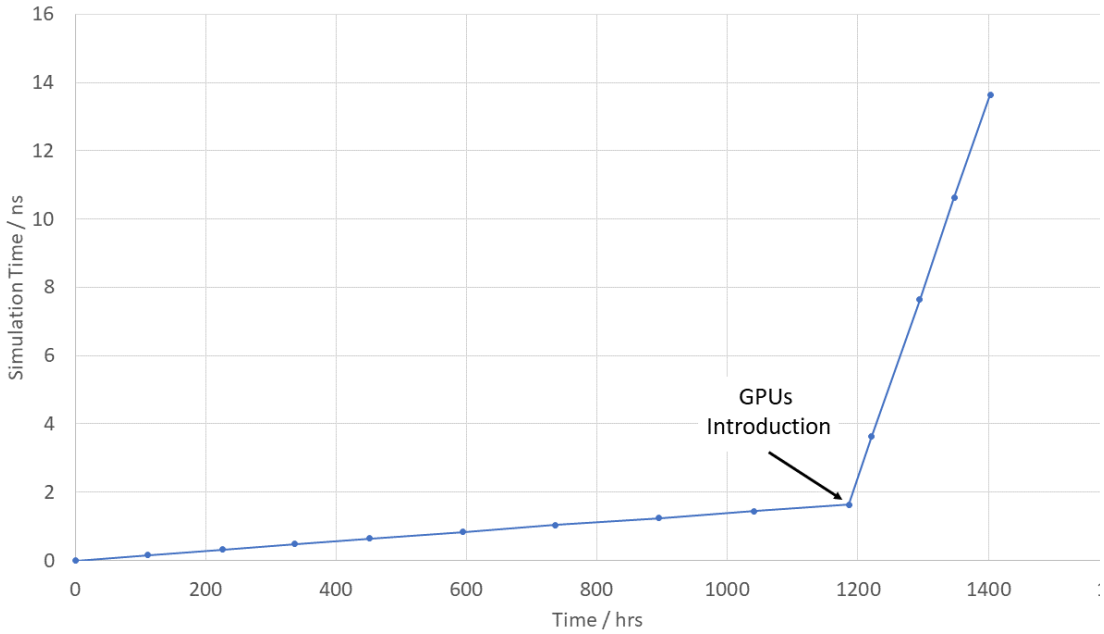


**Figure A.1.1** Plot of simulation time as a function of the amount of time taken for the simulation to run. The plot is of the eight-chain PMETAC system discussed extensively in Chapter 5. The point at which GPUs were introduced is marked on the plot.

Appendix 2: Graphs of the Time Evolution of Maximum Height of Brush for Polymer Brush Simulations in Studied Solutions.

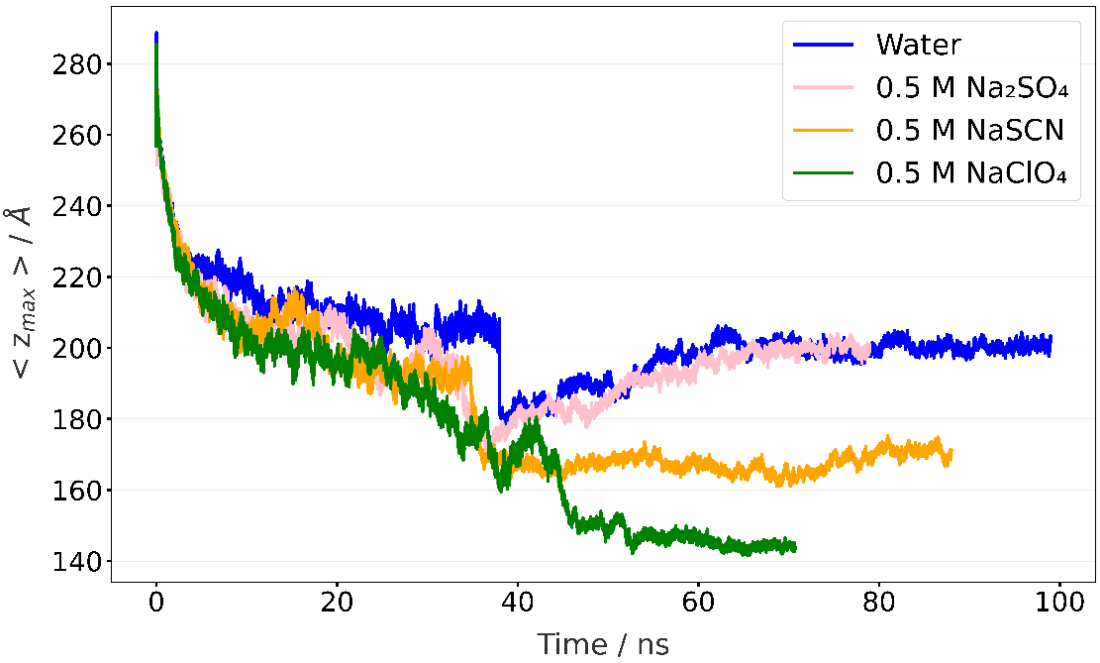


**Figure A.2.1** Time evolution of maximum height of brush for PMETAC (two-chain model) simulations in different salt solutions. PMETAC in water (blue), PMETAC in aqueous solution of 0.5 M sodium thiocyanate (orange), PMETAC in 0.5 M sodium sulfate (pink) and PMETAC in 0.5 M sodium perchlorate (green).

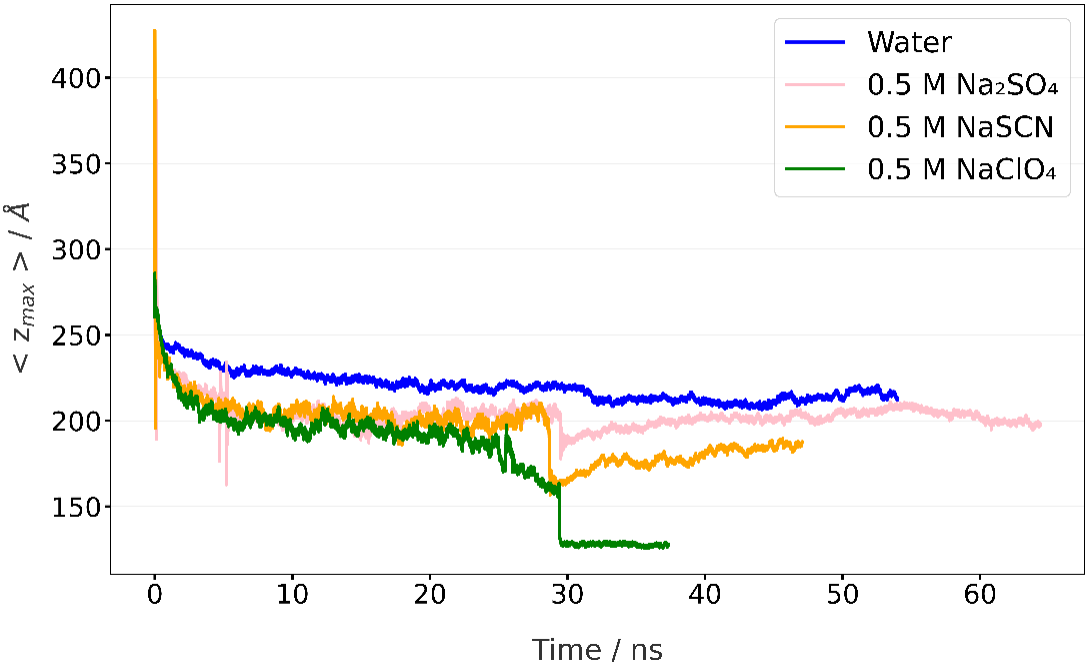


**Figure A.2.2** Time evolution of maximum height of brush for PMETAC (eight-chain model) simulations in different salt solutions. PMETAC in water (blue), PMETAC in aqueous solution of 0.5 M sodium thiocyanate (orange), PMETAC in 0.5 M sodium sulfate (pink) and PMETAC in 0.5 M sodium perchlorate (green).

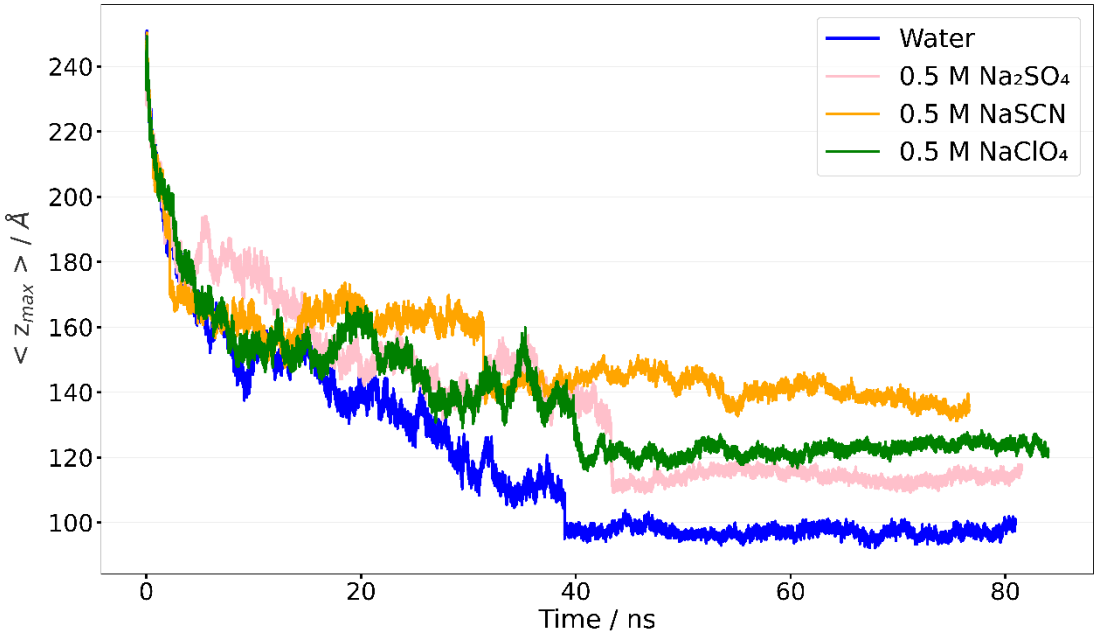


**Figure A.2.3** Time evolution of maximum height of brush for PSBMA (two-chain model) simulations in different salt solutions. PSBMA in water (blue), PSBMA in aqueous solution of 0.5 M sodium thiocyanate (orange), PSBMA in 0.5 M sodium sulfate (pink) and PSBMA in 0.5 M sodium perchlorate (green).

Appendix 3: Additional Lifetime Distribution Graphs of Chloride Counterions in the Two-Chain PMETAC Brush Systems.

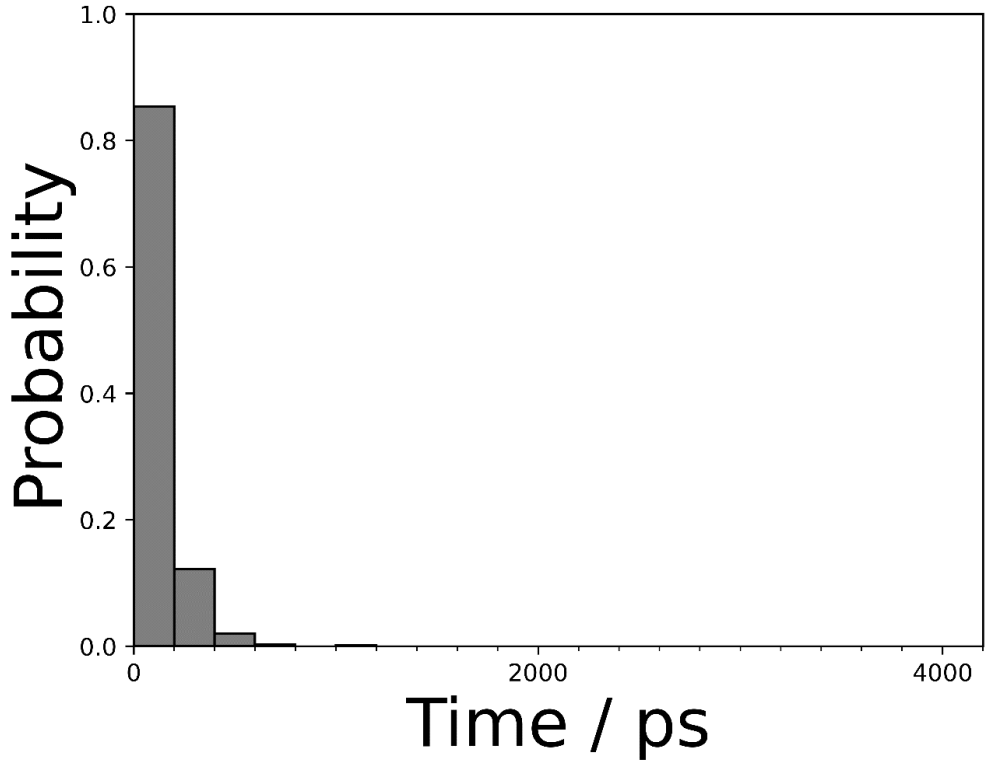


**Figure A.3.1** Plot of the normalised distribution of lifetimes for the $Cl^-$ counterions within 8.15 Å of the nitrogen atoms of the QA groups ($N_{QA}$) along the PMETAC chains (two-chain model) in 0.5 M NaSCN solution.

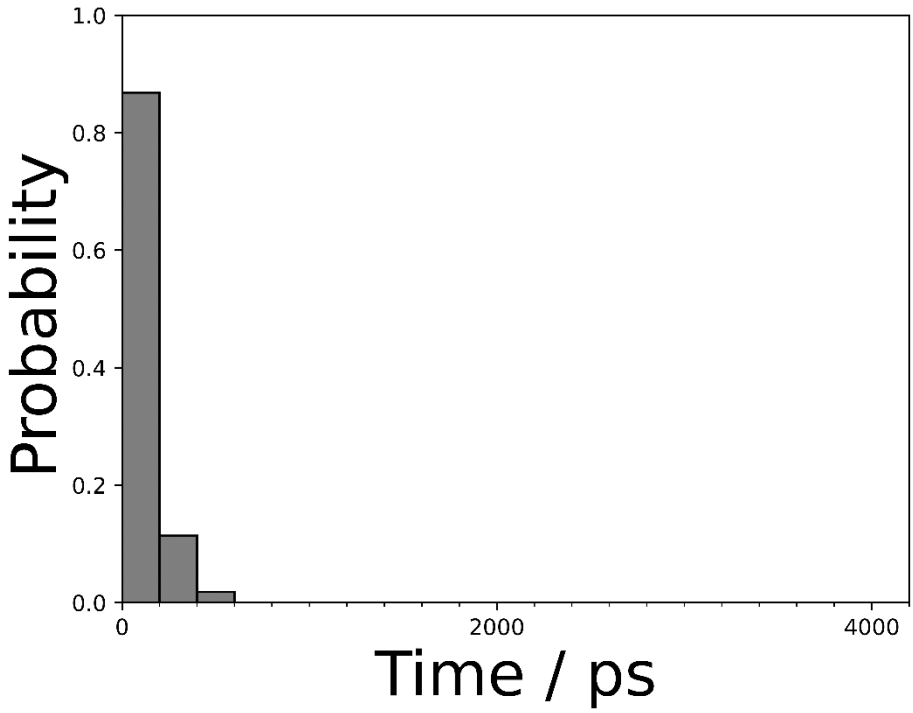


**Figure A.3.2** Plot of the normalised distribution of lifetimes for the $Cl^-$ counterions within 8.15 Å of the nitrogen atoms of the QA groups ($N_{QA}$) along the PMETAC chains (two-chain model) in 0.5 M $NaClO_4$ solution.

## Appendix 4: Percentage Values Describing the Change in Water Molecules within the PB systems.

**Table A.4.1** Table of the percentage loss of water molecules within the PMETAC brush (two-chain) in the presence of 0.5 M NaSCN and 0.5 M $NaClO_4$ solution. This is compared to the amount of water molecules in the PMETAC brush (two-chain) in water.

| **Electrolytic Solution** | **Percentage $H_2O$ loss** |
|---|---|
| **NaSCN** | 13 |
| **$NaClO_4$** | 34 |

**Table A.4.2** Table of the percentage gain of water molecules within the PSBMA brush (two-chain) in the presence of 0.5 M NaSCN and 0.5 M $NaClO_4$ solution. This is compared to the amount of water molecules in the PSBMA brush (two-chain) in water.

| **Electrolytic Solution** | **Percentage $H_2O$ Gain** |
|---|---|
| **NaSCN** | 29 |
| **$NaClO_4$** | 25 |

**Table A.4.3** Table of the percentage loss of water molecules within the PMETAC brush (eight-chain) in the presence of 0.5 M NaSCN and 0.5 M $NaClO_4$ solution. This is compared to the amount of water molecules in the PMETAC brush (eight-chain) in water.

| **Electrolytic Solution** | **Percentage $H_2O$ loss** |
|---|---|
| **NaSCN** | 13 |
| **$NaClO_4$** | 30 |

## Appendix 5: Percentage Values Describing the Proportion of Functional Groups Involved in Ion Pairing and Clustering in Polymer Brush systems

**Table A.5.1** Table of the percentage values of quaternary ammonium (QA) groups on the grafted PMETAC chains (two-chain model) bound to the external salt anions, ion pairs and higher-order ion clustering averaged over the trajectory for $ClO_4^-$ and $SCN^-$ anions

| **Ionic Species** | **Percentage of QA groups involved in ion binding** | **Percentage of QA groups involved in Ion Pairing** | **Percentage of QA groups involved in Ion Clusters** |
|---|---|---|---|
| **$SCN^-$** | 91 | 44 | 47 |
| **$ClO_4^-$** | 100 | 11 | 89 |

**Table A.5.2** Table of the percentage values of quaternary ammonium (QA) groups on the grafted PSBMA chains (two-chain model) bound to the external salt anions, ion pairs and higher-order ion clustering averaged over the trajectory for $ClO_4^-$ and $SCN^-$ anions

| **Ionic Species** | **Percentage of QA groups involved in ion binding** | **Percentage of QA groups involved in Ion Pairing** | **Percentage of QA groups involved in Ion Clusters** |
|---|---|---|---|
| **$SCN^-$** | 85 | 55 | 30 |
| **$ClO_4^-$** | 92 | 38 | 54 |

**Table A.5.3** Table of the percentage values of sulfonate groups on the PSBMA chains bound to the $Na^+$ cations, ion pairs and higher-order ion clustering averaged over the trajectory for the PSBMA brush (two-chain model) in 0.5 M $NaClO_4$ solution and 0.5 M NaSCN solutions.

| Electrolytic Solution | Percentage of sulfonate groups involved in ion binding | Percentage of sulfonate groups involved in Ion Pairing | Percentage of sulfonate groups involved in Ion Clusters |
|---|---|---|---|
| **NaSCN** | 38 | 33 | 5 |
| **$NaClO_4$** | 52 | 40 | 12 |

**Table A.5.4** Table of the percentage values of quaternary ammonium (QA) groups on the grafted PMETAC chains (eight-chain model) bound to the external salt anions, ion pairs and higher-order ion clustering averaged over the trajectory for $ClO_4^-$ and $SCN^-$ anions.

| Ionic Species | Percentage of QA groups involved in ion binding | Percentage of QA groups involved in Ion Pairing | Percentage of QA groups involved in Ion Clusters |
|---|---|---|---|
| **$SCN^-$** | 92 | 40 | 52 |
| **$ClO_4^-$** | 96 | 23 | 73 |

## Appendix 6: Plot of the Radial Distribution Function of the Quaternary Ammonium Groups and Sodium Cations in PSBMA Brush Systems and Diffusion Coefficient Values for Sodium Cations in PMETAC systems

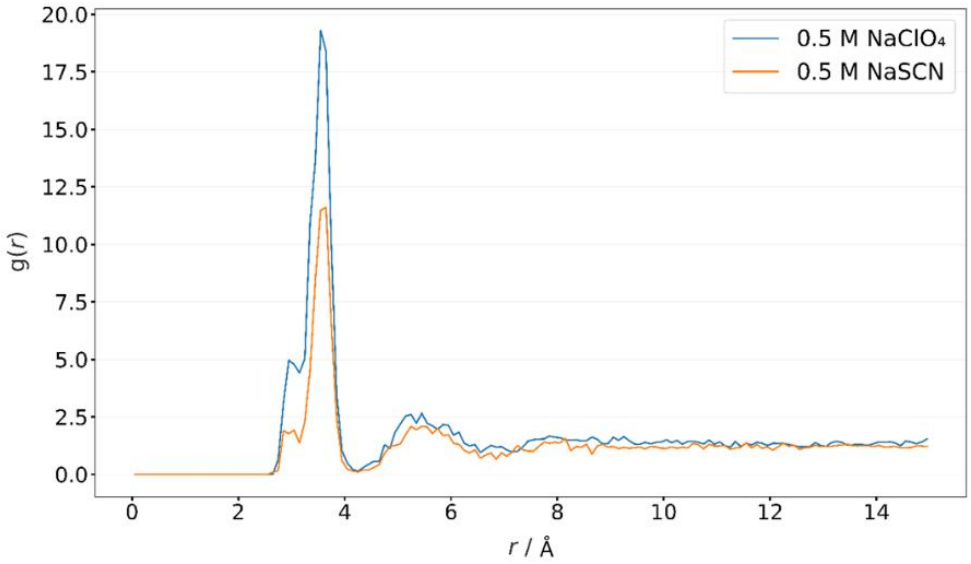


**Figure A.6.1.** Plot of the radial distribution functions (RDFs) of the nitrogen in the QA group ($N_{QA}$) of the PSBMA chains with the $Na^+$ cations in 0.5 M $NaClO_4$ (blue) and 0.5 M NaSCN (orange) solutions.

**Table A.6.1** Table of the calculated Diffusion Coefficient values and those values used in the ion pair calculations of the sodium cations in the studied PMETAC brush (two-chain) systems.

| **Solution** | **Diffusion Coefficient of $Na^+$ Cations / $Å^2$ $ns^{-1}$** | **Approximated Diffusion Coefficient of $Na^+$ Cations / $Å^2$ $ns^{-1}$** |
|---|---|---|
| **NaSCN** | 46.85 | 47 |
| **$NaClO_4$** | 45.57 | 46 |

Appendix 7: Plot of variation in end-to-end brush height of two-chain PMETAC brush model in studied salt solutions.

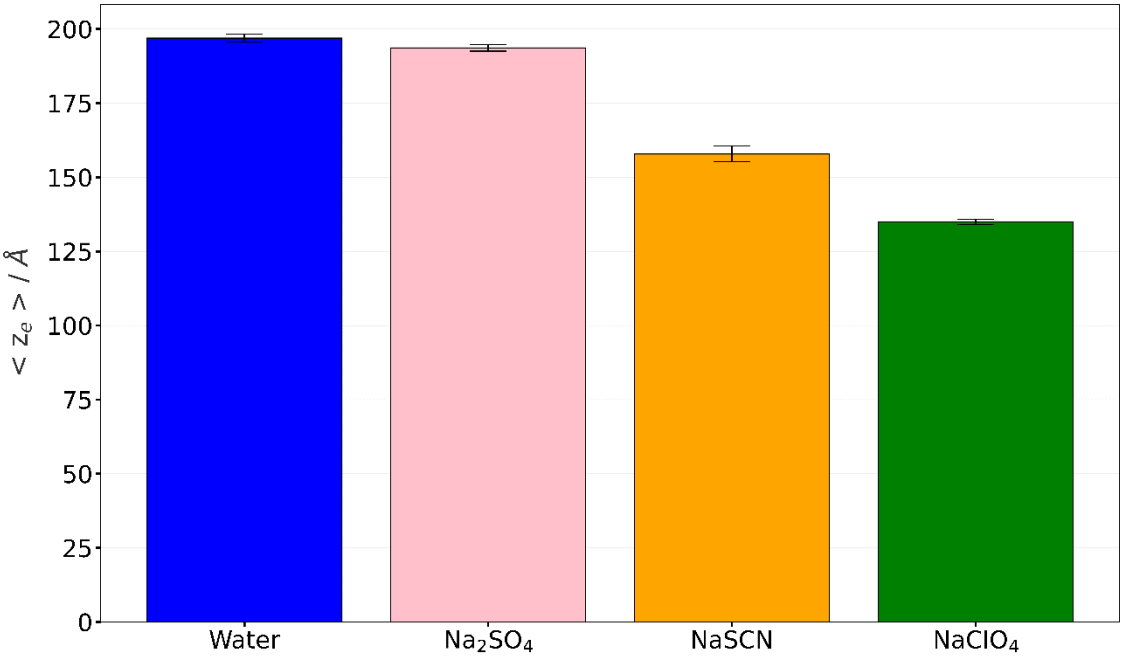


**Figure A.7.1** Plot of variation in end-to-end brush height (< $z_e$ >) of the two PMETAC chain brush model in the presence of water (blue), 0.5 M $NaSO_4$ (pink), 0.5 M NaSCN (orange) and 0.5 M $NaClO_4$ (green) solution. Error bars are shown representing the standard deviation of the set of end-to-end brush height values per PMETAC brush system.

Appendix 8: Plots of the conformational energies and second differences plots for Di-ammonium Di-Cations in Unhydrated Conditions.

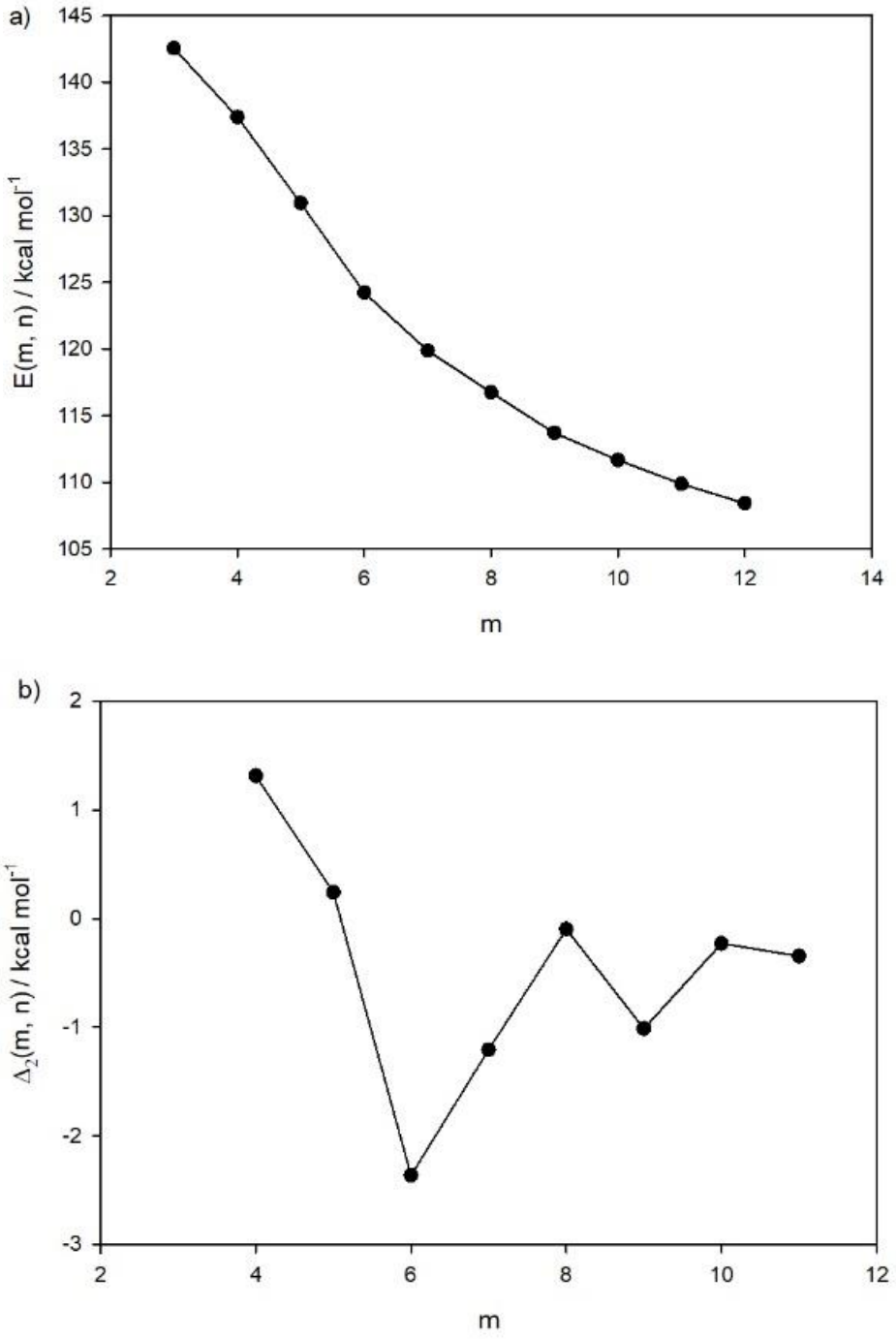


**Figure A.8.1:** a) A plot of the conformational energies as a function of carbon chain length for unhydrated $DA_m$ with $m$ = 3 - 12. b) A plot of second difference for unhydrated $DA_m$ with $m$ = 4 - 11.

Appendix 9: Plots of the second differences for Di-carboxylate Di-Anions in Unhydrated Conditions for the Different Energy Contributions.

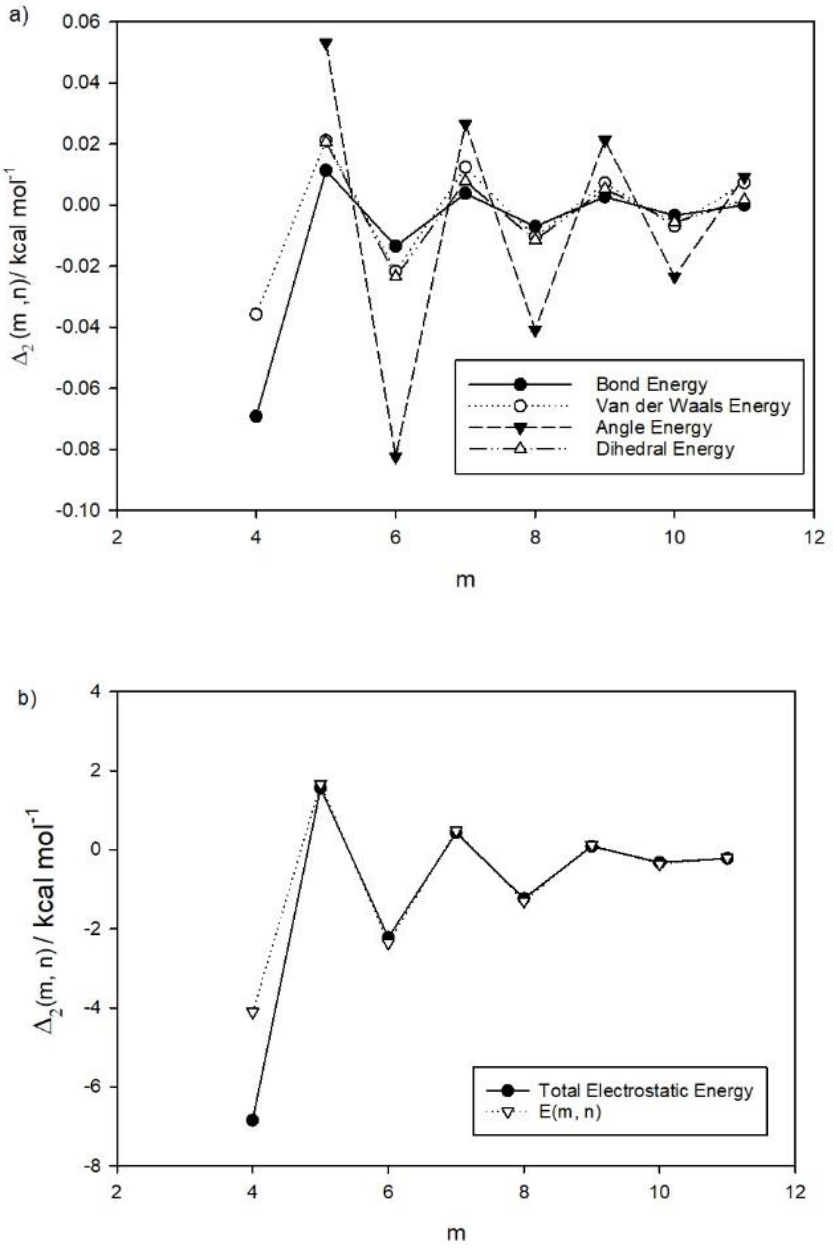


**Figure A.9.1:** a) Second Difference graph of the unhydrated $DC_m$ with $m$ = 3 - 12 for the energy contributions from bonds, angles, dihedral interactions, van der Waals interactions. b) Second difference graph of unhydrated $DC_m$ with $m$ = 4 - 11 for the energy contributions from electrostatic interactions comparing with the second difference graph for the conformational energies.

## Appendix 10: DFT Calculations for Di-carboxylate Di-Anions in Unhydrated Conditions

The odd-even effect was observed for the $DC_m$ in unhydrated, implicitly solvated and explicitly hydrated conditions. It was important to investigate if this pattern was originating from the $DC_m$ or from the computational programs used. DFT calculations were run for unhydrated $DC_m$ to validate this phenomenon. The energies of the $DC_m$ decrease as the chain length increases (Figure A.10.1a). This was observed in the basin-hopping global optimization calculations. A second difference graph (Figure A.10.1b) was calculated, and the odd-even effect was again observed.

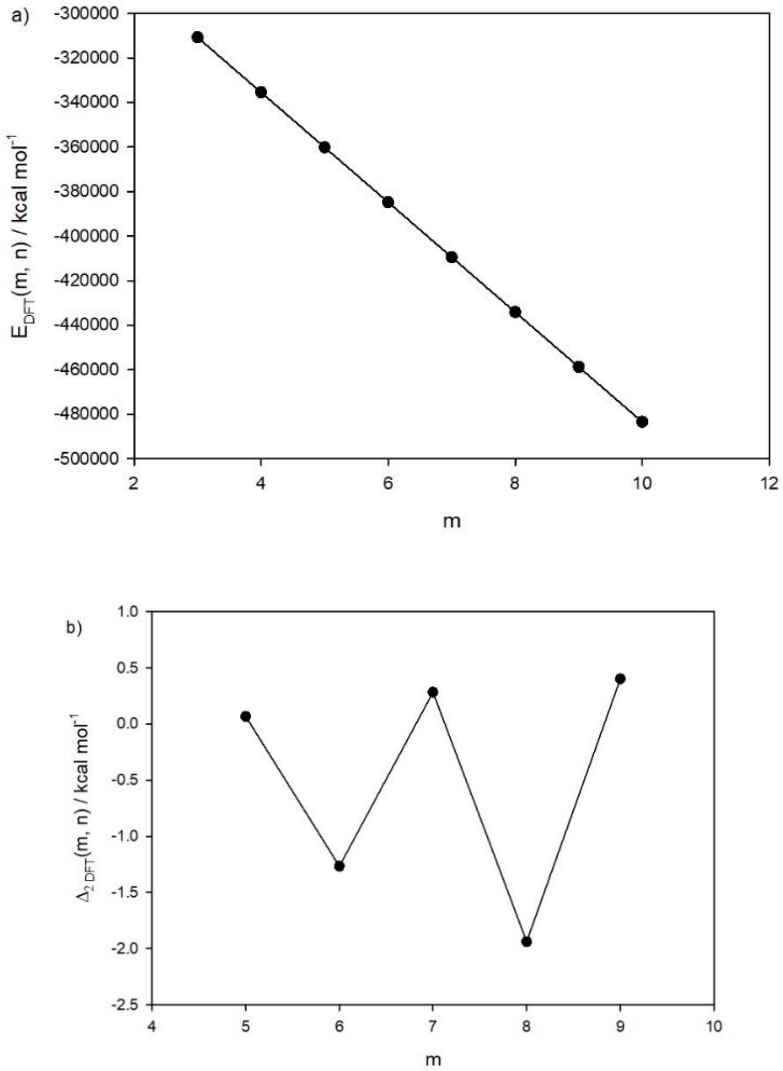


**Figure A.10.1**: a) Variation of the conformational energies from DFT calculations unhydrated $DC_m$ with $m$ = 3-10. b) Second Difference graph of unhydrated $DC_m$ with $m$ = 5-9.

## Appendix 11: Summaries for the Average Distance Values Between Charged Ends for Each Studied Di-ion.

**Table A.11.1.** Summary of the average $R_{NN}$ values for the three distinct structural regimes observed for $DA_m(H_2O)_n$. The minimum $R_{NN}$ value corresponds with the fully folded $DA_m$ conformation.

| ***m*** | ***n* range studied** | **Average $R_{NN}$ for the linear conformation / Å** | **Average $R_{NN}$ for the folded conformation / Å** | **Minimum $R_{NN}$ and corresponding *n* value** | |
|---|---|---|---|---|---|
| | | | | **$R_{NN}$ / Å** | ***n*** |
| **3** | 1-12, 15, 20 | 5.12 | 4.49 | 3.81 | 11 |
| **4** | 1-12, 15, 20 | 6.43 | 5.48 | 4.91 | 15 |
| **5** | 1-12, 15, 20 | 7.66 | 5.62 | 5.36 | 20 |
| **6** | 1-25 | 8.98 | 6.68 | 6.06 | 25 |
| **7** | 1-15, 20 | 10.26 | 7.84 | 7.43 | 20 |
| **8** | 12-18, 20 | 11.55 | 7.49 | 6.97 | 18 |
| **9** | 16-24 | 12.73 | 8.98 | 4.48 | 24 |
| **10** | 18-25 | 14.01 | 8.86 | 8.42 | 22 |
| **11** | 18-30 | 15.28 | 9.58 | 7.22 | 25 |

**Table A.11.2:** Summary of the average $R_{CC}$ values for the three distinct structural regimes observed for $DC_m(H_2O)_n$. The minimum $R_{CC}$ value corresponds with the fully folded $DC_m$ conformation.

| ***m*** | ***n* values studied** | **Average $R_{CC}$ for the linear conformation / Å** | **Average $R_{CC}$ for the folded conformation / Å** | **Minimum $R_{CC}$ and corresponding *n* value** | |
|---|---|---|---|---|---|
| | | | | **$R_{CC}$ / Å** | ***n*** |
| **3** | 1-12, 15, 20 | 5.11 | 3.50 | 3.25 | 15 |
| **4** | 1-12, 15, 20 | 6.42 | 4.67 | 4.05 | 20 |
| **5** | 1-12, 15, 20 | 7.65 | 4.84 | 4.61 | 20 |
| **6** | 1-12, 15, 20 | 8.95 | 5.26 | 5.13 | 20 |
| **7** | 1-12, 15, 20 | 10.28 | 5.40 | 4.58 | 20 |
| **8** | 1-16 | 11.48 | 5.90 | 5.73 | 14 |
| **9** | 1-16, 20 | 12.74 | 6.07 | 4.89 | 20 |
| **10** | 1-20 | 14.12 | 6.34 | 6.05 | 17 |
| **11** | 1-20 | 15.24 | 6.01 | 5.93 | 19 |

Appendix 12: Plots of the conformational energies and plots of the corresponding second difference for Di-ions in Implicit Solvated Conditions

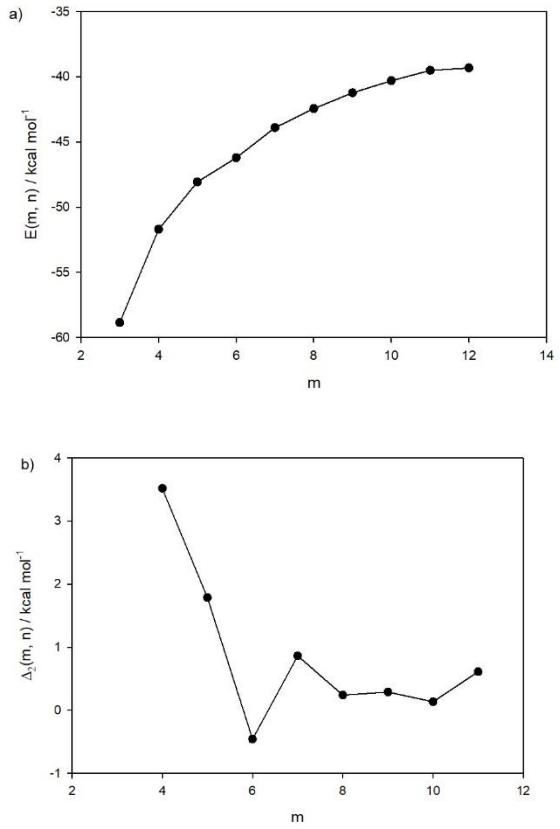


**Figure A.12.1:** a) Variation of the conformational energies implicitly solvated $DA_m$ with $m$ = 3-12. b) Second Difference graph of implicitly solvated $DA_m$ with $m$ = 4-11.

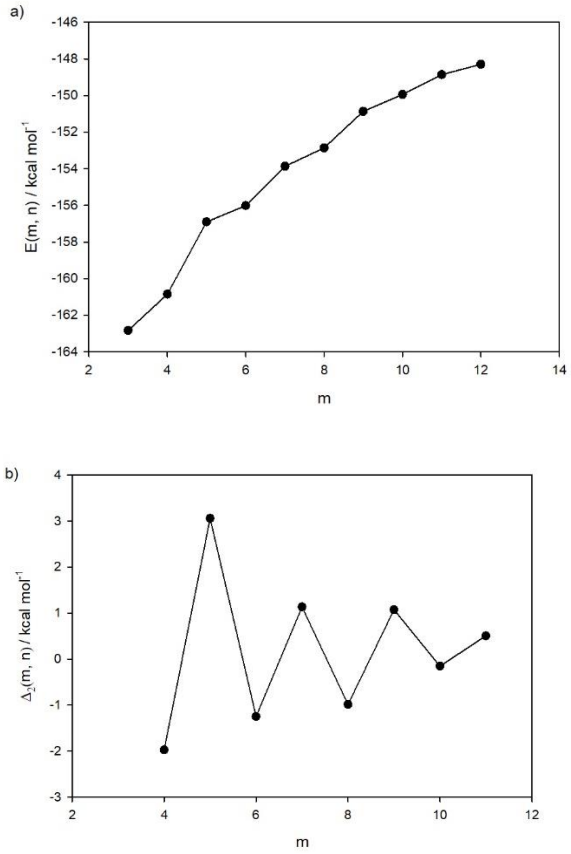


**Figure A.12.2:** a) Variation of the conformational energies for implicitly solvated $DC_m$ with *m* = 3-12. b) Second Difference graph of implicitly solvated $DC_m$ with *m* = 4-11).

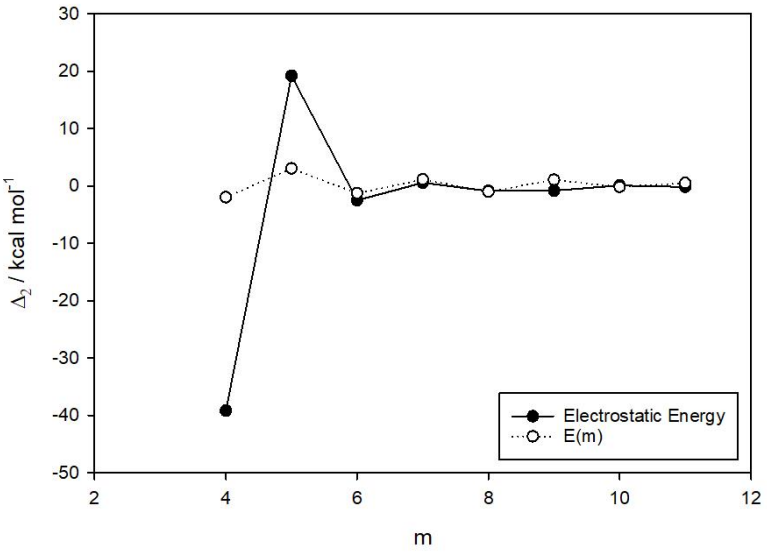


**Figure A.12.3:** Second Difference graph of implicitly solvated $DC_m$ with *m* = 4-11 for the energy contributions from electrostatic interactions compared with the second difference graph from the overall conformational energies.